Etude du pompage d'énergie non-linéaire par vibro impact

Tao Li

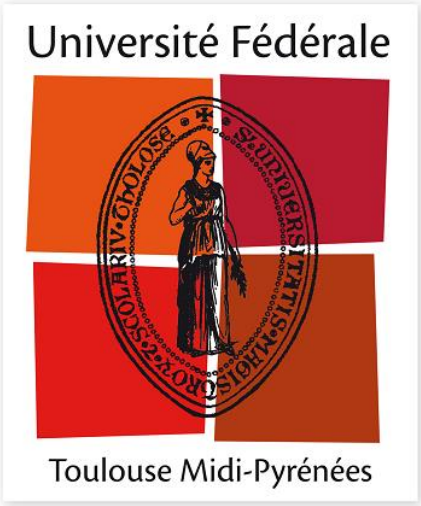

THÈSE

En vue de l'obtention du
DOCTORAT DE L'UNIVERSITÉ DE TOULOUSE

Délivré par:
Institut National des Sciences Appliquées de Toulouse (INSA Toulouse)

Discipline ou spécialité:
Génie Mécanique, Mécanique des Matériaux

Présentée par
Tao LI
Soutenue le mercredi 23 novembre 2016

Sujet de la thèse:
Study of nonlinear targeted energy transfer by vibro-impact

Jury:
M. Gaël CHEVALLIER, Professeur HDR, Université de Franche-Comté Besançon
M. Claude Henri LAMARQUE, Professeur HDR, ENTPE Vaulx-en-Velin
M. Pierre-Olivier MATTEI, Chargé de recherche HDR, LMA Marseille
M. Manuel PAREDES, Professeur HDR, INSA Toulouse

École doctorale:
Mécanique, Energétique, Génie civil et Procédés (MEGeP)
Unité de recherche:
Institut Clément Ader (ICA, CNRS UMR 5312)
Directeur(s) de Thèse:
(Directeur) M. Alain BERLIOZ, Professeur HDR, Université Paul Sabatier Toulouse
(Co-directeur) M. Sébastien SEGUY, Maître de Conférences, INSA Toulouse
Rapporteurs:
M. Gaël CHEVALLIER et M. Pierre-Olivier MATTEI

秋到丹枫秋已老

圖村故人

Here

You may find a lot of mistakes

But if there is a little that has inspired you

I would be satisfied

23/11/2016 Toulouse

Acknowledgements

Time like water, slowly slips away...
I, like a maple leaf,
turn yellow and mature,
it is time to summarize and re-start...
But, stop for a while, to remember and express my gratitude:

Mr. president Claude Henri LAMARQUE, Mr. Gaël CHEVALLIER, Mr. Pierre-Olivier MATTEI, Mr. Manuel PARADES, your criticism, encouragement, suggestions, discussions... each being a step-by-step contribution to my growth. Thank you all.

Mr. Alain BERLIOZ and Mr. Sébastien SEGUY, thank you for your supervision during the last three years. Without your help, how could all this be possible ?

Mr. Guilhem MICHON and Mr. Jean-Benoit ALIBERT, their help is very much appreciated.

Also, I thank the financial support of CSC and the working environment of laboratory ICA, as well as my colleagues who have accompanied me throughout those unforgettable periods of time.

Finally, my mother and father, although, they do not understand what I have done, they know that their son is doing something important and are always my first and last supporters.

Abstract

The objective of this thesis is to study the passive control of vibration by a Vibro-Impact (VI) Nonlinear Energy Sink (NES). Several aspects have been developed: the influence of parameters on response regimes, the optimization design mechanism under different excitations, the application to vibration control of nonlinear systems and the study of two VI NES in parallel.

Firstly, the influence of parameters on response regimes and bifurcation is analytically, numerically and experimentally studied, respectively. Different bifurcation routes and chaotic strongly modulated response are presented.

Then, the efficiency of typical response regimes is compared, and its mechanism lays the foundation for the optimization design of different parameters under different types of excitation.

Thirdly, the activation characteristic of VI NES is analytically studied and experimentally validated. An optimization design criterion is proposed for the vibration control of nonlinear system.

Finally, the vibration control by two VI NES in parallel is experimentally studied with the purpose of efficiency and robustness improvement. The principle of separate activation of VI NES is observed.

Keywords: Targeted Energy Transfer, Nonlinear Energy Sink (NES), Perturbation method, Impact damper

Résumé

L'objectif de cette thèse est d'étudier le contrôle passif des vibrations avec un absorbeur non linéaire de type Nonlinear Energy Sink (NES) à Vibro-Impact (VI). Plusieurs aspects ont été étudiés : l'influence des paramètres sur les régimes vibratoires observés, l'optimisation du design sous différentes excitations, l'application sur des systèmes vibratoires non linéaires et enfin l'étude de deux NES-VI en parallèle.

Tout d'abord, l'influence des paramètres de design sur les régimes vibratoires et les bifurcations est étudiée de façon analytique, numérique et expérimentale. Ainsi différentes bifurcations et des réponses fortement modulées de type chaotique sont présentées.

Ensuite, l'efficacité des régimes vibratoires est comparée, le mécanisme ainsi décrit constitue la base de l'optimisation du design de l'absorbeur face à différents types d'excitation.

Le mécanisme d'activation du NES-VI est étudié analytiquement puis validé expérimentalement. Un critère d'optimisation du design est proposé, puis appliqué sur différents systèmes au comportement vibratoire non linéaire.

Finalement, dans le but d'améliorer l'efficacité et la robustesse, le montage de deux NES-VI en parallèle est étudié expérimentalement. Le principe d'activation séparé est alors observé.

Mots-clés: Dynamique non linéaire, Nonlinear Energy Sink (NES), Méthode de perturbation, Absorbeur à impact

Table of contents

Introduction

Nowadays, large-scale applications of new materials like composite material, no matter for the reason of safety, or for the improvement of performance and comfort, can lead to complicated vibration phenomena. To control excessive vibrations, there exist different ways, and among them the passive control method is widely applied. Based on this passive method, a widely used device is Tuned Mass Damper (TMD), but it has many limitations, e.g., too important mass compared to that of a main system in one side, and the requirement of a precise tuning in the other side.

Recently, a type of nonlinear energy absorber termed as Nonlinear Energy Sink (NES) is extensively studied, and it is attached to a main system through nonlinear coupling. It is observed that the energy of this main system can be irreversibly transferred to the attached NES, and eventually be dissipated by NES through a series of transient resonance captures. In addition to these good performances, its mass is smaller than that of TMD and is easy to integrate as a result. The above phenomenon is termed as Targeted Energy Transfer (TET) or energy pumping.

To date, the initial study scope of TET is greatly extended, from linear main systems with one degree of freedom to nonlinear systems with many degrees of freedom, from NES with cubic nonlinearity to various other types like piece-wise or impact, and from the transient excitation to the periodic or random excitation, etc.. With so many researches, how to understand them and how to apply them are worth studying.

All energy absorbers should be coupled to main systems in a specific way, e.g., a linear spring for TMD and impacts for Vibro-Impact (VI) NES. Since the energy of a main system is transferred through this coupling, it plays a central role in the understanding of the underlying phenomenon, and this role can be viewed from different aspects. For instance, the ability of efficient TET in a broadband frequency directly depends on this nonlinear coupling. Another aspect is indirectly reflected by nonlinear normal modes or response regimes by deeply studying the corresponding Hamiltonian system, which is decided mainly by the type of nonlinearity. In addition, the interacting force can also be a useful index for the understanding of the variation of motion.

From the latter two aspects come two typical analytical methods: the study of Hamiltonian systems with the presentation of the results around a frequency energy plot and the study of damped systems with an asymptotic method, with which Slow Invariant Manifold (SIM) can be obtained for further analysis. The reason why they are important is that other complicated factors are neglected as many as possible, e.g., the type of outside excitation. Applicable for this principle, the interacting force has the potential to

play an intermediate role for the explanation of the dynamics of a system with different outside conditions, such as excitation types.

It has been found that the response regime of 1:1 resonance is responsible for efficient TET. Since the efficiency of TET is so tightly related to response regimes, the study of TET can be divided into the following two sub-problems: the influences of parameters on the occurrence of response regimes and the efficiency of different response regimes. In this way, the role of different parameters that seem so different from their own angles is the same from the viewpoint of response regimes. More specifically, for optimization design, the selection of parameters is to make the effective response regimes exist. Since response regimes can exist for both periodic and transient excitations, the optimization design mechanism should be based in the efficiency comparison of typical response regimes and be explained in the same way. Therefore, if the optimal response regime for periodic excitation with a single frequency was definite, the optimal mechanism for periodic excitation with a range of frequency could be explained in the same way.

Then, the following question is: how the optimal response regime is activated. If this activation is independent of the type of main systems, the optimization design of NES to control the vibration of a system can be simplified to the following question: how to activate NES at its best state. In this sense, whether the vibration control of a main system is effective cannot be assured, but the efficient activation of NES is guaranteed. Actually, its final role is decided by its relative importance in energy dissipation compared to other factors. Maybe, this conception is not the best in theory, but it could be applicable and efficient to some extent in practice.

From the above analysis, the following five questions are raised for the study of VI NES:

- Whether possible and how to establish a common bridge for the understanding of the dynamics of a same system under different excitations ?
- Whether the influence of parameters on the dynamics of a system coupled with VI NES can be decomposed into the following two sub-problems: the influence of parameters on the occurrence of response regimes and the efficiency comparison of response regimes ?
- Whether the optimization design mechanism of parameters under different excitations is the same ?
- Whether it is possible to simplify the optimization design of VI NES to control the vibration of nonlinear systems into the problem of the activation of VI NES at its best state ?
- Whether the addition of VI NES can improve the efficiency and robustness of TET ?

As responses to the above questions, the manuscript of this thesis is composed of five chapters.

In the first chapter, a general introduction of TET is presented in detail. At first, the dynamics of structure is presented, especially nonlinear aspects. Then, typical vibration control methods are compared and NES as a recent passive control device is

demonstrated. Thirdly, typical tools for the study of nonlinear dynamics are introduced. Fourthly, the study of NES with cubic nonlinearity is presented to demonstrate general characteristics of a NES. Finally, the state of the art of vibration absorber by VI, i.e., impact damper and VI NES, is introduced in detail and is specially examined from the viewpoint of TET.

The second chapter is concentrated on the study of the influence of different parameters on response regimes and their bifurcations. At first, an interacting force is introduced in the analytical analysis to explain complicated response regimes. Then, typical response regimes are presented around SIM. Thirdly, the influence of parameters is analyzed. Finally, different response regimes and bifurcation routes are experimentally observed.

The next chapter is around the efficiency comparison of different response regimes and the common optimization design mechanism for different types of excitation. At first, the efficiency of different response regimes is numerically observed under periodic and transient excitations, and they are analytically analyzed. Finally, experiments under periodic excitation with a single frequency, with a range of frequency and under transient excitation are carried out, respectively. Experimental results agree well with numerical results and validate the existence of a common criterion for optimization design under different excitations.

In the fourth chapter, the activation characteristic of VI NES is explored, and the optimization design of VI NES to control the vibration of nonlinear systems is also studied. Firstly, the activation characteristic is analyzed around SIM. As a result, the proportional activation of VI NES and its same activation for different frequencies can be obtained. Based on this, an optimization design criterion of VI NES for the vibration control of nonlinear systems is conceived. Secondly, the above two characteristics are numerically observed. Then, experimental observations further validate this activation mechanism. Finally, an application of this optimization design procedure to control chatter during a turning process is carried out, and numerical results prove its feasibility.

In the fifth and last chapter, another VI NES is added to study the possibility of efficiency and robustness improvement by the addition of VI NES. Firstly, existing analytical and numerical results are briefly introduced. Then, experiments under periodic excitations are carried out, and different response regimes are observed. In addition, the efficiency of vibration control by different combinations of clearances is compared. Finally, transient experiments are performed, and the principle of separate activation is observed. It means the efficiency and robustness improvement for free vibration. Generally, the response regime with two impacts per cycle is found tightly related to the effective control of vibration, no matter under periodic excitation or the transient case.

Finally, a conclusion is addressed. Then, future researches based on the work of this thesis are presented.

CHAPTER 1

Dynamics of targeted energy transfer

Abstract

The first chapter is dedicated to the presentation of a general background about the dynamics of structure and the framework of this thesis. Firstly, basic dynamics of structures is introduced. Then, vibration control methods are introduced and compared. Thirdly, the state of art of NES, especially VI NES, is presented in detail. Finally, objectives of this thesis are presented.

Contents

1.1 Linear and nonlinear systems

In nature, systems can be categorized into two main classes: linear systems and nonlinear systems.

1.1.1 Principal characteristics of linear systems

Superposition principle is a major characteristic of linear systems. It states that the net response at a given place and time caused by two or more loads is the sum of the response which would have been caused by each load individually. So that if input A produces response X and input B produces response Y, then input (A + B) produces response (X + Y).

In static, for example, a cause and an effect is proportional, i.e., a stress and a strain for linear material. In dynamic, the superposition principle is reflected by the linear modal superposition, i.e., free and forced vibrations can be conveniently expressed as a linear combination of individual linear motions.

1.1.2 Sources of nonlinearity

Although, studies of linear systems have been mature, linear behavior is an exception and nonlinearity is generic. Typical resources of nonlinearities are presented as follows [Kerschen *et al.*, 2006]:

- Geometric nonlinearity: it arises from the potential energy when a structure undergoes large displacements (e.g., pendulum). The relationship between restoring force and displacement can no longer be approximated as linear for large displacement as in the case of small displacement. These kinds of geometric nonlinearities are frequently encountered for large deformations of flexible elastic continua such as beams, plates and shells.
- Nonlinear material: it can be observed when the constitutive law between stresses and strains is nonlinear (e.g., foams and resilient mounting systems like rubber isolators) and its dynamics are normally complicated.
- Damping: dry friction effects (bodies in contact, sliding with respect to each other), hysteric damping and helical wire rope isolators are typical examples. Whether they should be considered depends on their relative importance.
- Boundary conditions: free surfaces in fluids, vibro-impacts due to loose joints or contacts with rigid constraints, clearances, imperfectly bonded elastic bodies and certain external nonlinear body forces. A common characteristic is the little change of displacement but with a sudden change of velocity at the boundary.

1.1.3 Typical characteristics of nonlinear systems

For nonlinear systems, principles established from linear systems no longer apply and the following typical nonlinear dynamics is demonstrated:

- The possibility of multiple, co-existing stable equilibrium positions and each with its own separate domain of attraction.
- Sudden transitions between stable attractors caused by nonlinear hysteresis phenomenon (i.e., jump) .
- Transitions from regular motions to beating and even chaotic motions, where the dynamics seems to be unpredictable, irregular and random-like.
- Chaotic explosion (intermittent or strongly modulated), where regular responses explode into responses with chaotic behavior and introduce a global form of instability in the dynamics just for a small parameter change.
- Supercritical or subcritical Hopf bifurcation.
- The dimensionality of the dynamics changes when a bifurcation occurs.

1.2 Vibration control

The vibration of a structure should be controlled no matter for the reason of comfort, stringent performance requirement, or safety. To control vibration, many researches have been done and many control methods have been developed. These control methods can be categorized into the following two main classes: passive control and active control. As to the passive control method, three different energy absorbers will be presented and compared.

1.2.1 Active control

In the case of active control, an auxiliary device is connected to a main structure through an actuator to counteract undesirable vibrations as showed in Fig. 1.1. To implement active control method, sensors are needed to collect information about the states of motion and their signals are fed back to a controller which gives commands to an actuator.

Generally, this control method can be more effective in the vibration reduction, relatively insensitive to outside conditions, and applicable to multi-hazard situations. In return, its disadvantages are also evident. The cost of installation and maintenance may be high. In addition, it relies on external power. Therefore, its reliability and stability is doubtful.

1.2.2 Passive control

When excessive vibration energy is only reduced by its own dynamic properties, it is normally termed as passive control method. According to its principle of function, it can be classed into three main categories: energy dissipation (direct method), energy isolation (base isolation) and energy transfer (indirect method) as displayed in Fig. 1.2. The principle of energy dissipation is to convert the kinetic energy to heat by increasing the damping of the structure, e.g., by the use of frictional sliding or deformation of

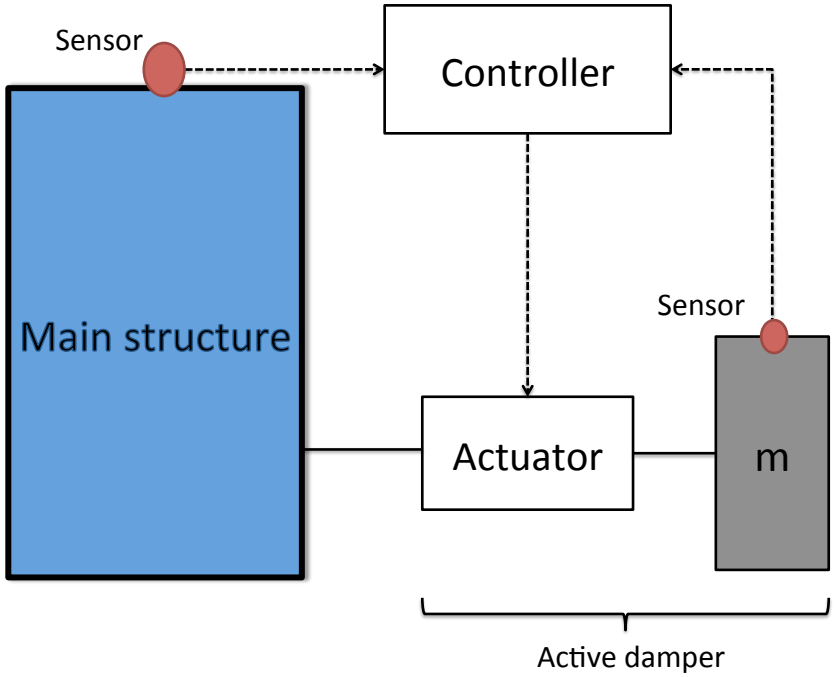

Fig. 1.1 Active control.

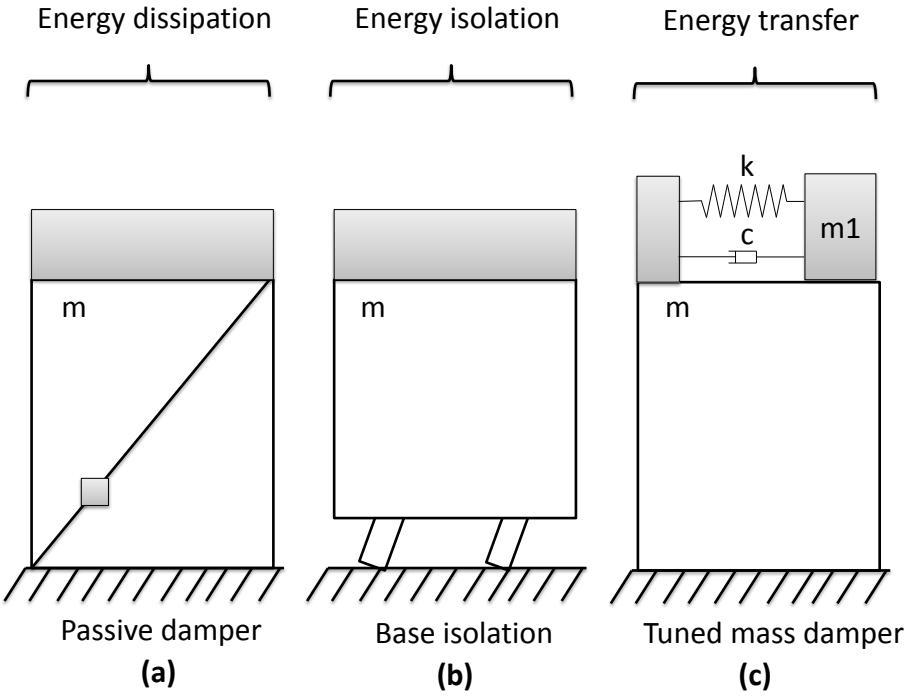

Fig. 1.2 Passive control.

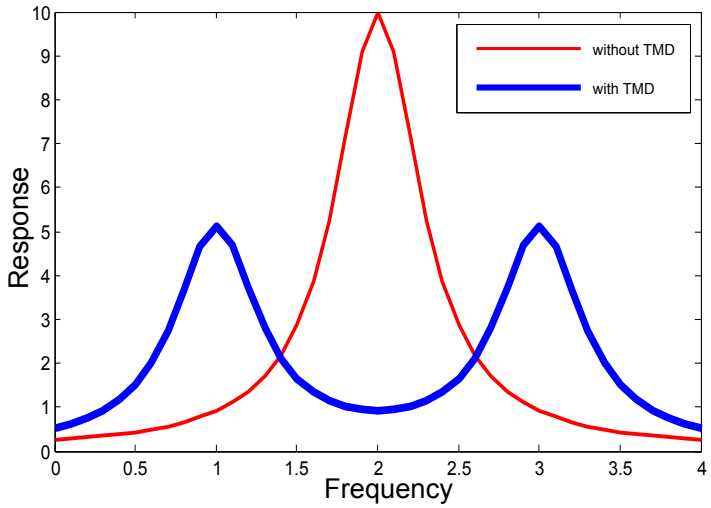

Fig. 1.3 Frequency response function of a main structure without and with TMD.

viscoelastic solids or fluids. For the energy isolation, it consists in isolating the structure and its components from potential damaging solicitations.

Compared to the above two methods, energy transfer involves a second structure which is attached to a principle structure and plays the role of attracting and dissipating excessive energy. The most popular and widely used device is indubitably Tuned Mass Damper (TMD) which is invented by Frahm in 1911 [Frahm, 1911]. This absorber is coupled to a main structure by a linear spring and dissipates excessive energy by viscous damping. It works at its optimal performance when its natural frequency is tuned to that of a principal structure. One frequency response function of a main structure without and with optimized TMD is showed in Fig. 1.3. The addition of TMD reduces the resonance peak at the expense of the occurrence of two other small peaks located at two sides of the resonance frequency.

The above mentioned characteristics make passive control method relatively less expensive, robust (e.g., still effective at earthquake) and independent of power supply. However, the response time may be a little significant. For example, TMD works just at a little range around natural frequency, and it will become invalid with the variation of the natural frequency of a main structure because of its aging and damage. In addition, the attached mass is relatively important compared to that of a main structure, classically 10%. Considering the above inconvenience, the possibility of other ways of coupling by means of nonlinearity has been extensively studied recently and will be introduced in the following part.

1.2.3 Nonlinear Energy Sink

Nonlinear Energy Sink (NES) is a type of energy absorber whose principle of damping belongs to that of the passive and indirect control method. In the aspect of configuration,

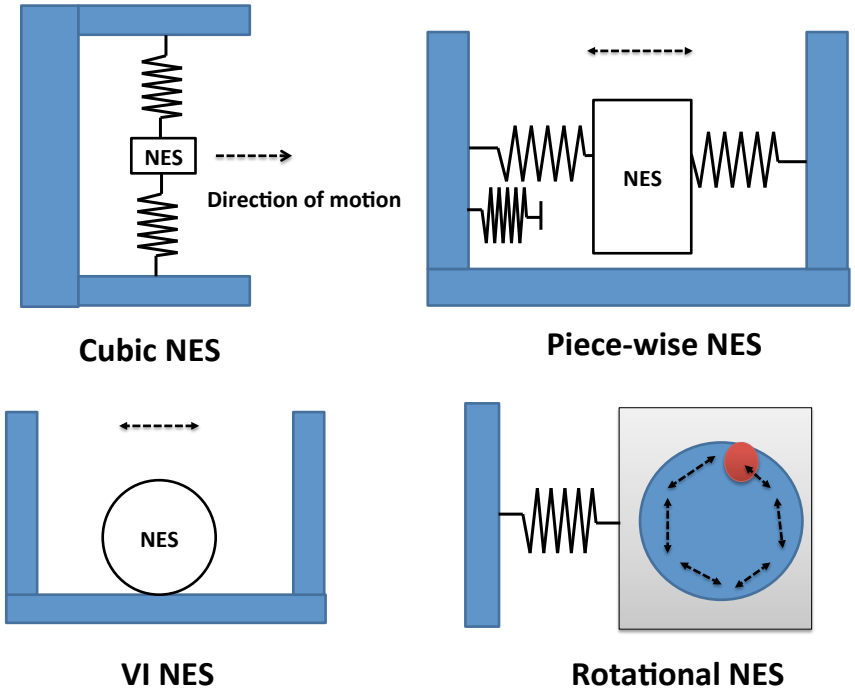

Fig. 1.4 Schematic representation of different types of NES.

NES is comparable to TMD, i.e., a small auxiliary mass is attached to a main structure. However, it is attached to a principal structure through essential nonlinearity. Through this way of coupling, NES can act as a broadband energy absorber by entering into resonance at a wide range of frequency. In addition, a substantial characteristic is that the energy of a main structure is irreversibly transferred into the attached NES and rapidly dissipated by NES. This process is referred as energy pumping or Targeted Energy Transfer (TET) [Lee *et al.*, 2008 ; Vakakis *et al.*, 2008].

Compared to TMD, NES has two main advantages. Firstly, the mass of NES is just several percent of the principal structure and is greatly reduced compared to that of TMD. Secondly, the essential nonlinearity of NES permits resonance during a large band of frequency rather than merely the natural frequency of a principal structure as in the case of TMD.

Theoretically, the type of nonlinearity is not defined clear and can possess many diverse forms. The first papers are around NES with pure cubic nonlinearity [Gendelman *et al.*, 2001 ; Vakakis and Gendelman, 2001]. Later other types of nonlinearity are studied in detail in the context of NES, e.g., non-smooth NES [Lamarque *et al.*, 2011], Vibro-Impact (VI) NES [Nucera *et al.*, 2007 ; Nucera *et al.*, 2008 ; Karayannis *et al.*, 2008 ; Lee *et al.*, 2009 ; Gendelman, 2012 ; Gourc *et al.*, 2015a ; Gendelman and Alloni, 2015 ; Gendelman and Alloni, 2016 ; Pennisi *et al.*, 2016], rotational NES [Gendelman *et al.*, 2012 ; Sigalov *et al.*, 2012], bi-stable NES [Mattei *et al.*, 2016 ; Benacchio *et al.*, 2016]. A schematic representation of different NESs studied in literature is demonstrated

in Fig. 1.4. Among them, the cubic NES will be introduced in detail later as an example to demonstrate TET. Then the state of art for VI NES will be reviewed and the study of VI NES from the viewpoint of TET is the motivation of this thesis.

1.3 Analysis tools of nonlinear dynamics

Some basic concepts and principal study methods are presented here, no matter used in the past study of TET or to be used in this thesis.

1.3.1 Nonlinear Normal Mode (NNM)

Linear normal mode is a central conception for linear systems. However, this concept does not apply any more for nonlinear systems in its original form. NNM has been introduced by Rosenberg [Rosenberg, 1960] and it has been defined as: an undamped discrete or continuous system as a synchronous (vibration in-unison) periodic oscillation where all material points of the system reach their extreme values and pass through zero simultaneously. More information about this basic concept and its computation can be consulted in [Kerschen *et al.*, 2009 ; Peeters *et al.*, 2009] and one example of the application of NNM can be consulted in [Festjens *et al.*, 2014]. Based on NNM, one main characteristic of TET, i.e., transient and sustained resonance captures, can be well understood [Lee *et al.*, 2005].

1.3.2 Harmonic Balance Method (HBM)

HBM is used to calculate periodic solutions of nonlinear systems. This technique assumes that the motion is periodic in time and approximates it by means of a finite Fourier series. HBM has an advantage in the aspect of its application to strongly nonlinear systems compared to other perturbation methods. Its precision of calculation depends on the used number of harmonics. However, it cannot obtain any information about the transient process.

1.3.3 Multiple Scales Method (MSM)

In addition to HBM, there are many other perturbation methods, e.g., averaging method and MSM. In essence, they are equivalent to each other. Their application is restricted to the assumption of weak-nonlinearity except HBM. In this way, the derived analytical solutions of nonlinear systems lie close to those of the corresponding linearized systems. In this thesis, MSM will be applied.

By MSM, not only the oscillatory solution is developed according to a small parameter, the variable of time is also expressed in the function of many time scales. The method of multiple scales is widely used in the field of nonlinear dynamics. Many examples of this method are treated in a book by Nayfeh [Nayfeh, 2011]. These methods mentioned

above normally are used after reducing the dimension of the problem by changing variables. The method of complexification first introduced by Manevitch [Manevitch, 2001] allows the reduction of the variables of displacement and velocity into a single complex variable and therefore decomposes the dynamics of the system into one slow part and another fast part.

MSM can also be applied to the study of transient dynamics and is a suitable tool for the understanding of nonlinear TET phenomena. Another advantage is that it can be used with symbolic manipulation programs, which is essential for its application to complicated nonlinear systems. It is stated that MSM is the simplest and involves the least algebra [Nayfeh, 1995].

1.3.4 Non-smooth temporal transformations (NSTTs)

Instead of taking sine and cosine functions as bases in perturbation methods, NSTTs employs saw-tooth and square wave functions as bases [Pilipchuk, 2002 ; Pilipchuk, 2015]. This technique can be applied to obtain solutions of a discontinuous system such as systems coupled with VI NES.

1.3.5 Numerical method

Although analytical methods have the ability to provide detailed information about the influence of parameters on the dynamics of systems, they may become inaccurate with the increase of nonlinearity and are also limited to systems with low dimensionality. As the compensation of analytical methods, many useful numerical methods have been developed. Their key advantage is that they are fairly easy to use and most of them provide exact solutions to equations of motion. Therefore numerical methods are more often used to acquire periodic solutions of nonlinear systems and to analyze bifurcations.

About periodic solutions, their stability and basin of attraction can be determined by a shooting method, whose principle of function is explained in [Nayfeh and Balachandran, 2008]. A continuation method is used to monitor modal lines as one parameter of the system evolves. A shooting procedure combined with the so-called pseudo-arc length continuation method is presented in [Peeters *et al.*, 2009]. One asymptotic numerical method can also be used to accomplish the above goal through the software Manlab developed by LMA of Marseille [Cochelin and Vergez, 2009]. In addition, other softwares can also be applied such as AUTO [Doedel *et al.*, 2007] and Matcont [Dhooge *et al.*, 2003].

1.3.6 Stability and bifurcation analysis

By analytical or/and numerical method, periodic solutions can be obtained. Then its stability can be analyzed by the following three ways: (a) direct numerical integration of equations of motion; (b) computing their Floquet multipliers; or (c) studying the

topological structure of numerical Poincaré maps. In this way, bifurcation diagrams can be constructed with respect to control parameters.

1.3.7 Time and frequency analysis

To understand the nonlinear dynamics better, it is necessary to study the variation of frequency with time. For TET, the frequency probably is not constant, which requires the use of wavelet transform or Hilbert transform [Hahn, 1996 ; Peng *et al.*, 2005 ; Huang, 2014] rather than Fourier transform which is limited to stationary signal.

1.4 NES with cubic nonlinearity

As mentioned above, the phenomenon about TET is initially studied for the NES with cubic nonlinearity, and its study is generalized to NES with other forms of nonlinearity later. The reason why the study of cubic NES is introduced in detail here is twofold. In one side, its essential characteristics around the concept of TET may still apply for other types of NES, e.g., VI NES. Moreover, different methods and study branches can be well demonstrated. In the other side, difficulties and unresolved issues are introduced and will constitute the objectives of this thesis.

1.4.1 Analytical methods

Two main analytical methods are used during the study of TET, and classed according to whether the damping of system is considered. The first work about TET dates back to 2000 by Vakakis and Gendeleman [Gendelman *et al.*, 2001 ; Vakakis and Gendelman, 2001]. When damping is neglected, the underlying Hamiltonian system is studied and may be a good reference for the corresponding system with week damping. Specifically, a relation between regimes and energy is obtained and presented in a diagram termed as Frequency Energy Plot (FEP) [Vakakis *et al.*, 2003] as showed in Fig. 1.5. FEP can be applied to predict the behavior of a system with weak damping as displayed in Fig. 1.6, in which the motion of this system is projected to FEP. It is found that there exist different orbits: fundamental orbits, sub-harmonic orbits and special orbits, which are marked out by black bullets. As a result, three ways of TET are observed: fundamental TET through 1:1 resonance, subharmonic TET through subharmonic orbits and TET initiated by non-linear beating, which corresponds to special orbits. When a system is perturbed from a state in rest , special orbits may be activated and can play the role of connecting fundamental orbits. This explains an essential characteristic of TET, i.e., the irreversible transfer of energy from a principal system to the attached NES. However, these special orbits cannot be activated except a large enough initial energy, called energy activation threshold. A more detailed introduction can be referred in [Lee *et al.*, 2008]. However, the study with this method is based on a relationship between dynamics and energy. Since energy is composed of two elements: frequency and

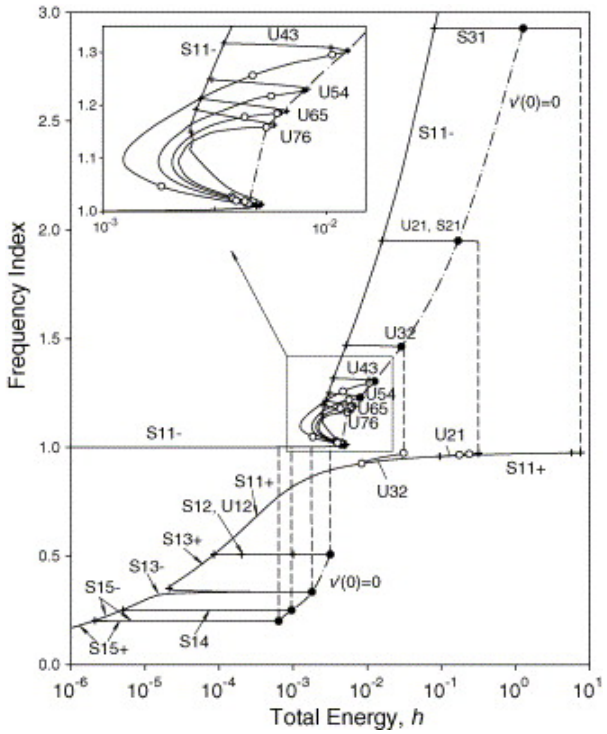

Fig. 1.5 FEP from [Lee *et al.*, 2005].

amplitude. A more refined study about the influence of frequency and amplitude should be carried out, respectively.

In addition to an activation threshold, the regime with 1:1 resonance is another important characteristic . Therefore, it is reasonable to study the dynamics of a system coupled with NES around this important regime. To directly study the system with week damping, one analytical method has been introduced in [Gendelman, 2004]. This approach is based on MSM under the hypothesis of 1:1 resonance. Solutions are decoupled in different time scales. A relationship of motion in a slow time scale is obtained and is called Slow Invariant Manifold (SIM). The bifurcation of NNM (i.e., deformation of SIM) is proved to be responsible for TET. In essence, SIM represents an intrinsic characteristic of the system and will not be influenced by damping and outside excitations. The above method is also generalized to NES with non-polynomial nonlinearities [Gendelman, 2004]. For different types of NES, different forms of SIM are showed in Fig. 1.7, and each SIM is related to their own nature.

About the resulting SIM of this method, its implications should be further studied, and Its relationship to other parameters such as damping and outside excitation should be also clarified. Moreover, possible common characteristics of SIM for different forms of NES should also be exploited.

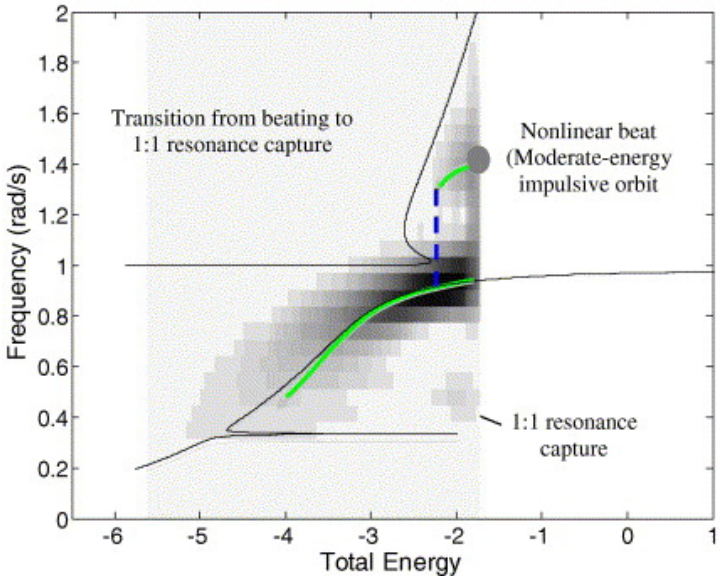

Fig. 1.6 Damped transitions in FEP [Kerschen *et al.*, 2008].

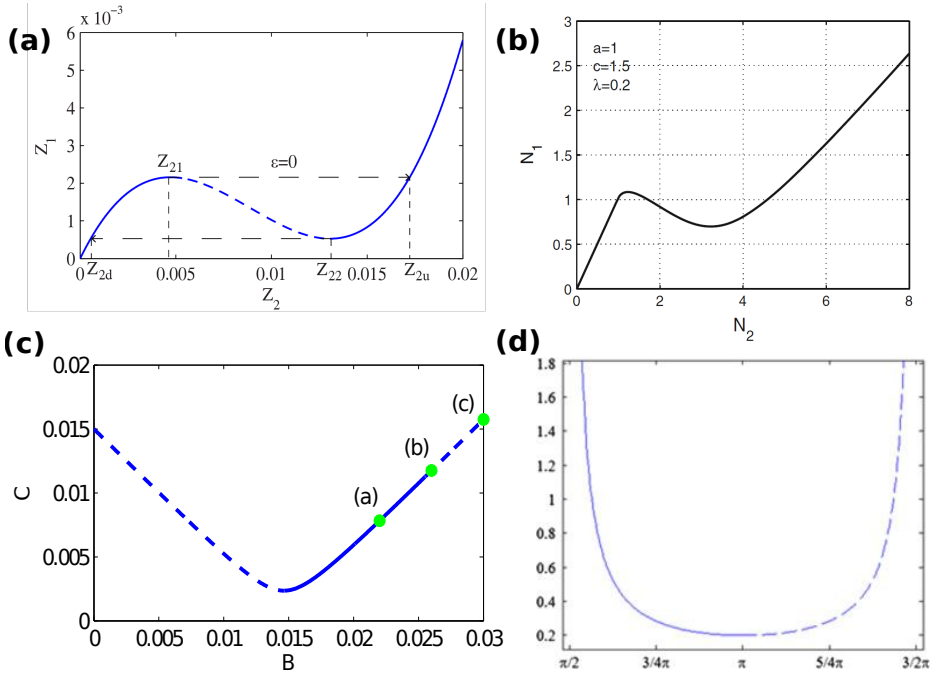

Fig. 1.7 Different forms of the topological structure of SIM: (a) cubic NES [Gourc *et al.*, 2014]; (b) piecewise NES [Lamarque *et al.*, 2011]; (c) VI NES [Gourc *et al.*, 2015a ; Gendelman and Alloni, 2015]; (d) rotational NES [Sigalov *et al.*, 2012].

1.4.2 Study under different excitations

NES with cubic nonlinearity under transient, periodic and random excitations has been extensively studied. The earliest study is concentrated on transient excitation. For periodic excitation, a special regime called Strongly Modulated Response (SMR) has been studied [Gendelman *et al.*, 2008]. TET is also studied for quasi-periodic and random excitations [Starosvetsky and Gendelman, 2011].

As for optimization design, the early studies are dedicated and limited to the study of the TET phenomenon itself, and the optimization problem is not totally solved. In [Manevitch *et al.*, 2007a ; Manevitch *et al.*, 2007b], an optimization design of parameters is accomplished by studying the underlying Hamiltonian system. The concept of Limiting Phase Trajectories (LPT) is defined and observed related to optimal response regimes. In [Nguyen and Pernot, 2012], an optimized design criterion is proposed, and parameters of cubic NES should be selected in order that the initial energy is located a little higher than that of a so-called first relative maximal point. The efficiency of cubic NES and TMD is compared under a frequency range around the natural frequency of a main system in [Starosvetsky and Gendelman, 2008], in which modulated responses seem to be more efficient than steady state responses. Limited experimental results in [Gourc *et al.*, 2014] give further proof that the energy of a main system is more reduced when SMR occurs. To conclude the above non-exhaustive cited studies, the study of TET under transient and periodic excitation is carried out, separately, and their relationship is not clear. Therefore, the question is whether there exists some relationship. The same question can be asked about the optimization design of NES. The above question about the optimization design under different excitations will constitute one objective of this thesis.

1.4.3 Applications

Applications can be classed into two categories: to control a linear system around one resonance frequency, and to control instability and limit cycle. For the initial study of TET, the main system is supposed to be a linear system, or the equation of system can be simplified into that of a simple system, regardless the number of degree of freedom and the type of excitations. In this sense, the equation of motion will be simple to treat by analytical development or numerical simulation, and it is called classic applications. Therefore, its main objective is to control the vibration around the interested frequency. Under this context, TET has been applied to diverse fields. TET in the domain of acoustics has been studied [Bellet *et al.*, 2010 ; Bellet *et al.*, 2012 ; Mariani *et al.*, 2011] and an experimental device is displayed in Fig. 1.8. Continuous structures have also been studied, i.e., supported beam [Georgiades and Vakakis, 2007a ; Avramov and Gendelman, 2010], tension-compression bar in [Georgiades *et al.*, 2007 ; Panagopoulos *et al.*, 2007 ; Tsakirtzis *et al.*, 2007] and plate [Georgiades and Vakakis, 2007b].

As for nonlinear systems, the application objective can be classed into two catego-

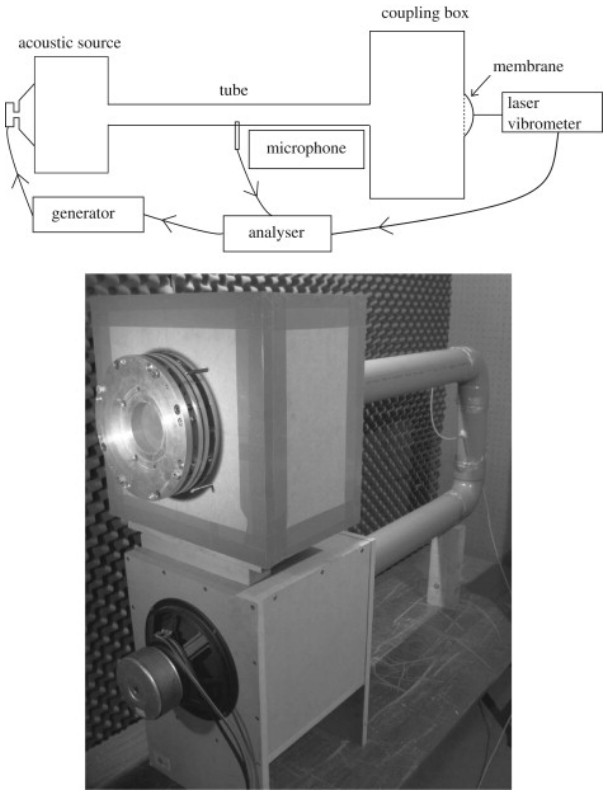

Fig. 1.8 An experimental device of NES used in [Bellet *et al.*, 2010].

ries: to control the stable points to the smallest and to increase the attraction domain of stable points to the largest. In another word, the performance of limit cycles and their stability should be improved. Around these two objectives, the vibration control of different nonlinear systems with NES has been studied. In [Gendelman and Bar, 2010], the application of NES to control the limit cycle of oscillation of Van der Pol has been researched. Aeroealastic instability control has been studied in [Lee *et al.*, 2007 ; Lee *et al.*, 2007]. In the domain of machining, the control of chatter with NES has been studied [Gourc *et al.*, 2015b]. Cubic NES also has been applied to control the vibration of helicopters [Bergeot *et al.*, 2016]. To improve the robustness of NES, cubic NES in parallel is studied in [Vaurigaud *et al.*, 2011 ; Savadkoohi *et al.*, 2012].

From the above analysis, the attention of study is transferred to the study of complicated nonlinear systems with NES, which is a usually encountered case in engineering practice. From the literature, the study of linear and nonlinear systems is normally carried out separately. In fact, the type of nonlinearities is so diverse from the viewpoint of principal systems. However, the type of recent NES is more limited and its study with linear system is simpler. Therefore, it will be one objective of this thesis to study the possible characteristics of NES, regardless of the type of main systems. Meanwhile, the improvement of robustness by multi-NES will also be studied.

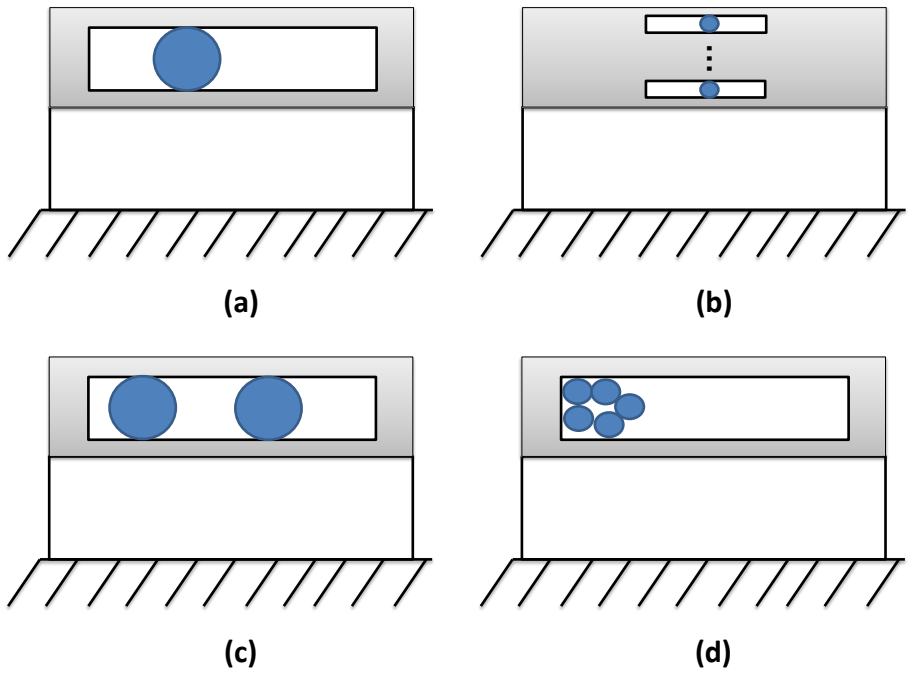

Fig. 1.9 Different forms of impact damper: (a) one ball; (b) multiple balls in parallel; (c) multipile balls in series connection; (d) particle damper.

1.5 VI NES

Although considerable studies about cubic NES are introduced, VI NES is the research subject of this thesis. In this part, its configuration and principle of energy reduction is introduced at the first place. Then, the state of art around impact damper is presented and unresolved problems are also discussed. Finally, the study of VI NES based on the framework of TET is demonstrated in detail.

1.5.1 Principle of function

Vibration and impact is a common phenomenon in nature and engineering [Ibrahim, 2009 ; Babitsky, 2013]. In most cases, it is detrimental and should be avoided. However, it has also been applied to control vibration seventy years ago [Lieber and Jensen, 1945] and a damper termed as acceleration damper is used. In the subsequent researches, it has been termed as impact damper, and recently as VI NES in the context of TET.

An impact damper is defined as a small object (e.g., a ball) which can move freely in a clearance of a principal structure, and the small object may be attached to the principle structure with or without spring as showed in Fig. 1.9(a). Other forms of impact damper can also exist, such as multiple impact dampers in parallel (Fig. 1.9(b)), multiple impact dampers in series (Fig. 1.9(c)) and particle damper (Fig. 1.9(d)). The energy of the principle structure is transferred by impacts and dissipated also by impacts

or by the friction between them. The most important control mechanism is the exchange of momentum during collisions. This characteristic is best represented by the regime with two impacts per cycle, which is known as the fundamental regime of resonance capture in the context of TET [Lee *et al.*, 2009]. Compared to TMD and cubic NES, it is proved to respond rapidly once the system is perturbed, and it is also simpler to implement.

1.5.2 Studies of impact damper

Extensively studies have been carried out around impact damper. The following words can be applied to distinguish different researches: implicated approaches (e.g., theoretical, numerical and experimental), application domain, the number of impact dampers and their form of coupling, the form of excitation and the friction, etc. Only the part that a linear system is coupled with one damper or several dampers in parallel under free vibration, under excitation with single frequency vibration and a range of frequency is introduced here. More information in detail can be consulted in [Ibrahim, 2009].

Although different researches have been developed for their own objectives, they can be categorized into two main categories: bifurcation and optimization design. Of course, this two objectives may occur together.

The exact analytical solutions of a single particle impact damper and their stability are obtained by Masri [Masri, 1965 ; Masri and Caughey, 1966]. The stability analysis defines the domains over which the modulus of all eigenvalues of certain matrix relating conditions after each of two conservative impacts is less than unity. Later the analytical study is generalized to the system coupled with n-unit impact damper under periodically excitation [Masri, 1969 ; Masri, 1970]. It is found that properly designed multiple impact dampers are more efficient than the case with single unit.

The steady state responses and their stability regions are obtained for an impact pair under excitation with two ranges of frequency, which are close or away from the natural frequency of a main system in [Bapat *et al.*, 1983 ; Popplewell *et al.*, 1983]. Later, the same study is carried out for the excitation with a prescribed periodic displacement [Bapat and Bapat, 1988]. Except the influence of parameters on response regimes, the influence of parameters (e.i., mass ratio, coefficient of restitution and clearance) is studied for a single unit impact damper under free and forced vibrations [Bapat and Sankar, 1985]. The optimized parameters are found to be different under these two different excitation types. These results are further experimentally validated in [Ema and Marui, 1994].

For transient excitation, the free decay of impact damped oscillations under a wide range of oscillator amplitude is studied in [Brown, 1988], the starting response regime with a finite number of impacts per cycle is proved useful in energy reduction.

A design procedure [Popplewell and Liao, 1991] is proposed and the suggested optimum regime is actually corresponding to the minimal point in the SIM obtained in [Gourc *et al.*, 2015a]. For the results according to this design procedure, there are some discrepancy between analytical calculation and numerical results. It probably results from the negligence of the influence of frequency on the stability.

By the systematic methods proposed in the papers by Peterka and Blazejczyk [Blazejczyk-Okolewska, 2001 ; Peterka and Blazejczyk-Okolewska, 2005], different response regimes and bifurcation types can be explained, such as symmetric and asymmetric two impacts per cycle, beating and intermittent chaos, and different routes to chaos. In addition, the dynamics has also been studied with Poincare maps [Sung and Yu, 1992] and Lyapunov exponential [Yoshitake *et al.*, 2007].

1.5.3 Studies of VI NES

Recently, vibration control by vibro-impact is studied in the frame of TET, and it is termed as VI NES. The application of VI NES to control seismic induced vibration has been studied numerically and experimentally by Nucera [Nucera *et al.*, 2007 ; Nucera *et al.*, 2008] and a VI NES is attached to a main structure by a spring. It has been observed that VI NES is able to effectively diminish undesirable energy once induced by seismic. The mechanism of TET has been well demonstrated. The above system is further studied by Lee [Lee *et al.*, 2009], in which some new tools are proposed as an effort to study the dynamics in a systematical way. Its underlying Hamiltonian system is studied, and as a result, a FEP is constructed as for the case of cubic NES. Special orbits as well as three mechanisms of TET are observed. It is demonstrated that a superior shock absorption by VI NES is attained for intermediate clearances, small coupling frequencies and large mass ratios.

With damping, an analytical study with MSM is carried out for a system coupled with VI NES under transient excitation [Gendelman, 2012]. Then, it is generalized to the periodic excitation case. SIM is obtained and applied to explain the slow variation of motion, and it is proved to be a good tool to predict the variation of responses under both transient and periodic excitations. In addition, SMR are experimentally observed and explained [Gourc *et al.*, 2015a]. Its chaotic characteristic is explained for the first time [Gendelman and Alloni, 2015 ; Gendelman and Alloni, 2016].

In the aspect of application, VI NES is applied to quench the chatter of a turning process [Gourc *et al.*, 2015b]. The analytical study has been carried out and is only treatable with the simplification of the underlying time-delayed equation. As a result, the obtained analytical results cannot reliably predict experimental results. As the case of cubic NES, this difficulty probably exists once VI NES is coupled to complicated systems. The preliminary experimental results with two-thirds reduction of velocity demonstrate its effectiveness of energy reduction. However, a feasible and precise design of VI NES to control vibration of nonlinear systems will be difficult, which will be one of the objectives of this thesis.

1.5.4 Asymptotic analysis of VI NES

The mechanical model of a LO coupled with a VI NES is showed in Fig. 1.10. VI NES is attached to a cavity and can move freely during the clearance between VI NES

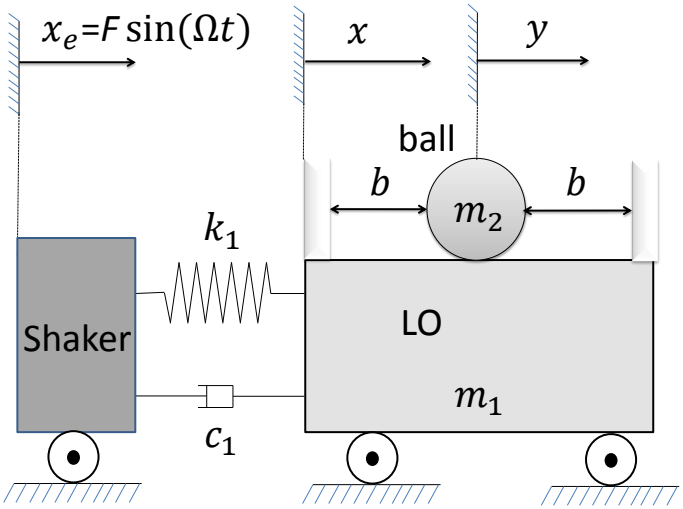

Fig. 1.10 Schema of a LO coupled with a VI NES under periodic excitation.

and LO. The following asymptotic analysis has been developed by E. GOURC [Gourc, 2013] and it lays the analytical foundation of this thesis.

The equation of motion between impacts is described as follows:

$$\begin{aligned} &m_1\frac{d^2}{dt^2}x\left(t\right)+c_1\frac{d}{dt}x\left(t\right)+k_1x\left(t\right)=k_1x_e\left(t\right)+c_1\frac{d}{dt}x_e\left(t\right)\\ &m_2\frac{d^2}{dt^2}y\left(t\right)=0\\ &\forall\left|x-y\right|<b \end{aligned} \tag{1.1}$$

where x, m_1, c_1 and k_1 are the displacement, mass, damping and stiffness of the LO respectively. y and m_2 are displacement and mass of VI NES. b represents the length of the clearance. $x_e\left(t\right)$ is the displacement imposed on the base and it will contribute two parts of force to the LO: the stiffness part and the damping part.

After nondimensionalization, the above equations is simplified:

$$\begin{aligned} &\ddot{x}+\epsilon\lambda_1\dot{x}+x=\epsilon G\sin\Omega\tau+\epsilon^2\lambda_1G\Omega\cos\Omega\tau\\ &\epsilon\ddot{y}=0\\ &\forall\left|x-y\right|<b \end{aligned} \tag{1.2}$$

The corresponding physical parameters are expressed as follows:

$$\begin{aligned} &\epsilon=\frac{m_2}{m_1},\quad {\omega_0}^2=\frac{k_1}{m_1},\quad \tau=\omega_0t,\\ &\lambda_1=\frac{c_1}{m_2\omega_0},\quad \Omega=\frac{\omega}{\omega_0},\quad G=\frac{F}{\epsilon} \end{aligned}$$

where ϵ represents the mass ratio between VI NES and LO. ω_0 denotes the natural angular velocity and f_0 denotes the natural frequency of LO. τ represents the dimensionless

time.

The dots denote differentiation with respect to dimensionless time τ. $\epsilon G \sin \Omega\tau$ and $\epsilon^2 \lambda_1 G\Omega \cos \Omega\tau$ represent the force contribution of displacement and that of velocity of excitation respectively imposed on LO. The latter term is conserved here to demonstrate its physical meaning and is neglected during the following analysis because of its small magnitude.

When $|x - y| = b$, impacts occur. The relation between after and before impact is obtained under the hypothesis of the simplified shock theory and the condition of total momentum conservation:

$$\begin{aligned} &x^+ = x^-, \quad y^+ = y^- \\ &\dot{x}^+ + \epsilon\dot{y}^+ = \dot{x}^- + \epsilon\dot{y}^-, \quad \dot{x}^+ - \dot{y}^+ = -r\left(\dot{x}^- - \dot{y}^-\right), \\ &\text{for } |x - y| = b \end{aligned} \tag{1.3}$$

where r is the restitution coefficient and the superscripts $+$ and $-$ indicate time immediately after and before impact.

It is seen that the velocity before and after impact experiences a sudden change in its direction and thus results in what is known as non-smooth dynamics. Actually, the process of the change of velocity is more complex than the used analytical treatment, but the method used here has been proved simple, useful and effective.

Specifically, three particular techniques have been developed over the years in order to transform the complicated non-smooth process into smooth ones. These include the power-law phenomenological modeling, the Zhuravlev and Ivanov non-smooth coordinate transformations, and the Hertzian contact law [Ibrahim, 2009].

New variables representing the displacement of the center of mass and the internal displacement of the VI NES are introduced as follows:

$$v = x + \epsilon y, \quad w = x - y \tag{1.4}$$

Substituting Eq. (1.4) into Eqs. (1.2) and (1.3), the equation between impacts in barycentric coordinate are given as:

$$\begin{aligned} &\ddot{v} + \epsilon\lambda_1 \frac{\dot{v} + \epsilon\dot{w}}{1 + \epsilon} + \frac{v + \epsilon w}{1 + \epsilon} = \epsilon G \sin \Omega\tau + \epsilon^2 \lambda_1 G\Omega \cos \Omega\tau \\ &\ddot{w} + \epsilon\lambda_1 \frac{\dot{v} + \epsilon\dot{w}}{1 + \epsilon} + \frac{v + \epsilon w}{1 + \epsilon} = \epsilon G \sin \Omega\tau + \epsilon^2 \lambda_1 G\Omega \cos \Omega\tau \\ &\forall |w| < b \end{aligned} \tag{1.5}$$

and the impact condition (1.3) is rewritten as:

$$\begin{aligned} &v^+ = v^-, \quad w^+ = w^-, \\ &\dot{v}^+ = \dot{v}^-, \quad \dot{w}^+ = -r\dot{w}^-, \quad \text{for } |w| = b \end{aligned} \tag{1.6}$$

From here on, MSM is used to analyze the solution in different orders and time scales. Multiple scales are introduced in the following form:

$$\begin{aligned} v(\tau;\epsilon) &= v_0(\tau_0,\tau_1,\ldots) + \epsilon v_1(\tau_0,\tau_1,\ldots) + \ldots \\ w(\tau;\epsilon) &= w_0(\tau_0,\tau_1,\ldots) + \epsilon w_1(\tau_0,\tau_1,\ldots) + \ldots \\ \tau_k &= \epsilon^k \tau, \quad k = 0,1,\ldots \end{aligned} \tag{1.7}$$

A detuning parameter (σ) representing the nearness of the forcing frequency Ω to the simplified natural frequency of the LO is introduced:

$$\Omega = 1 + \epsilon\sigma \tag{1.8}$$

Substituting Eqs. (1.7) and (1.8) into Eqs. (1.5), (1.6), equating coefficients of like power of ϵ and only conserving the first two orders:

order ϵ^0 between impacts:

$$\begin{aligned} &D_0^2 v_0 + v_0 = 0 \\ &D_0^2 w_0 + v_0 = 0, \quad \forall |w_0| < b \end{aligned} \tag{1.9}$$

order ϵ^0 once impacts:

$$\begin{aligned} &v_0^+ = v_0^-, \quad w_0^+ = w_0^-, \\ &D_0 v_0^+ = D_0 v_0^-, \quad D_0 w_0^+ = -r D_0 w_0^-, \quad \text{for } |w_0| = b \end{aligned} \tag{1.10}$$

order ϵ^1 between impacts:

$$\begin{aligned} D_0^2 v_1 + v_1 = &-2D_0 D_1 v_0 - \lambda_1 D_0 v_0 - w_0 + v_0 \\ &+G\sin(\tau_0 + \sigma\tau_1) \end{aligned} \tag{1.11}$$

For order ϵ^1, only the term related to LO is conserved and will be used later. Combining the first and second order, the SIM and fixed points could be obtained.

From the analysis of order ϵ^0, v_0 represents an ideal undamped harmonic oscillator expressed as follow:

$$v_0 = C(\tau_1)\sin(\tau_0 + \theta(\tau_1)) \tag{1.12}$$

From the standpoint of w_0, Eq. 1.9 and Eq. 1.10 represent a harmonically forced impact oscillator with symmetric barrier. For the regime of 1:1 resonance with two impacts per cycle, its solution can be searched in the following form:

$$w_0 = C(\tau_1)\sin(\tau_0 + \theta(\tau_1)) + \frac{2}{\pi}B(\tau_1)\Pi(\tau_0 + \eta(\tau_1)) \tag{1.13}$$

where $\Pi(z)$ is a non-smooth sawtooth function [Pilipchuk, 2002 ; Pilipchuk, 2015]. This folded function and its derivative are depicted in Fig. 1.11 and are expressed as follows:

$$\Pi(z) = \arcsin(\sin z) \quad M(z) = \tfrac{d\Pi}{dz} = sgn(\cos z) \tag{1.14}$$

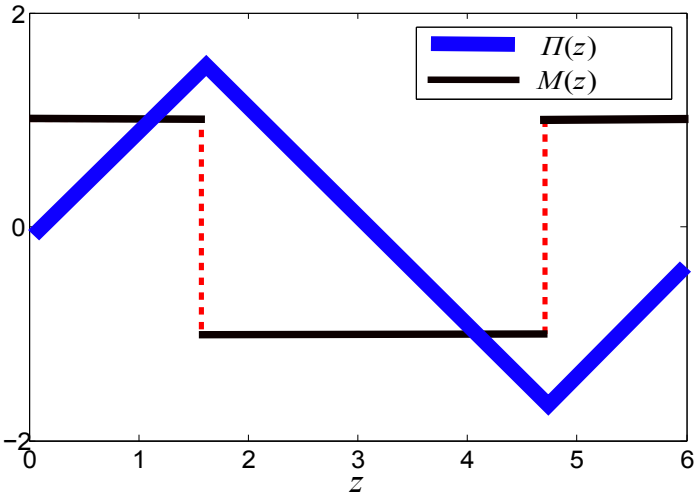

Fig. 1.11 Representation of the non-smooth functions $\Pi(z)$ and $M(z)$.

According to Eq. (1.13) and (1.14), impact occurs at $T_0 = \pi/2 - \eta + j\pi$ with $j = 0, 1, 2, \ldots$. The impact condition $|w_0| = b$ is rewritten with Eq. (1.13) as:

$$C\cos(\eta - \theta) = b - B \tag{1.15}$$

Rewriting now the inelastic impact condition (1.10) yields:

$$C(1+r)\sin(\eta - \theta) = \frac{2}{\pi}B(1-r) \tag{1.16}$$

Combining Eqs. (1.15) and (1.16), a relation between B and C is obtained as follows:

$$C^2 = \left(1 + \frac{4(1-r)^2}{\pi^2(1+r)^2}\right)B^2 - 2bB + b^2 \tag{1.17}$$

To obtain the fixed points, the equation at the next order should be analyzed and will be presented in the next chapter, and the stability analysis of fixed points can be accomplished by direct numerical integration of Eqs. (1.9) and (1.10) or by the following commonly used method.

The characteristic of asymptotic stability is important for the consistency of practical application of vibro-impact system. A vibro-impact system like a LO coupled with a VI NES is asymptotically stable if it returns eventually to the original motion after a small perturbation. The essential idea of the method is to evaluate the propagation of small errors in difference equations. It can be imagined that the effect of a slight perturbation of the absolute displacement and velocity of the secondary mass or the main mass, Δw and $\Delta \dot{w}$, is monitored at subsequent collisions. The perturbation may affect the instants of some of the later collisions but in a manner consistent with the equations of motion and periodicity requirements. The accumulated errors can be expressed as follows:

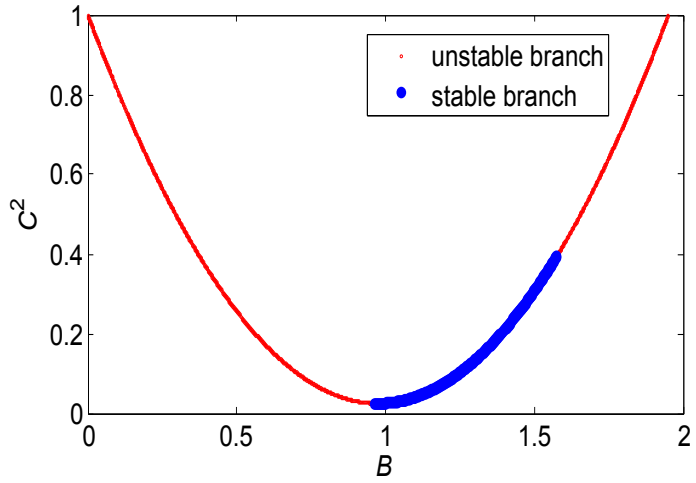

Fig. 1.12 SIM of VI NES: one stable branch in thick line, two unstable branches in thin line.

$$\begin{Bmatrix} \Delta w_{(N+1)} \\ \Delta \dot{w}_{(N+1)} \end{Bmatrix} = \left[P\right] \begin{Bmatrix} \Delta w_1 \\ \Delta \dot{w}_1 \end{Bmatrix} \tag{1.18}$$

and

$$\left[P\right] = \left[P_N\right] \left[P_{(N-1)}\right] \cdots \left[P_i\right] \cdots \left[P_1\right] \tag{1.19}$$

A subscript like i designates properties at the ith collision. The periodic motion is asymptotically stable if and only if all the modules of the eigenvalues of matrix $\left[P\right]$ are strictly less than unity [Masri, 1965 ; Masri and Caughey, 1966 ; Bapat *et al.*, 1983]. The results with the application of the above method are obtained and showed in Fig. 1.12. The points p1 and p2 represent the bifurcation points in which the regime with two symmetric impacts per cycle loses its stability, specifically the saddle-node bifurcation for p2 and the symmetric break bifurcation for p1. For the point p0, a grazing bifurcation occurs and the regime with three impacts per cycle comes into being [Peterka, 2003].

1.6 Objectives and work of this thesis

The presented studies about cubic NES demonstrate the research of TET in different aspects, and impact damper, as a member of NES in the context of TET, may also be investigated from this new horizon. Its study state demonstrates that its main limitation comes from the used analytical methods. The recent study of impact damper around the name of VI NES highlights some new characteristics. However, its study is not comprehensive. Therefore, the objective of this thesis is to study VI NES in this new context of TET. The chapters of this thesis are organized as follows:

The second chapter is dedicated to the study of typical response regimes, and the influence of parameters on these response regimes and bifurcations around SIM. At first, different typical response regimes are introduced. Then the influence of parameters on bifurcations is studied. Finally, different response regimes and bifurcation routes are experimentally studied.

In the next chapter, the efficiency of different response regimes is compared. The common optimization design mechanism of VI NES under periodic and transient excitations is studied. Firstly, numerical simulations are carried out to compare efficiency of different response regimes and parameters. Then, experiments are constructed under periodic and transient excitations, respectively. Results are applied to compare the efficiency of different response regimes and obtain the optimization design relation between different types of excitation.

In the fourth chapter, the objective is to explore the activation mechanism of VI NES and then, to propose an optimization design criterion of VI NES for the vibration control of nonlinear systems. Firstly, the activation characteristic of VI NES is analyzed around SIM. Then, an optimization design procedure of VI NES is proposed for vibration control of nonlinear systems. In the numerical and experimental parts, the activation characteristic is validated. Finally, a preliminary application to control chatter during a turning process is carried out.

In the last chapter, a VI NES is added to explore the possibility of efficiency and robustness improvement. A LO coupled with two VI NES in parallel are experimentally studied. Different experiments under different excitations are carried out. Different response regimes are observed and their contributions to vibration control are compared. Moreover, the principle of separate activation is studied by transient experiments.

CHAPTER 2

Influence of parameters on response regimes

Abstract

The objective of this chapter is to study the influence of parameters on response regimes and bifurcations of a LO coupled with a VI NES. Firstly, the analysis is developed around SIM. Then, five typical response regimes are demonstrated by numerical simulations. In addition, the coherence between numerical and analytical results is analyzed. Thirdly, the influence of different parameters is investigated around SIM. Finally, different response regimes, bifurcation routes and SMR are experimentally validated.

Contents

2.1 Theoretical analysis

There are already many researches about the dynamics of VI NES system, and more specifically speaking, about response regimes and bifurcations. However, the study is performed on cases studies, and it is necessary to perform a comprehensive study.

Recently, it is observed that transient resonance capture is important for vibration control, and its corresponding response regime is that with two impacts per cycle of VI NES. Therefore, it is natural to put the focus on this regime.

Since the fixed point of this regime can be calculated, it is possible to perform an analytical study firstly, and with numerical and experimental validation later.

As mentioned in the first chapter, VI NES has been studied in the domain of TET as a member of NES and MSM has been used as analytical study method. As a result, SIM and fixed points can be obtained. The following analytical development is a continuation of the former study [Gourc, 2013].

A typical SIM (Eq. (1.17)) with $b = 1$ and $r = 0.6$ is showed in Fig. 2.1, and three typical points p0, p1 and p2 are marked out.

In order to obtain the fixed points and to study the non-stationary motion evolution on the SIM, Eq. (1.11) at the next order of approximation is analyzed. To identify terms that produce secular terms, the function of w_0 is expanded in Fourier series in the following way:

$$w_0 = C(\tau_1)\sin\left(\tau_0 + \theta(\tau_1)\right) + E\left(\tau_1\right)\sin\left(\tau_0 + \zeta\left(T_1\right)\right) + RFC \tag{2.1}$$

where RFC represents the remaining frequency components except resonance frequency. The component $C\left(\tau_1\right)$ is decided by the motion of LO and $E\left(\tau_1\right)$ is totally related to the motion of VI NES, and this time, it can be a variable rather than a constant. In this way, it opens another viewpoint to observe and analyze transient and not-steady responses. From the standpoint of experiments, $E\left(\tau_1\right)$ is related to the periodic impact force, i.e., impact strength and frequency. Therefore, Eq. (2.1) is a more general and relaxed analytical description of motion compared to former studies, in which only the response regime with two symmetric impacts per cycle is considered.

Substituting Eqs. (1.12), (1.13) and (2.1) into Eq. (1.11) and eliminating terms that produce secular terms give:

$$\begin{aligned} D_1 C &= -\frac{1}{2}\lambda_1 C - \frac{1}{2}E\sin\left(\Theta\right) + \frac{1}{2}G\sin\left(\eta\right) \\ D_1\eta &= \frac{1}{2}G\cos\left(\eta\right)/C - \frac{1}{2}E\cos\left(\Theta\right)/C + \sigma \end{aligned} \tag{2.2}$$

where

$$\begin{aligned} \Theta &= \zeta - \theta \\ \eta &= \sigma\tau_1 - \theta \end{aligned} \tag{2.3}$$

Θ represents the phase difference related to LO and VI NES. η represents the phase difference related to LO and outside excitation.

The fixed points can be obtained by equating the right side of Eq. (2.2) to zero and then combining it with Eq. (1.17). In this way, the fixed points (number and position) can be obtained. Compared to the classic non-asymptotic method, its function is twofold. Firstly, its position can be used to judge the type of response regime. Secondly, its value can be precisely calculated for 1:1 resonance, which may be related to the optimal response regime. Meanwhile, the corresponding equivalent force E between LO and VI NES can be used to analyze the complicated performance.

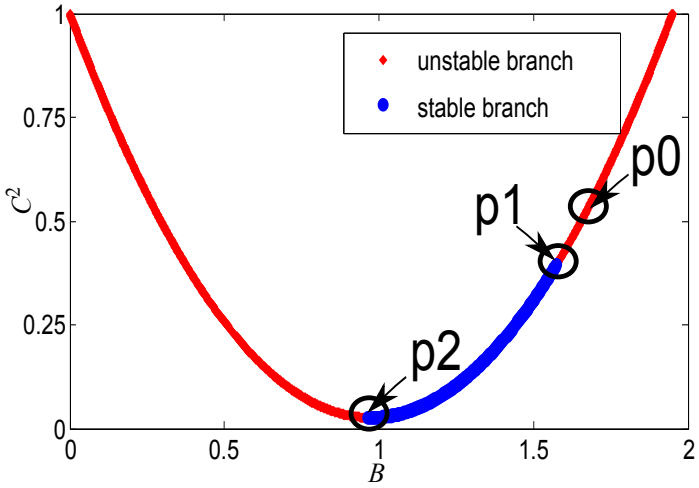

Fig. 2.1 SIM of VI NES: two unstable branchs in red, one stable branch in blue and three critical points p0, p1 and p2.

2.2 Response regimes

In this part, a criterion to categorize different response regimes is firstly introduced. Secondly, typical response regimes by numerical study are showed. Then, an analytical explanation for the variation of response regimes is carried out. Finally, the influence of frequency on the variation route of response regimes is studied.

2.2.1 Regime classification criterion

Normally, the frequency ratio is applied to categorize response regimes, e.g., the same frequency for 1:1 resonance. By this way, the transform from time domain to frequency domain, e.g., Fourier transform and wavelet transform, is needed to judge the frequency components and their relationship. And it is the case widely used in the study of cubic NES. However, the classification for VI NES will be simpler since the impact number per cycle of the main system is a clear and direct index. In [Peterka, 2003], the regime is labeled by the quantity $z = p/n$, where p is the number of impacts and n is the number

TABLE 2.1 Parameters of the experiment

Physical Parameters			
m_1	$4.168\,kg$	c_1	$3.02\,Ns/m$
k_1	$11.47 * 10^3\,N/m$	m_2	$32\,g$
Reduced Parameters			
ϵ	0.76%	λ	1.80

of excitation periods T during the considered impact motion period. It is proved to be rather convenient and will be applied in this thesis.

2.2.2 Variation of response regimes

The experimental identified parameters in Table 5.1 will be used for simulation with Eqs. (1.2) and (1.3). The value related to relative and barycentric motion can be obtained by Eq. (1.4).

With the variation of the clearance, five different response regimes exist under outside excitation frequency of $8.5\,Hz$ and they are categorized by the value of z as showed in Fig. 2.2. The first, second and third column represents the displacement of LO, relative displacement and projection of motion (i.e., yellow curve) into SIM respectively. z can be observed from the second column combined with the first column, i.e., the total occurrence times of the extreme relative displacement value (i.e., b or $-b$) during one period of LO. Fig. 2.2(a) is chosen as the representation for all cases with $z > 2$, in which $z = 3$ and $z = 4$ co-exist. In this case, the time difference between impacts is not equally distributed as showed in the middle subfigure and the stable projected motion is located at the right unstable branch of SIM and it is far from the stable blue branch as showed in the right subfigure. Moreover, the number of impacts increases with the decrease of clearance, but the impulse strength decreases. Fig. 2.2(b) represents two asymmetric impacts per cycle with $z = 2$. The time difference between two impacts are not the same, the projected motion is closer to the stable blue thick branch. Fig. 2.2(c) represents two symmetric impacts per cycle with $z = 2$. It is seen in the right subfigure that the steady projected motion can be represented by a point in the stable branch of SIM except the transient process at the beginning. A SMR is presented in Fig. 2.2(d), the alternative appearance of $z = 2$ and $z < 2$ can be seen in the middle and right subfigures. For the part $z = 2$, the case with two impacts per cycle occurs and its variance is governed by the blue stable branch. For the part $z < 2$, the case with sparse impacts occurs, its variation law is not known. This irregularity is also demonstrated by the variation of displacement amplitude of LO in the left subfigure, which reveals the chaotic characteristic of SMR [Gendelman and Alloni, 2015 ; Gendelman and Alloni,

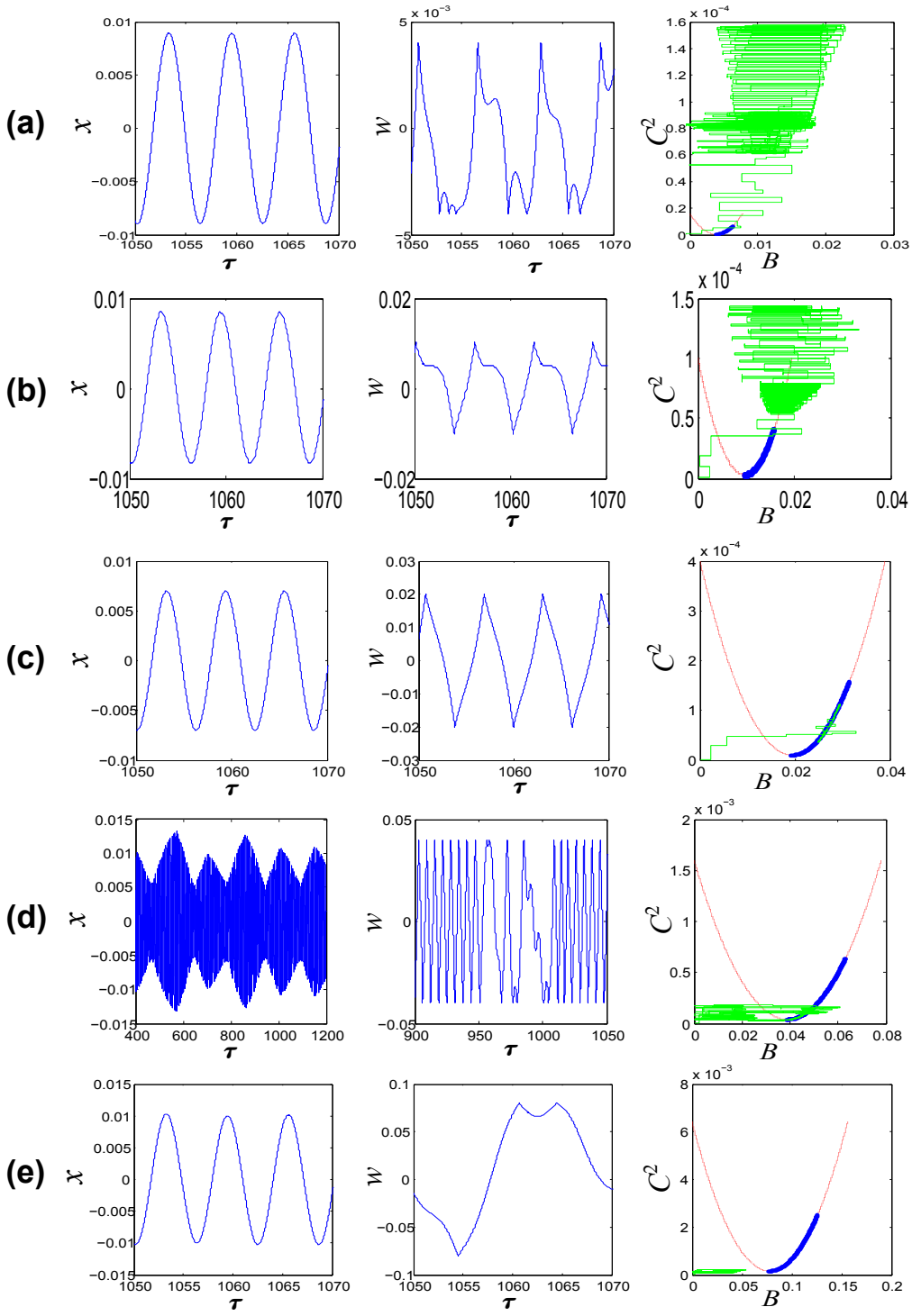

Fig. 2.2 Displacement of LO in the first column, relative displacement in the second column and motion of system projected into SIM in the third column for different response regimes: (a) $z > 2$; (b) $z = 2$ and asymmetric; (c) $z = 2$ and symmetric; (d) $z = 2$ and $z < 2$ for SMR; (e) $z < 2$.

2016]. Fig. 2.2(e) demonstrates loose impact case with $z < 2$, in which transient 1:1 resonance with continuous two impacts per cycle does not exist. In this area, the response is irregular. From the variation of impact number and displacement amplitude of LO in Fig. 2.2, it is seen that the average value of z with long time duration decreases and the average value of displacement amplitude of LO (x) decreases at the first place and then increases.

2.2.3 Areas of SIM

From the third column of Fig. 2.2, it is seen that the relative position of motion projected into SIM varies with the clearance. According to the value of C^2, 4 areas can exist. This law of variation by numerical study can also be analytically obtained and the result is showed in Fig. 2.3(a).

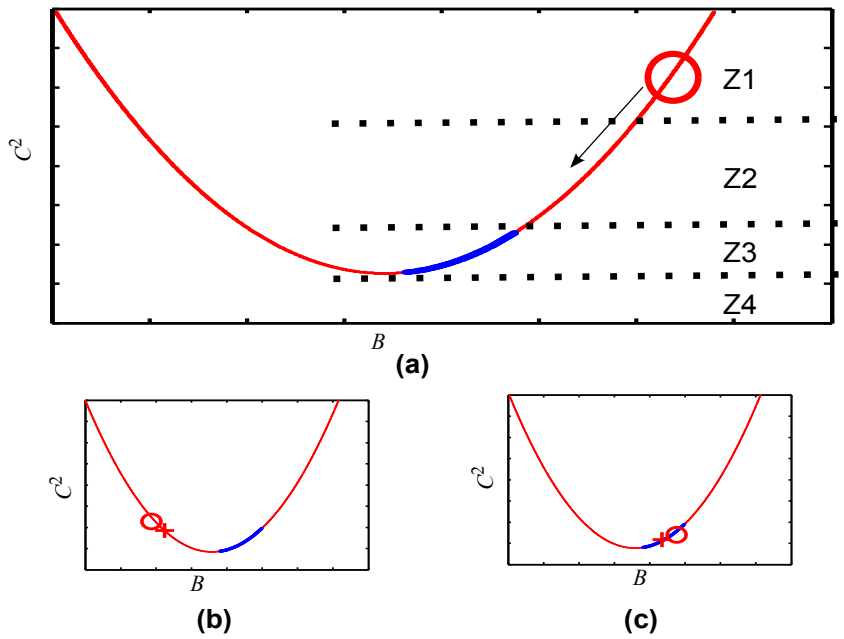

Fig. 2.3 Areas of SIM: (a) 4 typical areas; (b) a first case in Z3; (c) a second case in Z3.

With the increase of the clearance, one of the fixed point represented by red circle will move along the SIM from area Z1 with $z > 2$ to $z = 2$ through a series of grazing bifurcation. In area Z2, the regime with two asymmetric impacts per cycle persists until the critical point between stable blue branch and the right unstable red branch, in which the double period bifurcation occurs. Then the regime with two symmetric impacts per cycle occurs. If the above process is continued, there exist two routes. The first case is showed in Fig. 2.3(b), the two unstable points will approach each other and then disappear. The response regime is SMR demonstrated in Fig. 2.2(d) and the duration time of transient 1:1 resonance part will decrease with the increase of clearance, which is nume-

rically observed by an outside excitation frequency 8.5 Hz. Another case is demonstrated in Fig. 2.3(c) with an outside excitation frequency 8 Hz. Two fixed points exist in the stable branch and then disappear by collision with each other. During the evolution of this case, there exist two possible solutions, i.e., two symmetric impacts per cycle and SMR. The irregular regime in area 4 will appear after the collision of fixed points at the end of the above two cases with further increase of the clearance. The above analysis process for the variation of regimes can be applied to other parameters, although the specific variation route will depend on the specific parameters. In return, different bifurcations and routes can be explained with the above analysis approach.

2.2.4 Numerical analysis of SMR

Here, a numerical analysis of SMR is performed with Hilbert Transform (HT) and Wavelet Transform (WT). The time history of response ($v \approx x$) are firstly showed in Figs. 2.4 and 2.5.

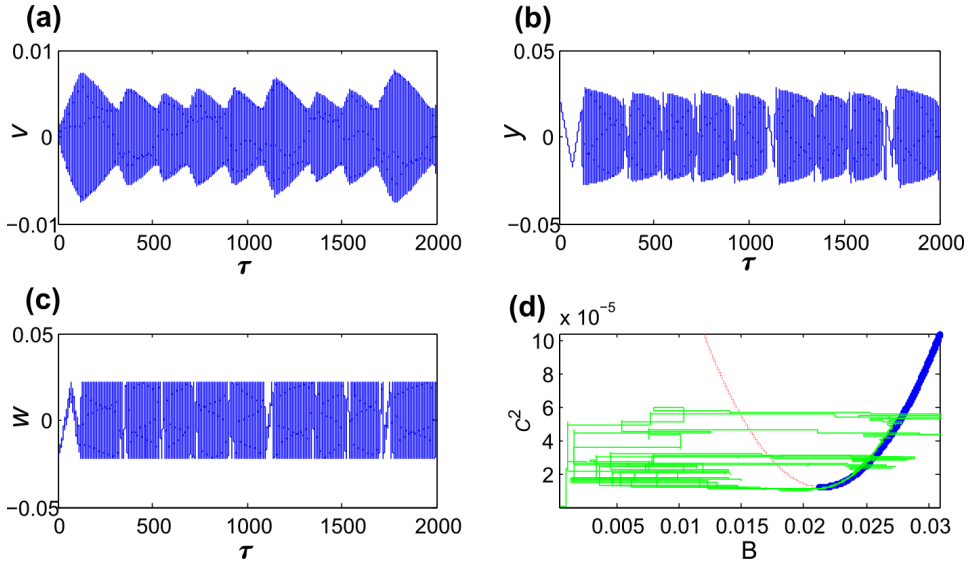

Fig. 2.4 SMR with $b = 0.22, G = 0.02$, $x_0 = 0.02, \dot{x_0} = 0, y_0 = 0.06, \dot{y_0} = 0$: (a) displacement of the center of gravity; (b) displacement of VI NES; (c) relative displacement; (d) projection of motion into SIM.

It is seen that the local maximum value of v is different every time, which is different from that of NES with cubic nonlinearity. In [Gendelman and Alloni, 2015 ; Gendelman and Alloni, 2016], this chaotic characteristic is deeply explained, and it will be further explained in this thesis. The 1:1 transient resonance captures can be observed from the phase and phase difference between v and y in Fig. 2.5(b). The nearly constant phase differences demonstrate the resonance capture as showed in a large view in Fig. 2.5(d). In addition, the slow variation of the phase difference shows the slow variation of response regime with two impacts per cycle, which corresponds to different stable fixed points of

SIM. In Fig. 2.5(e-h), the time history of frequency of v and y is obtained by HT and WT, respectively. In Fig. 2.5(e-f), the transient noisy that results from impacts should be excluded to get the true frequency component. The same frequency component is observed as the case of NES with cubic nonlinearity.

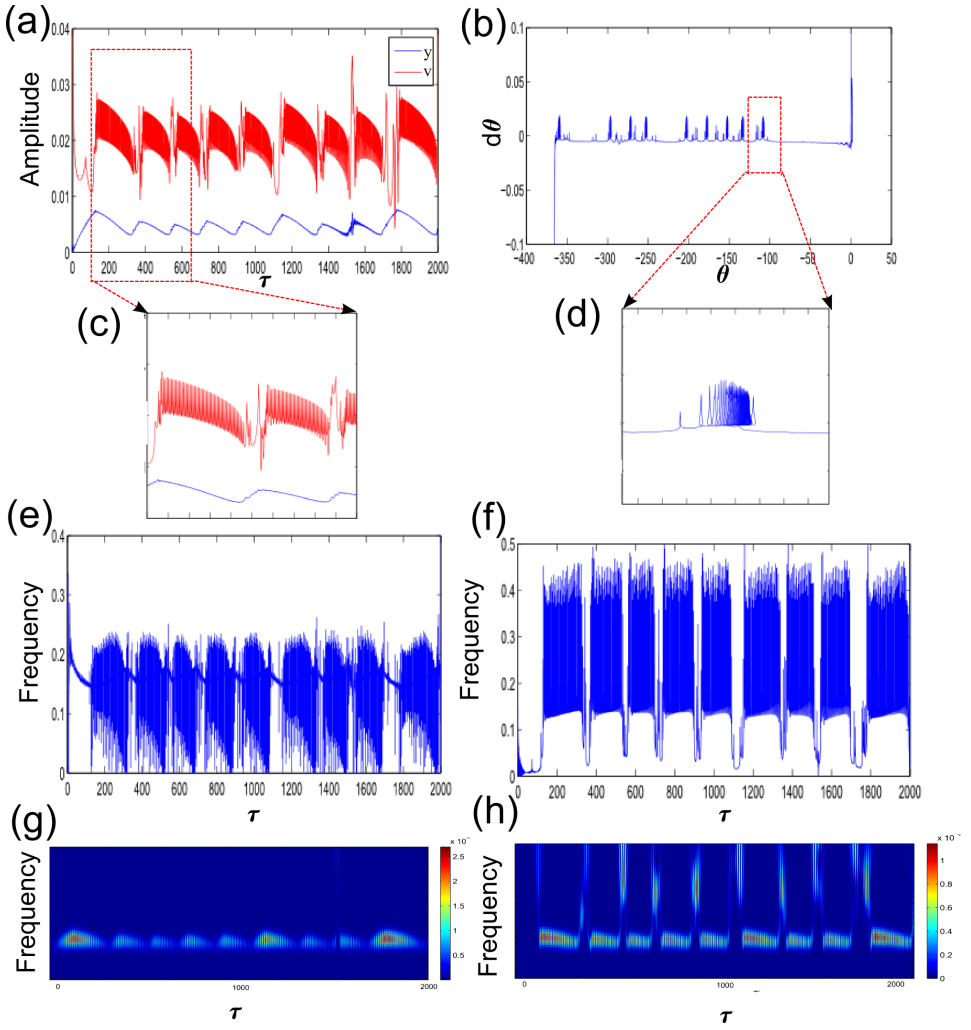

Fig. 2.5 SMR with $b = 0.22, G = 0.02$, $x_0 = 0.02, \dot{x_0} = 0, y_0 = 0.06, \dot{y_0} = 0$: (a) envelope of v and y; (b) phase and phase difference; (c-d) enlarged views of (a-b); (e-f) instantaneous frequency by HT; (g-h) instantaneous frequency by WT.

2.2.5 Transition phenomena and optimization design criteria

From the above analysis, there exist two possible transition routes with two different transition regions, which are respectively defined as hysteresis region and beat motion. The former corresponds to the Fig. 2.3(c) in which the response regime is ambiguous (1:1 resonance or SMR). The latter corresponds to the Fig. 2.3(b) characterized by the SMR of main system [Peterka, 1996]. Two boundaries can be analytically obtained by

two bifurcation conditions, i.e., the bifurcation showed in Fig. 2.6(a) and the bifurcation demonstrated in Fig. 2.6(b). The first one is defined by the contact point between the left unstable red branch and the stable blue branch and the other condition is obtained by the collision of the two fixed points. For a frequency bandwidth, the above two transition regions are obtained and showed in Fig. 2.6(c). A1 represents the hysteresis region, which is numerically validated by co-existence of SMR and 1:1 resonance, which has been experimentally observed in [Bapat *et al.*, 1983]. A2 represents the beat motion region. The point P1 represents the singular point in which the continuous transition without SMR (i.e., no intermittency) exists. From the variation of displacement amplitude of LO in Fig. 2.2, it is reasonable to assume that the optimal energy dissipation exists at the point where 1:1 resonance disappears, which is represented by the red cross in Fig. 2.6(c). Different response regimes in different areas (i.e., Z1, Z2, Z3 and Z4) are also validated by numerical results and they are represented by the squares, circle and star. The optimal mechanism will be studied deeper in the next chapter.

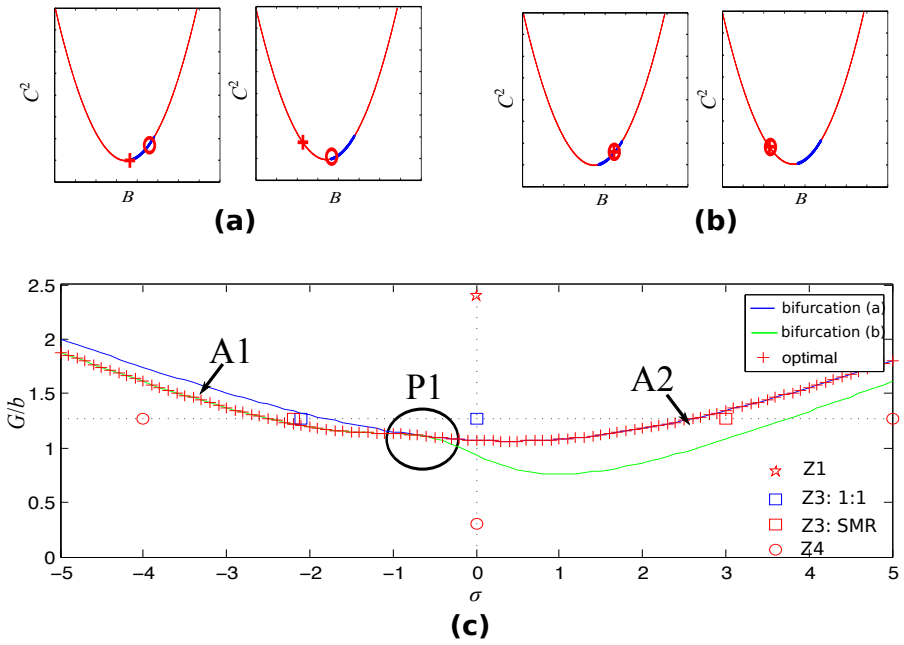

Fig. 2.6 Transition phenomena: (a) saddle-node bifurcation boundary; (b) Hopf bifurcation boundary; (c) transition regions.

2.3 Influence of parameters

In this part, the influence of different parameters is analyzed in detail. The bifurcation with frequency as the control parameter is analyzed and it is important for the optimization design of system under periodic excitation with a range of frequency, which will be discussed in the next chapter. The influence of mass ratio and damping on the

transition process is also discussed. In the last part, the influence of restitution coefficient is also studied.

2.3.1 Influence of frequency

With the variation of relative value between the amplitude of outside force and clearance (i.e., G/b), the relative position of Frequency Response Function (FRF) of the main system will vary and it will result in the location change of the projected motion in the SIM. This phenomenon has been experimentally observed in [Gourc *et al.*, 2015a]. For a fixed G, this relative location will change from area Z1 to Z4 (i.e., from black thick dotted curve to blue thin curve) with the increase of b as showed in Fig. 2.7. For any relative location, just some interval of frequency can situate in area Z3 (e.g., red fine dotted curve and green thick curve), in which the most efficient energy reduction by TET is possible, no matter in the form of resonance capture by the 1:1 resonance regime or just one part of the process in resonance capture by SMR. This is the reason why one optimal designed parameter will not still be optimal for another frequency. The fact is that the 1:1 resonance regime for all range of frequency is not possible.

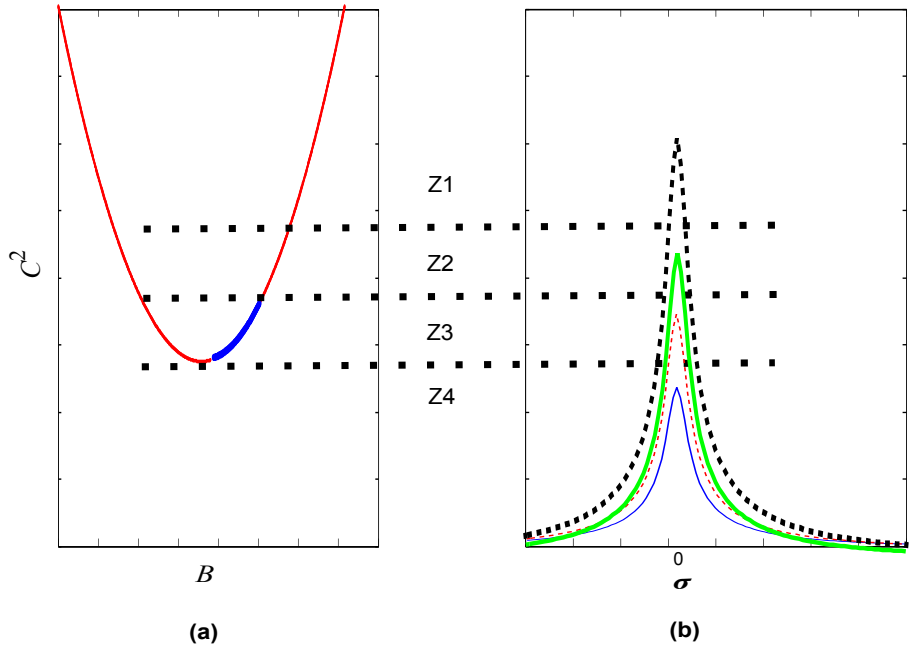

Fig. 2.7 Influence of frequency on the dynamics around SIM: (a) SIM; (b) relative position of FRF.

Another phenomenon is about possible types of bifurcations and routes during sweep experiments (e.g., observed in [Yoshitake *et al.*, 2007]). All possible cases can be explained clearly. For the case of fine blue line in Fig. 2.7(b), there will not exist any route to irregular response. However, there will be two possible routes for the case represented by

the thick black dotted line, i.e., the first route can go up along the line as follows: two symmetric impacts, then two asymmetric impacts, then increase the number of impacts until total irregular response. The second route can go down along the line in the following way: two symmetric impacts, then SMR, then decrease of the duration time for the 1:1 resonance part of SMR until total irregular response. The typical cases with fine red dotted line and thick green line can be a little different but can be explained in the same way. For the past researches about the parameter optimization for a frequency range around resonant frequency, different cases have been observed and explained. However, the study is incomplete and the goal is not clear. From Fig. 2.7, the optimization criterion is clear and it is just to make the objective bandwidth of frequency locate in the area Z3 as wide as possible. Normally, the objective bandwidth of frequency is around the natural frequency of LO, therefore the case with fine red fine dotted line would be better.

2.3.2 Influence of mass ratio and damping

The SMR projected in SIM is showed in Fig. 2.8(a). More information about the variation mechanism of the displacement of LO and relative displacement can be seen in Fig. 2.2(d). In the stable branch in thick blue curve, the good prediction with a high correlation between the theoretical blue curve and the numerical green curve is seen and enlarged in Fig. 2.8(c), which cannot be obtained by the traditional analytical approach comprehensively summarized in [Ibrahim, 2009]. For the analytical method firstly developed in [Gendelman, 2012], its objective is to analyze the transient resonance capture (two impacts per cycle) during free vibration and it is also applied to periodically forced vibration. Its application requires small magnitude of mass ratio and damping. For the transition part between non 1:1 resonance and 1:1 resonance as showed in Fig. 2.8(b) and Fig. 2.8(c), the vertical value difference of every vertical yellow line is decided by the energy dissipation during impacts related to the mass ratio and the restitution coefficient (the influence of the restitution coefficient will be explained later) and that of every horizontal yellow line is decided by the energy dissipation related to the damping of LO. Large energy reduction resulted from large mass ratio and damping will result in the failure of this approach, i.e., the prediction of SIM to projected motions, although it may increase the efficiency of energy reduction.

From Fig. 2.2(d), it is seen that the response is strongly modulated and the local maxima changes every time, which is defined as chaotic SMR in [Gendelman and Alloni, 2015 ; Gendelman and Alloni, 2016]. To explain its variation trend, the non 1:1 resonance motion of VI NES should be considered and its average action force on the LO should be developed in Fourier series. Its small amplitude in Eq. (2.1) reveals the cause for the increase of the amplitude of main system. This way of treatment is also fairly convenient to understand experimental results which will be explained in the experimental part.

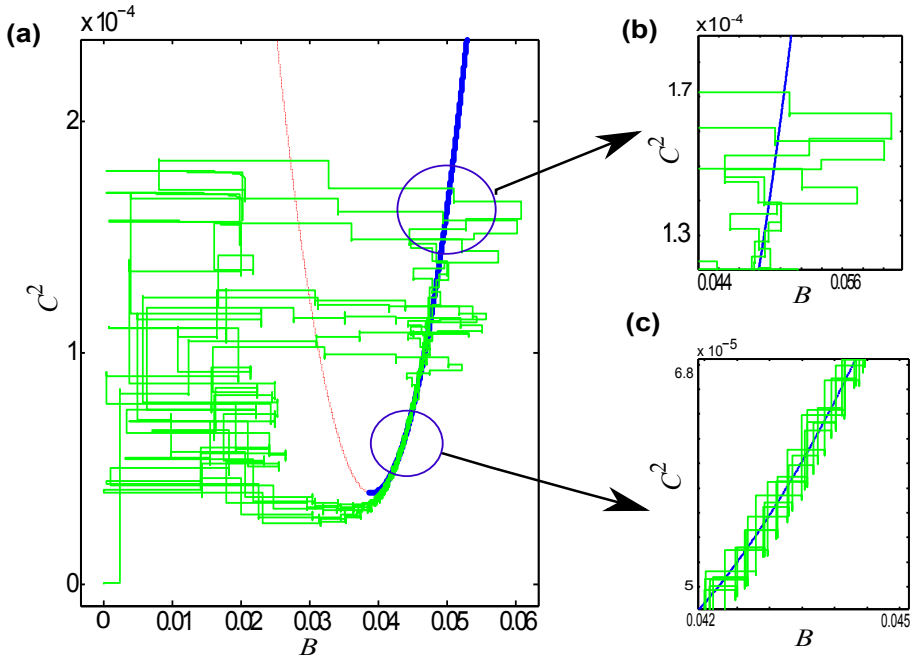

Fig. 2.8 SMR projected into SIM: (a) projected motion in green lines; (b) an enlarged view of transition part; (c) an enlarged view of 1:1 resonance part.

2.3.3 Influence of restitution coefficient

From Eq. (1.17) and Fig. 1.12, there exists a minimal value of C^2 for the occurrence of 1:1 resonance. When the restitution of coefficient is varied with the amplitude of LO (black dotted line) and other parameters fixed, the relative position of SIM will vary as showed in Fig. 2.9(a).

When $r = 1$ showed in red fine curve, it will locate in area Z1, in which the impact number is large but with low impact impulse strength. As a result, the energy dissipation is not high. With the decrease of r, the transition will follow along the black arrow in Fig. 2.9(b). When $r = 0.2$ showed in black thick dotted curve, the impact number will be low and impact pulse may be large. Globally, it will result in low efficiency. Therefore, an intermediate value will be optimal and lead to a maximal value of E in Eq. (2.1).

2.4 Experimental results

The objective here is to observe different response regimes with the variation of length of cavity. Their efficiency is not compared here and will be the objective of next chapter.

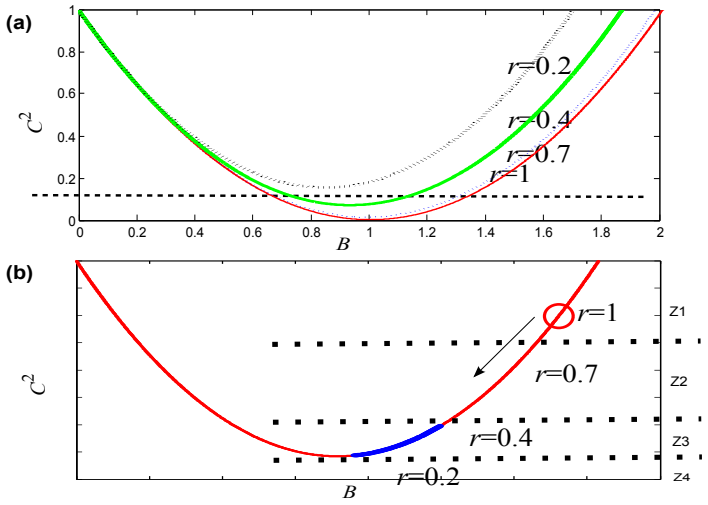

Fig. 2.9 Influence of the restitution coefficient: (a) SIMs with different r; (b) relative position for different r.

2.4.1 Experimental configuration

The experimental setup is presented in Fig. 2.10(a). It consists of a LO, with an embedded VI NES. The whole system is embedded on $10kN$ electrodynamic shaker. The displacement of the LO as well as the imposed displacement of the shaker are measured using contact-less laser displacement sensors. The acceleration of the LO is measured by a accelerometer. A detailed view of the VI NES is presented in Fig. 2.10 (b).

It simply consists of a closed cavity of length $d + 2b$, where d is the diameter of the ball and b can be adjusted by a cylinder in the cavity. The cylinder and the other side cover are made of hardened steel. The parameters of the system have been identified by performing modal analysis and are summarized in Table 5.1. The excitation frequency is fixed to 8 Hz.

2.4.2 Bifurcation route

The bifurcation route can be judged in different ways such as that showed by the variance of response in the columns of Fig. 2.2, but they require the displacement and velocity of VI NES to be known as a prerequisite, which is not allowed in our laboratory. Another way is to use a return map of time difference between every two consecutive impacts [Korsch *et al.*, 2007]. For a limited time of data acquisition with the excitation period given, the time of impact t_i can be measured as showed by red stars in right subfigures of Fig. 2.11(a-f). The acceleration of LO (blue curve) will change abruptly and then the time differences δt_i between these moments can be calculated. Two neighboring times δt_i and $\delta t_{(i+1)}$ can form one point $(\delta t_i, \delta t_{(i+1)})$, and every two points can constitute a vector with the first point $(\delta t_i, \delta t_{(i+1)})$ and the second point $(\delta t_{(i+1)}, \delta t_{(i+2)})$.

With the variation of clearance b, different response regimes have been observed.

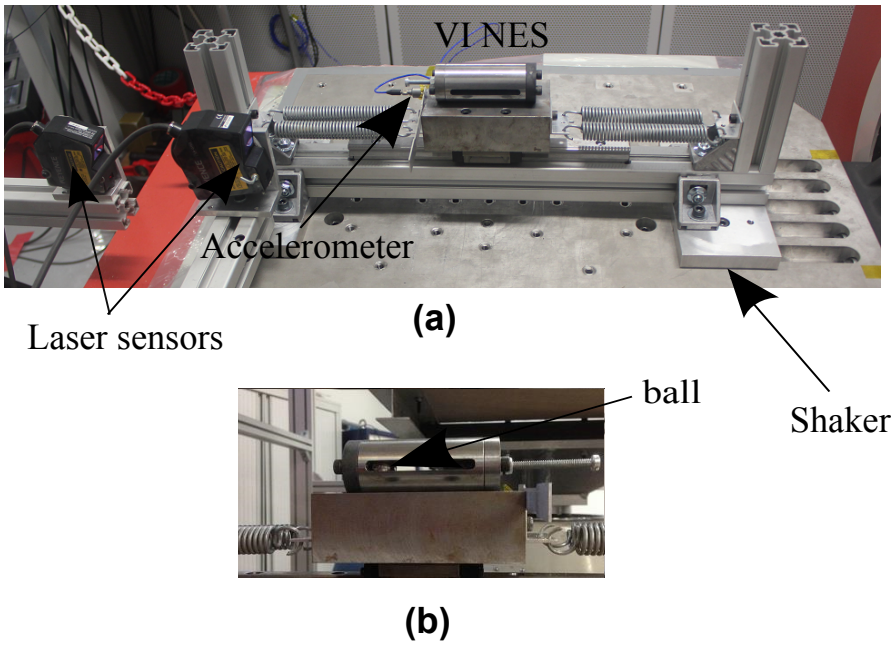

Fig. 2.10 Experimental setup: (a) the global configuration; (b) a detailed view of VI NES.

All left subfigures in Fig. 2.11(a-f) represent the time difference return map, the yellow dotted triangle can be expressed by L1: $\delta t_x + \delta t_y = T(1/8\,s)$, L2: $\delta t_x = T(1/8\,s)$ and L3: $\delta t_y = T(1/8\,s)$. The black dotted line can be expressed by L4: $\delta t_x = \delta t_y$. All right subfigures in Fig. 2.11(a-f) represent a typical sample of the acceleration of LO, in which the red stars denote the time of impact and the value of acceleration. Fig. 2.11(g) demonstrates the relative position of every regime in SIM. For $b = 0.3\,mm$, the results are showed in Fig. 2.11(a), there exist more than 3 impacts during one period, and the distribution of impact time is also irregular, which maybe chaos and need further verification. For $b = 2.5\,mm$ showed in Fig. 2.11(b), there exist three impacts every period and the impact time distribution is not equal but stable which is illustrated by the fact that all vector form a triangle, meanwhile all points are inside L1. For $b = 4\,mm$ in Fig. 2.11(c), the vector is located at the L1, which means it just exist two impacts every period. However, the absolute value of acceleration is not equal. For $b = 7.5\,mm$ in Fig. 2.11(d), there also exist two impacts per cycle, but this time the absolute value of acceleration is almost equal. For $b = 11.5\,mm$ in Fig. 2.11(e), the case of two impact per cycle and no impact appears alternatively and the duration time of 1:1 resonance is short and irregular. For $b = 20\,mm$ in Fig. 2.11(f), all points is in the right and up side of L1, it means that two impacts per cycle does not exist during the whole process, i.e., transient resonance captures does not exist.

In summary, the relative position in the SIM moves with the increase of clearance as observed by the study in the last section. The value of acceleration (i.e., impulse

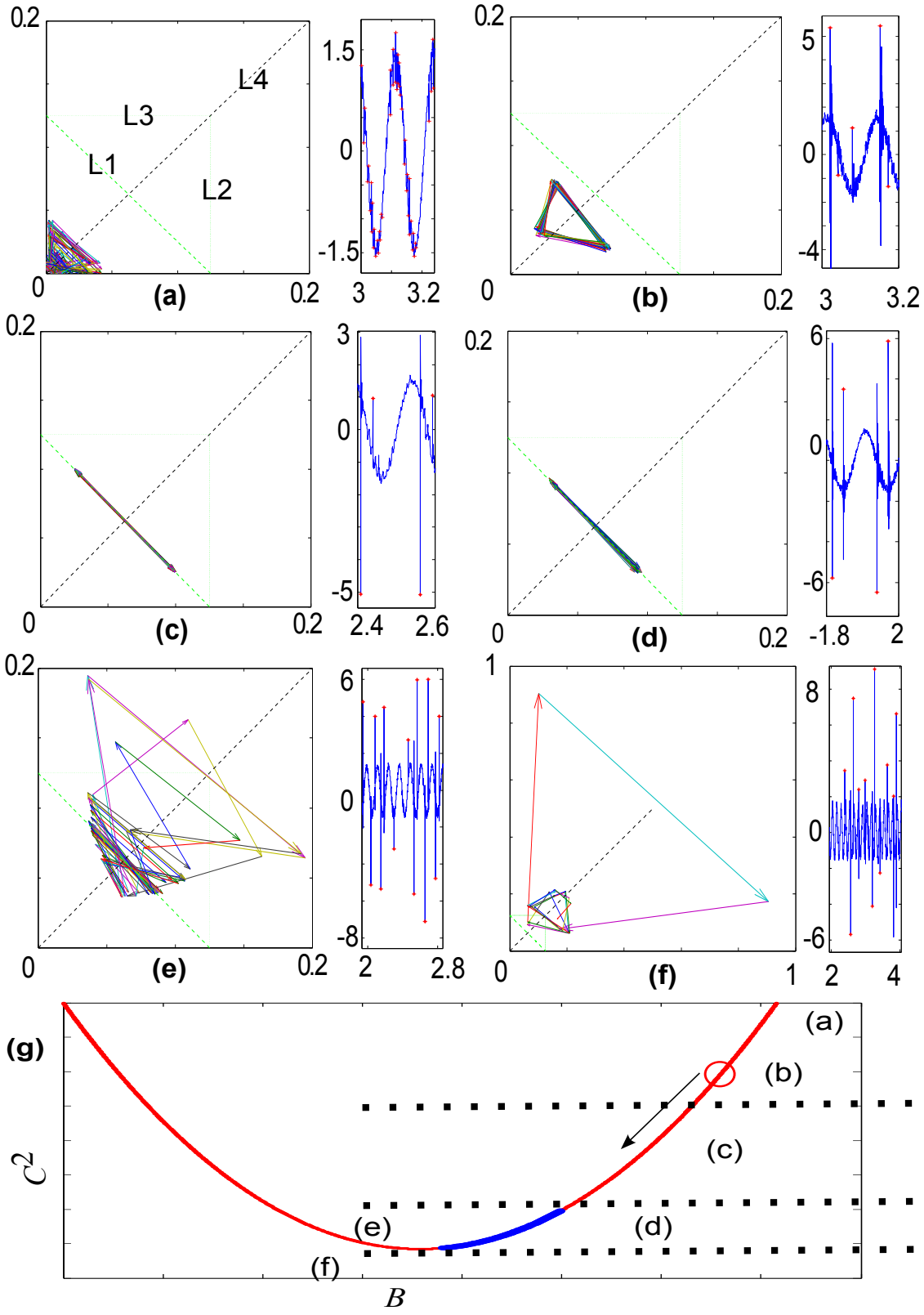

Fig. 2.11 Route of the variation of regimes: (a) b=0.3 mm with $z > 3$; (b) b=2.5 mm with $z = 3$; (c) b=4 mm, asymmetric resonance with $z = 2$; (d) b=7.5 mm, symmetric resonance with $z = 2$; (e) b=11.5 mm, SMR and partially with $z = 2$; (f) b=20 mm with $z < 2$; (g) location of different regimes in SIM.

strength) is small although with many impacts during one period for small clearances. Then it augments with the two impacts per cycle, and the efficiency of TET is the largest. A further increase of clearance, instantaneous large value (i.e., strong impulse strength) can exist, but it cannot persist during the whole process. From the former analytical analysis, the number and strength of impact impulse will decide the value of E in Eq. (2.1) directly and it will decide the efficiency of TET, which is validated by the experimental results here.

2.4.3 TET during SMR

A SMR with $b = 15\,mm$ is demonstrated in Fig. 2.12, which is characterized by the intermittency of 1:1 resonance (i.e., two impacts per cycle) and the chaotic strongly modulated amplitude of LO. In Fig. 2.12(a), the acceleration of LO during $5\,s$ is demonstrated by the blue curve and points of the impact moment represented by red stars illustrate the time and acceleration value of impact moments. The intermittency is demonstrated by the irregular occurrence and duration time of 1:1 resonance as showed by the distribution of impact points in Fig. 2.12(a) and also by transient escape in the return map of time difference showed in Fig. 2.12(b). In Fig. 2.12(c), the black curve and red curve represent the displacement (mm) of shaker and LO respectively, which is superimposed with the acceleration of LO. Here, the influence of the amplitude and frequency of impact to the energy reduction is showed by the variation of the amplitude of LO. The transient resonance captures are seen by two impacts per cycle, in which TET is possible. In the first equation of Eq. (2.2), the amplitude variation of main system at the slow time scale is decided only by the amplitude (i.e., E) which is obtained by Fourier transfer and has the same frequency as that of LO, provided that the damping of LO and outside excitation are fixed. For the decrease period of the amplitude of LO, two impacts per cycle and large value of impact impulse strength are required to guarantee the condition of 1:1 resonance and large impact damping as showed in Fig. 2.12(e). Otherwise, it will increase for not enough dense impacts illustrated in Fig. 2.12(f) or not big enough impact impulse even with two impacts per cycle as showed in Fig. 2.12(d). Therefore, although 1:1 resonance (two impacts per cycle) is necessary for TET, their efficiency is different for different 1:1 resonance regimes as is showed by the difference of acceleration value for the same 1:1 resonance regime from the above experimental results and is also analytically represented by different points at the stable blue branch in Fig. 1.12. Or it is reasonable to suppose that the most efficient case is the one with not only 1:1 resonance but also the largest impact impulse strength in impact moments as may be presented by the optimal curve proposed in Fig. 2.6, which will be studied further in the following chapter.

If we look closely, there exist small peaks of the acceleration during the period defined as no impacts period as has been used in the analysis. One example is showed for the time around $t = 2.7\,s$ in Fig. 2.12(f). This phenomenon is probably caused by the small inclination of the LO which results in the location of the ball in one side rather than in

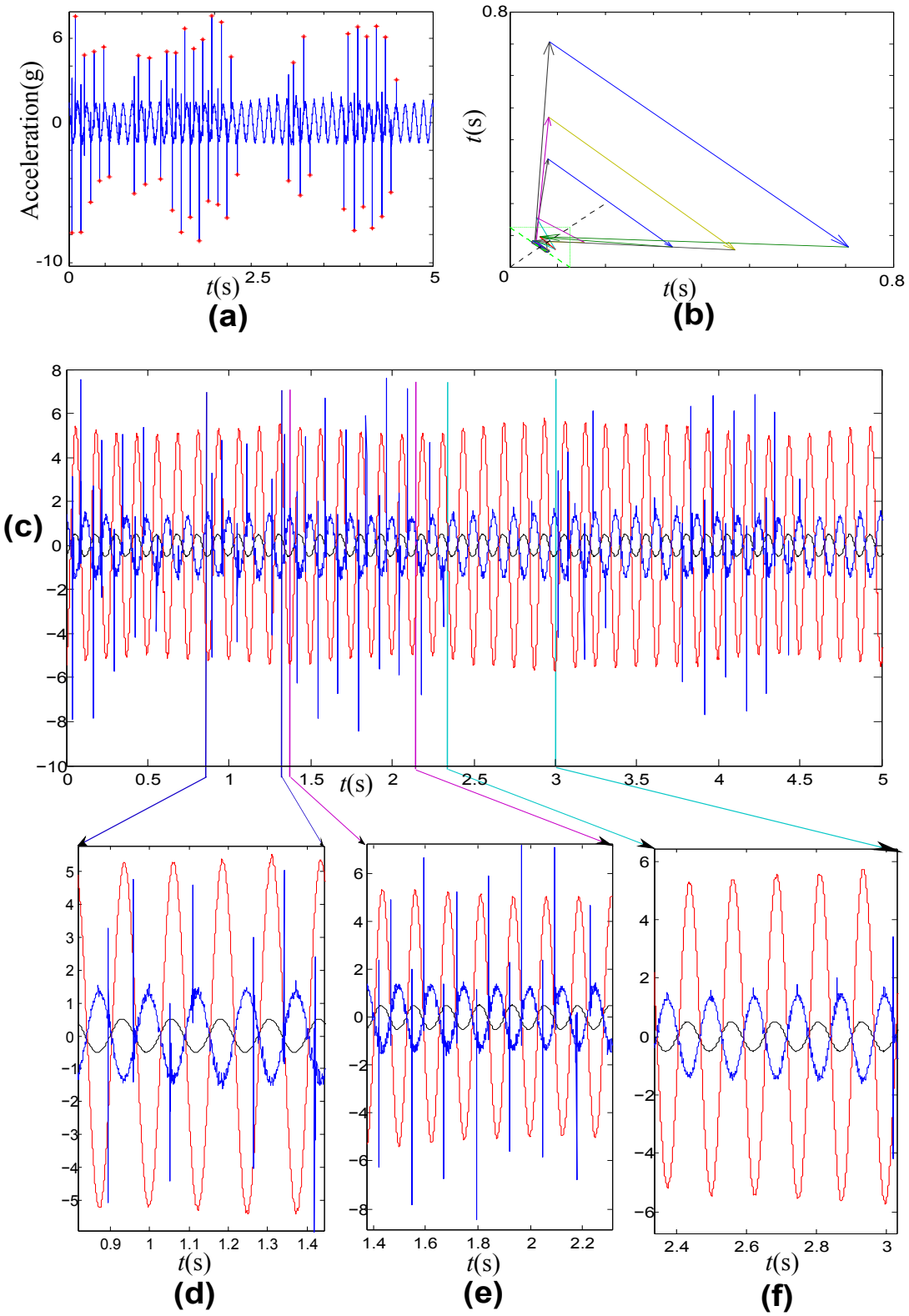

Fig. 2.12 TET during SMR: (a) the acceleration of LO; (b) the return map of time difference; (c) the superposition of the acceleration (blue curve) and the displacement (red curve) of LO and the displacement of shaker (black curve); (d-f) enlarged views of (c).

the middle [Bapat, 1995]. Another problem is that the time difference is not equal for two consecutive impacts per cycle as has not been predicted by analytical results, which is possibly caused by the damping between LO and VI NES, the inclination of LO and the difference of the restitution coefficient at each side [Bapat *et al.*, 1983]. Although the above two phenomena have not been considered in the analytical study, they do not influence the above obtained analysis for the dynamics and the TET during the SMR.

2.5 Conclusion

In this chapter, all response regimes are analyzed around the SIM. The influence of parameters and initial conditions on the dynamics is demonstrated with analytical and numerical results at the first place. Then, experimental results prove the existence of different regimes and different bifurcation routes, and TET during SMR is also demonstrated.

The general equation (i.e., Eq. (2.2)) is not only used to solve fixed points but also to explain the variation of complicated regimes from free and forced excitations. In addition, it can explain the complicated amplitude variation of experimental results. From the viewpoint of interacting force, the analysis method can be generalized since impact systems are similar, such as impact oscillator and impact damper.

The way to analyze all regimes around SIM provides another viewpoint for several reasons. Firstly, SIM is strongly related to the TET and the response regimes are interesting in terms of vibration control. Then, the design of all parameters can be analyzed in the same criterion and it can be described as: to make the suitable response regimes exist.

Another interesting result is the experimental results about SMR. Except the strongly irregular characteristic (maybe chaotic), it also demonstrates different efficiency of TET for different transient regimes. It can be imagined that they are parts of a constantly varying transient vibration. Therefore, the results here can act as a reference for free vibration.

Since typical response regimes have been clearly identified, the next objective is to compare their efficiency in terms of vibration control. It will be presented in the next chapter.

CHAPTER 3

Efficiency comparison of response regimes

Abstract

The objective of this chapter is to provide a common optimization design criterion of VI NES for different excitation types. To accomplish this goal, the efficiency of typical response regimes is compared. Firstly, the efficiency comparison of response regimes is numerically performed under periodic and transient excitations, and influences of parameters are studied. Then, the optimization design relationship between different excitations is analyzed. Finally, they are verified by experimental results.

Contents

3.1 Numerical study

The objective of this chapter is to compare the efficiency of different response regimes through the variation of parameters. From the viewpoint of engineering application, the length of cavity (clearance) is more controllable than other parameters. Therefore, it will be chosen as the design parameter. About possible response regimes, they have been studied in the former chapter and are quantized by z as demonstrated in Fig. 2.2 in Sec. 2.2.2. The system under periodic and transient excitations will be studied consecutively to observe efficiency of TET and its corresponding response regimes. During the analysis, the important role of SIM will be demonstrated.

For all simulations, Eqs. (1.2) and (1.3) are used and the following parameters are fixed except that it is specially pointed out: $\lambda_1 = 1.43, \epsilon = 0.84, r = 0.6$.

3.1.1 Periodic excitation with a fixed frequency

The parameters and initial conditions are fixed as follows: $G = 0.02, \sigma = 0, x_0 = 0, \dot{x_0} = 0, y_0 = 0, \dot{y_0} = 0$. To compare efficiency, two indices are used: the average displacement amplitude ratio in terms of energy (Ae) and maximal displacement amplitude ratio (Am). The displacement without VI NES is chosen as the reference. The difference between the above two indices can be distinguished from modulated displacement of SMR and its amplitude is no longer stable.

With the increase of the length of cavity b, different response regimes have been observed and classed according to their efficiency as showed in Fig. 3.1.

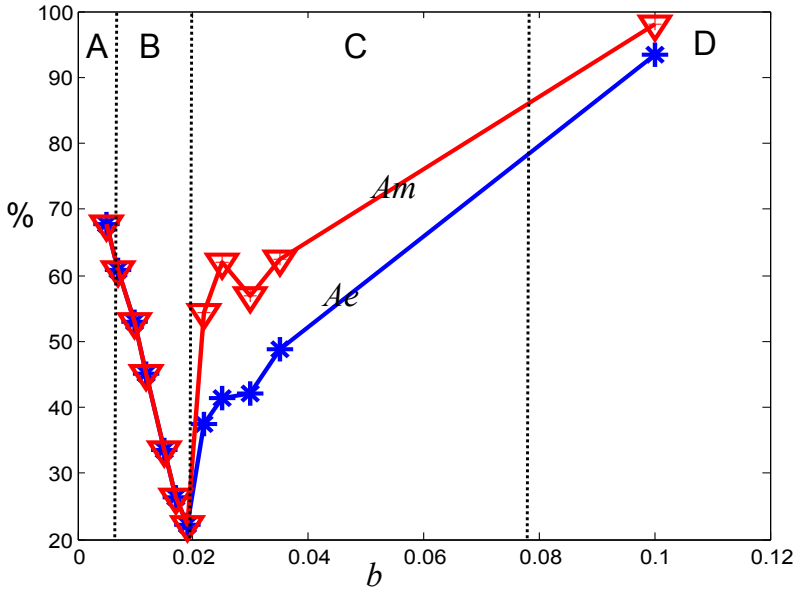

Fig. 3.1 Efficiency of TET for different response regimes under periodic excitation: blue asterisk represents the average amplitude of LO and red upside-down triangle represents the maximal amplitude of LO.

Area A with more than two impacts per cycle, area B with two impacts per cycle (asymmetric or symmetric), area C as SMR with partial duration of two impacts per cycle, area D as irregular response without any duration of two impacts per cycle. It is found that only the response regime with two impacts per cycle is steady with the same Am as Ae. It is observed that the optimal value lies at the boundary between two impacts per cycle and SMR. The following conclusion can be made: the response regime with two impacts per cycle is more efficient than the case with more than two impacts per cycle. However, the result of efficiency comparison of SMR and the two impacts per cycle depends on the specific conditions. For the same case with two impacts per cycle, the symmetric case is more efficient than the asymmetric case.

To better understand the above numerical results, the analytical results will be demonstrated here. Specifically, the fixed points obtained from Eq. (1.17) and Eq. (2.2) (the stable state of this equation), and its variation in the SIM will be used to judge the response regime and to precisely calculate the value of design parameters.

From analytical calculation, two fixed points (circle stable point and cross unstable point) can be obtained as showed in Fig. 3.2. According to their positions, three different areas are observed : with more than two impacts per cycle for fixed point in area A, with two impacts per cycle (full duration or partial duration) in area B and no duration of two impacts per cycle for area D.

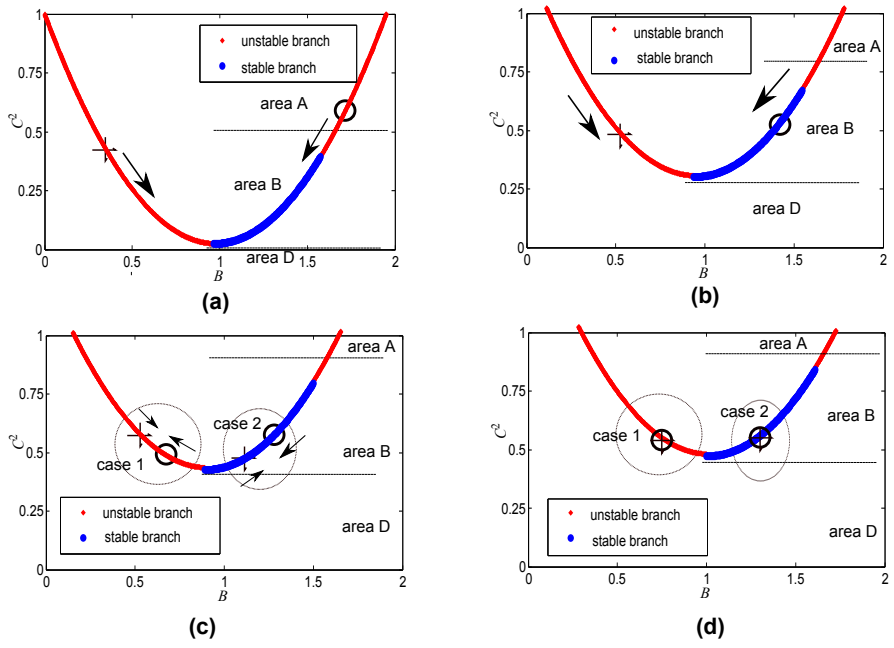

Fig. 3.2 Variation of fixed points with the increase of b: (a) response regime with $z > 2$; (b) two impacts per cycle with $z = 2$; (c) SMR with $z < 2$; (d) the limit point to exit SMR.

For small value of b, the response regime with more than two impacts per cycle occurs

and the location of fixed points is showed in Fig. 3.2(a). Actually, these two points only theoretically exists and cannot exactly describe the actual case, and its amplitude is usually not steady.

With the increase of b, relative locations between fixed points and SIM will change. In the case showed in Fig. 3.2(b), SIM will move up and results in the move of one fixed point from area A to B and another fixed point in the red unstable branch. In this case, the response regime with two asymmetric and symmetric impacts per cycle will consecutively occurs until one fixed point meet the minimal point in the SIM. Meanwhile, the efficiency of energy reduction is increased during this process as showed by the preceding numerical results. One important thing is that three important points can be analytically obtained: the boundary point between area A and area B, the boundary point between two symmetric and asymmetric impacts per cycle and the minimal point at SIM.

When one fixed point passes the minimal value of SIM, two cases can exist and denoted by circle for case 1 and ellipse for case 2 as showed in Fig. 3.2(c) and SMR will occur. For case 1, the stable point passes from the thick stable branch to the thin unstable branch. In this case, the optimization point is localized in the minimal point of SIM. In case 2, the unstable point in the thin unstable branch will move into the thick stable branch and finally meet with the other fixed point. In this case, SMR will be more efficient than the case with two impacts per cycle. Anyway, the above two cases can be analytically calculated. In the last chapter, the influence of frequency of excitation on the existence of these two cases is explained and it is showed that the case 1 applies for the excitation with the natural frequency of LO or even high frequency. A further increase of b, these two fixed points will meet and then disappear, there will be no fixed points as showed in Fig. 3.2(d).

From the above analysis, the variation of E can be conversely inferred from the variation of C with the variation of b. For the optimal case with minimal C, E related to interaction force is the largest. Moreover, its variation mechanism is inverse to that of C. For SMR, the transient interaction force E can be inferred from the corresponding steady value and can be used to explain the variation mechanism of SMR. In this thesis, this value is used to establish the bridge between transient and periodic excitation.

In summary, the efficiency of different response regimes is numerically obtained and analytically explained. The optimal response regime is the limit between that with two impacts per cycle and SMR for the excitation with the natural frequency of LO.

3.1.2 Transient excitation

In order to compare with the periodic excitation, the transient excitation for the same system is studied. The following parameters and initial conditions are used for all simulations: $G = 0, x_0 = 0.02, \dot{x_0} = 0, y_0 = b, \dot{y_0} = 0$, and only b is varied.

With the variation of b, one response type with $b = 0.01$ is chosen to demonstrate all possible stages during the whole process. Different tools are used to explain the

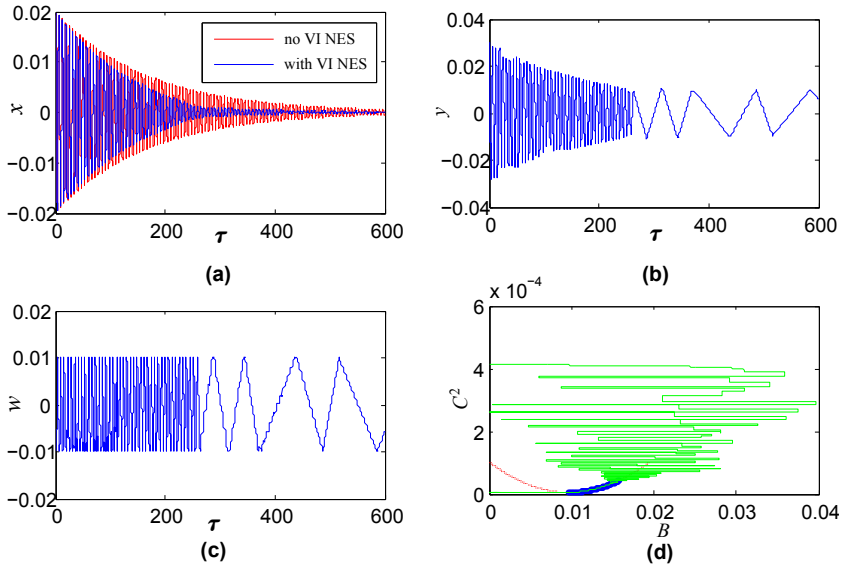

Fig. 3.3 A typical response with $b = 0.01$: (a) the displacement of LO with and without VI NES; (b) the displacement of VI NES; (c) the relative displacement; (d) the project of motion into SIM.

dynamics from different points of view as showed in Figs. 3.3 and 3.4. The displacement of LO with and without VI NES, displacement of VI NES and relative displacement is demonstrated, respectively, from Fig. 3.3(a-c). In Fig. 3.3(a), the efficiency of VI NES is clearly observed by the difference between blue and red curve. In Figs. 3.3(b) and (c), the transient resonance between LO and VI NES is clearly showed. In Fig. 3.3(d), the motion is projected to SIM and the ability of SIM to govern the transient resonance is showed.

Evidently, the response undergoes different stages during the whole process, which is showed by the relative displacement during the whole process as showed in Fig. 3.4(a). At the starting place, the regime with more than two impacts per cycle (i.e., $z > 2$) is excited as showed in Fig. 3.4(b). Then the two asymmetric and symmetric impacts per cycle consecutively appears in the stage 2 as demonstrated in Fig. 3.4(c). In Fig. 3.4(d), the stage with sparse impacts occurs when the energy of system is low. The above three parts are similar to stage A, B and D in the case of periodic excitation just without SMR and the change direction of regimes is fixed. The instantaneous energy distribution is showed in Fig. 3.4(e). From about $\tau = 100$ to $\tau = 200$, there exits strongly energy exchange. The accumulated energy dissipated by LO and VI NES is showed in Fig. 3.4(f). The above mentioned period of strong energy exchange can be observed from different perspectives. The energy decay inclination of LO is almost linear in Fig. 3.3(a), the projection of motion is controlled by SIM at these moments demonstrated in Fig. 3.3(d), the response regime is two impacts per cycle showed by the relative displacement in Fig. 3.4(c). In Fig. 3.4(f), the accumulated energy dissipated by the damping of

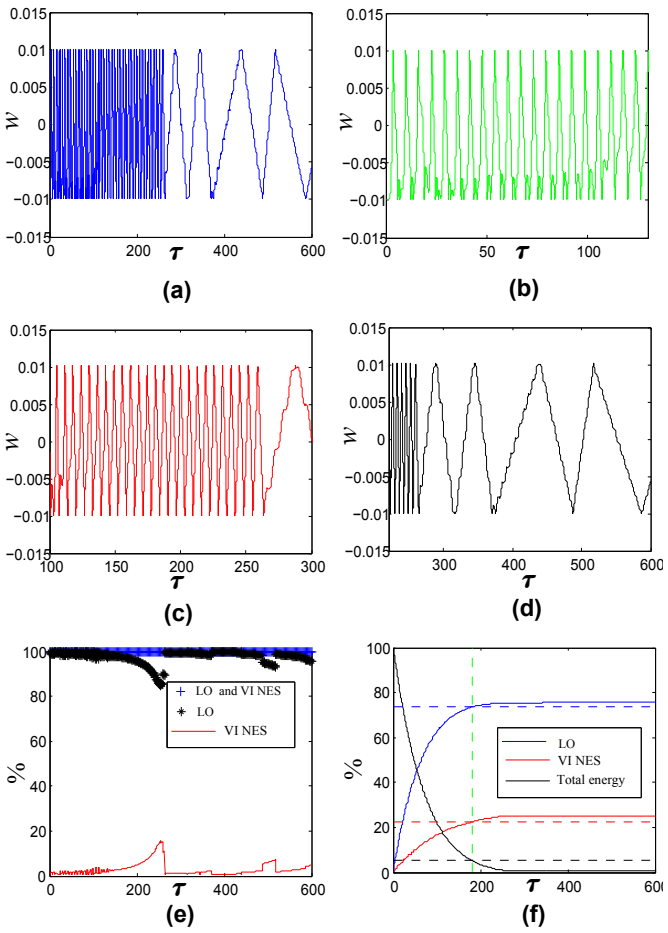

Fig. 3.4 A typical response with $b = 0.01$: (a) the whole duration of the relative displacement; (b) stage 1 with $z > 2$; (c) stage 2 with $z = 2$; (d) stage 3 with $z < 2$; (e) the instantaneous energy distribution between LO and VI NES; (f) the energy dissipated by LO and VI NES.

LO and impacts is compared. The time moment for 95% energy reduction of the initial energy of LO and the accumulated energy dissipated by VI NES during this period is used to characterize the efficiency of VI NES.

Based on the response regime at the starting stage for different values of b, three typical responses are showed in Fig. 3.5. The starting stage can be distinguished from the relative displacement in the first column of Fig. 3.5. The displacement of LO with and without VI NES is compared in the second column. The motion projected into SIM is demonstrated in the third column.

The efficiency comparison of different response regimes with various b is plotted in Fig. 3.6. The time needed for 95% energy reduction of LO and the corresponding accumulated percent of energy dissipated by VI NES are two indices used to characterize the energy reduction efficiency of VI NES. The left and right vertical axes denote the energy percent dissipated by VI NES and the corresponding dimensionless time needed.

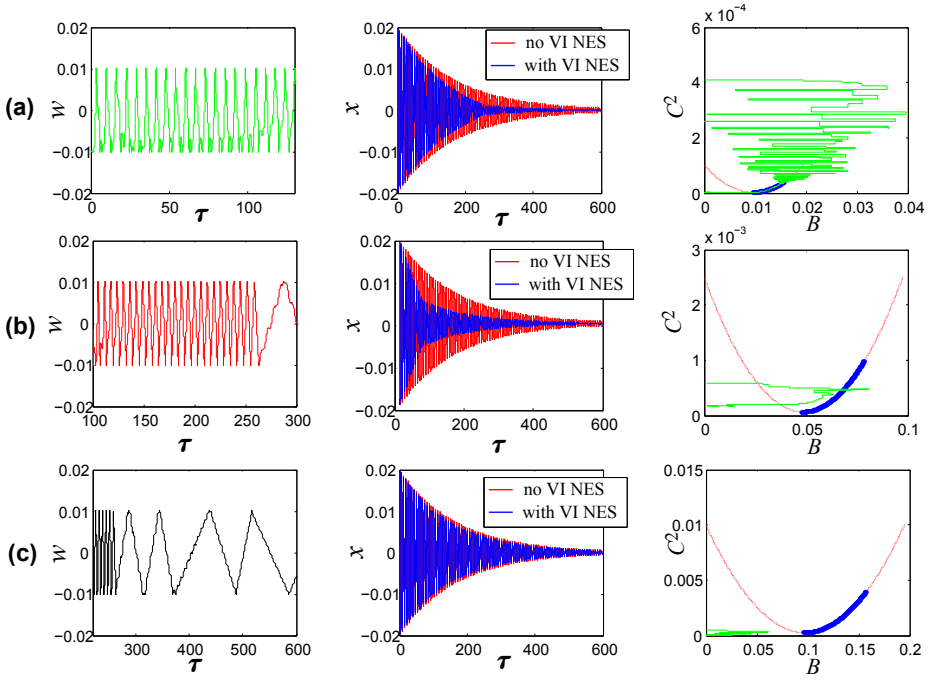

Fig. 3.5 Responses starting from different response regimes by the variation of b: (a) start from stage 1 with $b = 0.01$; (b) start from stage 2 with $b = 0.05$; (c) start from stage 3 with $b = 0.1$.

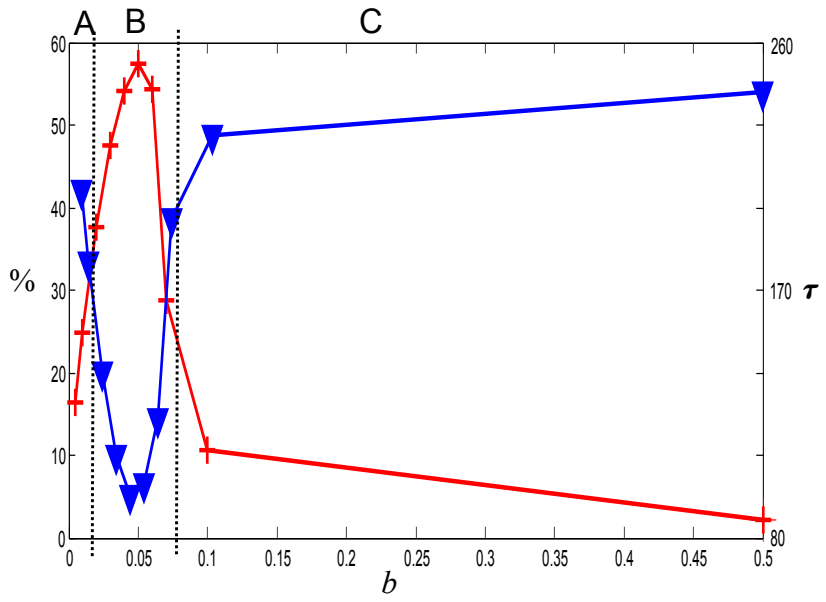

Fig. 3.6 Efficiency comparison of different response regimes with the variation of b: percent of energy dissipated by VI NES represented by red cross and time needed for the 95% energy reduction of LO denoted by blue top-down triangle.

It is observed that the most efficient case is obtained when the response starts from the stage 2, i.e., two impacts per cycle, which is well demonstrated by Fig. 3.5(b) with $b = 0.05$, the decay inclination is linear that can be seen from the variation of displacement denoted by the blue curve in its middle subfigure. It should be pointed out that the value of b is so intentionally chosen that these limited points can almost represent the typical starting point in the SIM. It is specially noticed that the starting point of the above optimal response for transient excitation is different from that of the optimal response regime for periodic excitation. The conclusion is that the optimal starting point should be located a little away from the lowest point in SIM and the specific distance remains unknown and will be discussed later.

3.1.3 Discussion

In Sec. 2.1, the general Eq. (2.1) governing the variation of motion is developed to further explain the transient transition process of response. This kind of process exists for SMR and response under transient excitation. In Sec. 3.1.1 and 3.1.2, efficiency variation mechanism of TET is obtained for periodic excitation with one frequency and transient excitation, respectively. The frequency of periodic excitation is chosen the same as the natural frequency of LO in order that they are comparable. In this section, their relation is established at the first place. Then, the obtained results are used to explain the existing problems in the previous studies and to provide possible optimization design criteria.

Transient and periodic excitation

For periodic excitation, the steady state response regime is identified by two impacts per cycle. The value of E in Eq. (2.1) can be analytically calculated and is related to one stable point in the blue stable branch in SIM. Of course, every point in the stable branch relates to a value of E and can be analytically obtained, though it may not actually exist. From the variation law of efficiency for different lengths of cavity under fixed periodic excitation (i.e., constant G), the value of C becomes smaller as the stable fixed point moves from up to down in the right branch. The sum of right hand side of Eq. (2.1) should be zero for the points in the branch. Therefore the value of E increases until the maximal value corresponding to the minimal point of SIM. A further increase of length of cavity b from the case of two impacts per cycle, the SMR showed in Fig. 2.2(d) appears and the corresponding actual value of E varies around an analytical calculated value during the whole process.

For transient excitation, there does not exist SMR. Response regime continuously transits from one type to another type with the decrease of C. However, the transient response can be approximately described by the steady state type, i.e., the above interaction force can be applied. Its effectiveness can be seen from the precise description of SIM for the resonance parts of the motion projection of SMR and transient response. We can imagine an outside force for any moment during the whole process as if the outside

excitation is abruptly added to hold this transient regime. The equivalent value of E can be obtained by the analytical results in the section 2. However, this value of the imagined force will not be constant. If the original starting place is set to the minimal point of SIM, the value of E will be the largest with a corresponding largest outside force. Yet, its duration will be very short. In contrast, if the starting point in SIM is designed to a very high point in the right red branch, its efficiency will also be very low considering the low efficiency at the start. Therefore, the design criterion is that the efficiency of TET should be not only high at the beginning but also last as long as possible. Theoretically, this optimal point can be obtained, but its analytical calculation should be very complex. Although it is still not analytically obtained here, its mechanism is further explained. For the former study about optimization mechanism of TET, most work is concentrated in the activation of TET. However, only the condition of activation is not enough for optimal objective because it should also possess a long enough duration. In [Nguyen and Pernot, 2012], one practical design criterion for cubic NES is proposed with applicability though may not optimal. But the underlying mechanism is not developed in detail. The design contradiction claimed in [Bapat and Sankar, 1985], i.e., different values for the same parameter under transient and periodic excitation, can also be explained. From the above analysis, the existence of difference of the same design parameter (i.e., b) is evident.

Periodic excitations with one frequency and with a range of frequency

To study the optimization design for excitations with a range of frequency in the vicinity of the natural frequency of a LO, the optimization design mechanism under one excitation with a specific frequency should be studied at the first place. When the frequency response function of LO is obtained during a range of frequency, the amplitude at different frequency points is different. The value at the point of natural frequency is maximal. If an optimal value of b is chosen according to the above analysis for the resonance point, the problem is that the value of b will not be still optimal for the other points and will result in SMR or irregular response without any duration of two impacts per cycle. If this value is optimally designed for other frequencies, the same dilemma occurs. Therefore, there does not exist one value of b optimal for all frequency. Although the value of b can be chosen to make the SMR appear for all frequency, it does not mean that this value is optimal. If the objective is to control the resonance value of LO, the problem is simplified to the case with one frequency. This design objective is reasonable and practical.

3.2 Experimental validation

The objective of this part is to experimentally verify the obtained optimization mechanism in the preceding section. For periodic excitation, the focus is to validate the periodic case with one single frequency at the first place and then to verify the results

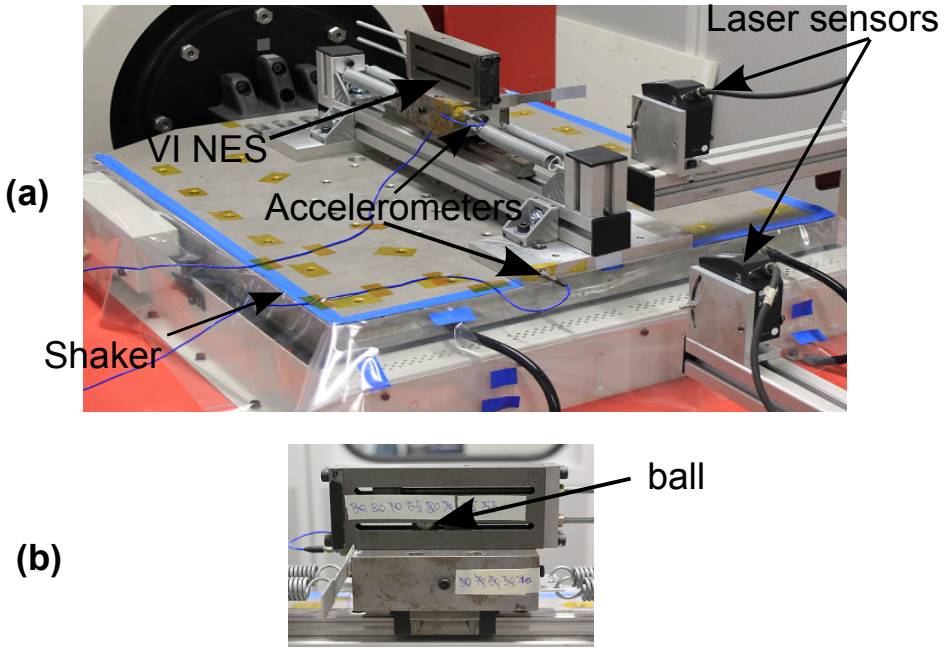

Fig. 3.7 Experimental setup: (a) global configuration; (b) a detailed view of VI NES.

under a range of frequency. As for transient excitation, the study with experimental validation is already partly done by Bapat [Bapat and Sankar, 1985], the experimental results here will provide more details about the efficiency of different transient response regimes and will be compared to the former study results.

3.2.1 Periodic excitation

Experimental setup

The global experimental configuration is showed in Fig. 3.7(a). A ball is put inside a cavity of LO and can freely move inside. The whole system is embedded on $10\,kN$ electrodynamic shaker. The displacement of the LO as well as the imposed displacement of the shaker are measured using contact-less laser displacement sensors. The acceleration of LO and shaker is measured by an accelerometer. A detailed view of the VI NES is presented in Fig. 3.7 (b). It simply consists of a closed cavity of length $d + 2b$, where d is the diameter of the ball and b can be adjusted by a cylinder in the cavity. The cylinder and the other side cover are made of hardened steel. The physical parameters of the system have been identified by performing modal analysis and are summarized in Table 3.1.

TABLE 3.1 Parameters of the experiment

Physical Parameters			
m_1	$4.7\,kg$	c_1	$3.02\,Ns/m$
k_1	$11.47 * 10^3\,N/m$	m_2	$32\,g$
b	$0 - 50\,mm$		
Reduced Parameters			
ϵ	$0.76\,\%$	λ_1	1.91
f_0	$7.86\,Hz$		
Single Frequency Test			
	f_r	$7.82 - 7.84\,Hz$	
shaker acceleration		$0.06\,g$	
Frequency Band Test			
	$f_s - f_e$	$6.5 - 9\,Hz$	
shaker acceleration		$0.06\,g$	

Fixed frequency excitation

The frequency of excitation slowly varies from 7.82 Hz to 7.84 Hz, which can be considered almost fixed to the value 7.83 Hz. This value is closed to the natural frequency $f_0 = 7.86$ Hz. Its acceleration is fixed to 0.06 g. The response without VI NES is recorded as reference and the results with VI NES is obtained by varying the value of b from 5-50 mm. It should be pointed out here the unit of b expressed in the experimental results is mm which is different from m for numerical results. The results are showed in Fig. 3.8. The time history of displacement of LO is showed, but only the stable period regardless of the starting and ending parts is used for calculation and comparison. Specifically, the time period 20-70 s is considered.

In Fig. 3.8(a), the displacement amplitude of LO decreases slowly with the increase of b. For $b = 5\,mm$ and $b = 10\,mm$, the response regime with three impacts per cycle occurs. The asymmetric two impacts per cycle appears for $b = 15\,mm$ and $b = 20\,mm$. Symmetric two impacts per cycle corresponds to $b = 25\,mm$ and $b = 27.5\,mm$. In Fig. 3.8(b), the variation trend is inverted as the increase of b. The response regime is always SMR, but the occasional duration time of two impacts per cycle is shorter and shorter. One specific SMR for $b = 35\,mm$ is demonstrated in Fig. 3.8(c). The value of local maximum points is different and irregular, which is demonstrated by the Y value of four points A, B, C and D. This kind of chaotic SMR [Gendelman and Alloni, 2015 ; Gendelman and Alloni, 2016] is experimentally validated from the point view of VI NES by the existence of intermittent strong impacts. Of course, it can be described directly by the strongly

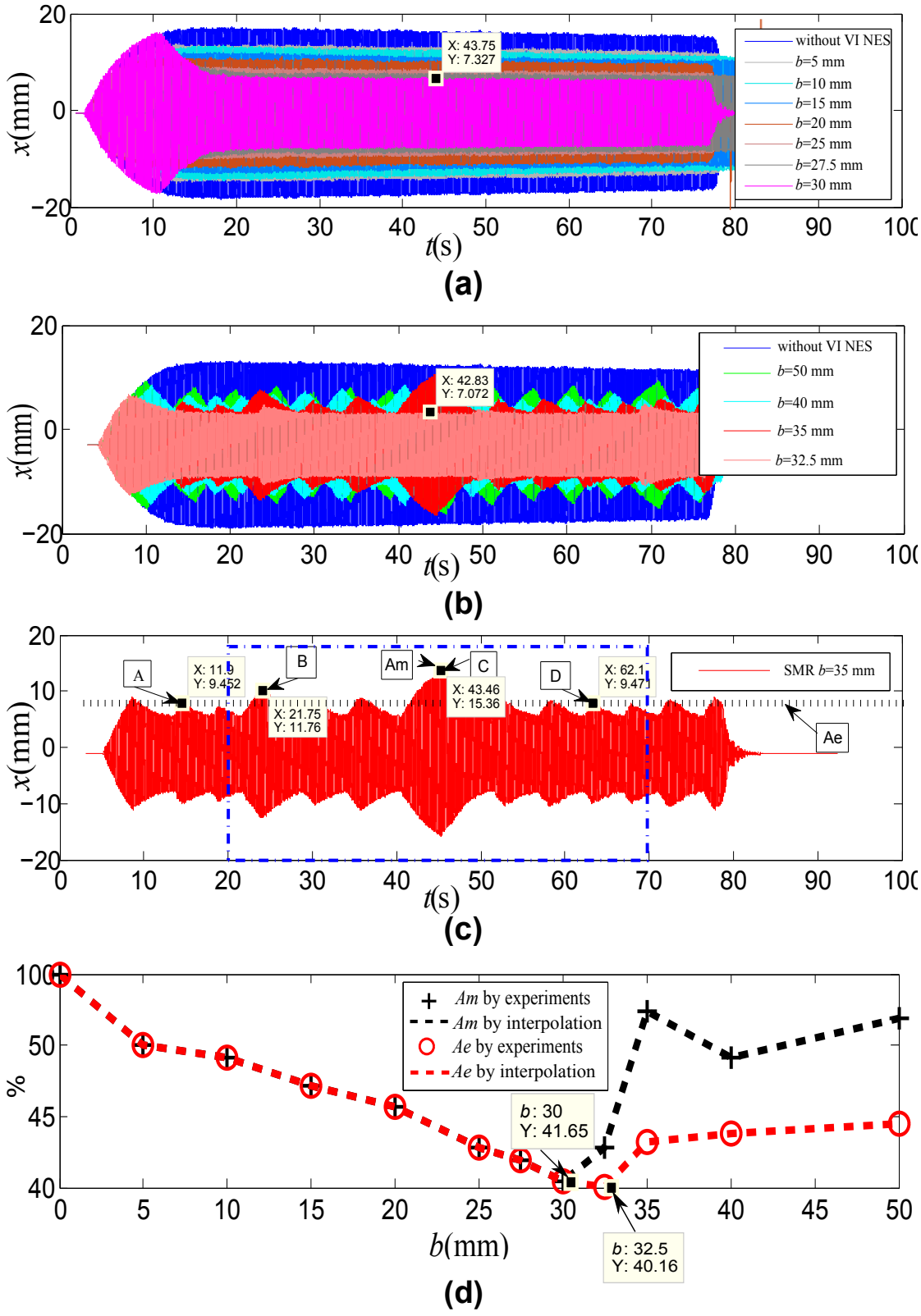

Fig. 3.8 Displacement of LO and TET efficiency of VI NES under periodic excitation with a fixed frequency and different b: (a) small b with $z > 2$ or $z = 2$; (b) large b with $z < 2$ (c) $b = 35mm$ with SMR; (d) TET efficiency.

modulated envelope of x as showed here. To compare the efficiency of different b, the data during 20-70 s denoted by blue dotted rectangle is used to calculate the equivalent amplitude (Ae) possessing the same energy, which is represented by the black dotted line. For not steady state response and specially SMR, the maximal amplitude (Am) during this process is recorded which is the vertical value of point C in this case. The calculated results are showed in Fig. 3.8(d) and the variation law observed in Fig. 3.1 is verified. One difference is that the numerically observed area D is not experimentally observed because of the limit of the length of cavity. The efficiency of the regime with two impacts per cycle ($b = 30\,mm$) and that of the SMR ($b = 32.5\,mm$) are almost the optimal value and the optimal value b can be inferred to be located between them. The obtained value $Ae = 40.16\,\%$ is very interesting from the viewpoint of energy reduction.

Frequency band excitation

To study the influence of b around the natural frequency of LO and the possibility of application of the above observed mechanism, the system periodically excited under a range of frequency is studied. The starting frequency f_s and ending frequency f_e during sweep is showed in Table 5.1 and the acceleration is still fixed to $0.06\,g$.

The displacement of LO is recorded for different b and is showed in Fig. 3.9. The shift of resonance peak between different experimental results comes from the difference of the starting record time. The maximal value of every sweep is indicated by different values of Y as showed in Fig. 3.9(a) and (b). For the frequency around resonance, the same mechanism described in the former section is well demonstrated by the value of Y. Its performance is also optimal for a medium value of b. The transition process of response for different value of b close to the optimal response is showed in Figs. 3.9(c-e). The optimal value locates between $b = 27.5\,mm$ (i.e., two impacts per cycle) and $b = 30\,mm$ (i.e., SMR). For $b > 30\,mm$, the efficiency will decrease for all frequency with the transition of response regime from SMR with long duration of two impacts per cycle to that with short duration and until totally no two impacts per cycle. In return, the efficiency for the resonance frequency will decrease with the decrease of b, but the response regime in other excitation frequencies will shift from SMR to two impacts per cycle and even to highly irregular response (i.e., many impacts per cycle and different from the above mentioned one), which means that their efficiency will increase at first and then decrease. In this way, the optimal mechanism for a range of frequency is clear. If the optimization design objective around resonance frequency is to control the maximal amplitude, the system can be optimized at the resonance frequency according to the above optimization design mechanism. In this optimal case, SMR will occur for other frequency close to resonance frequency and its duration of two impacts per cycle will increase with the decrease of the distance of this frequency from resonance frequency. Therefore, the optimal design for a range of frequency is directly related to that of resonance frequency. Although it is optimally designed for a range of frequency, VI NES will not work at its optimal state for other frequency except resonance frequency.

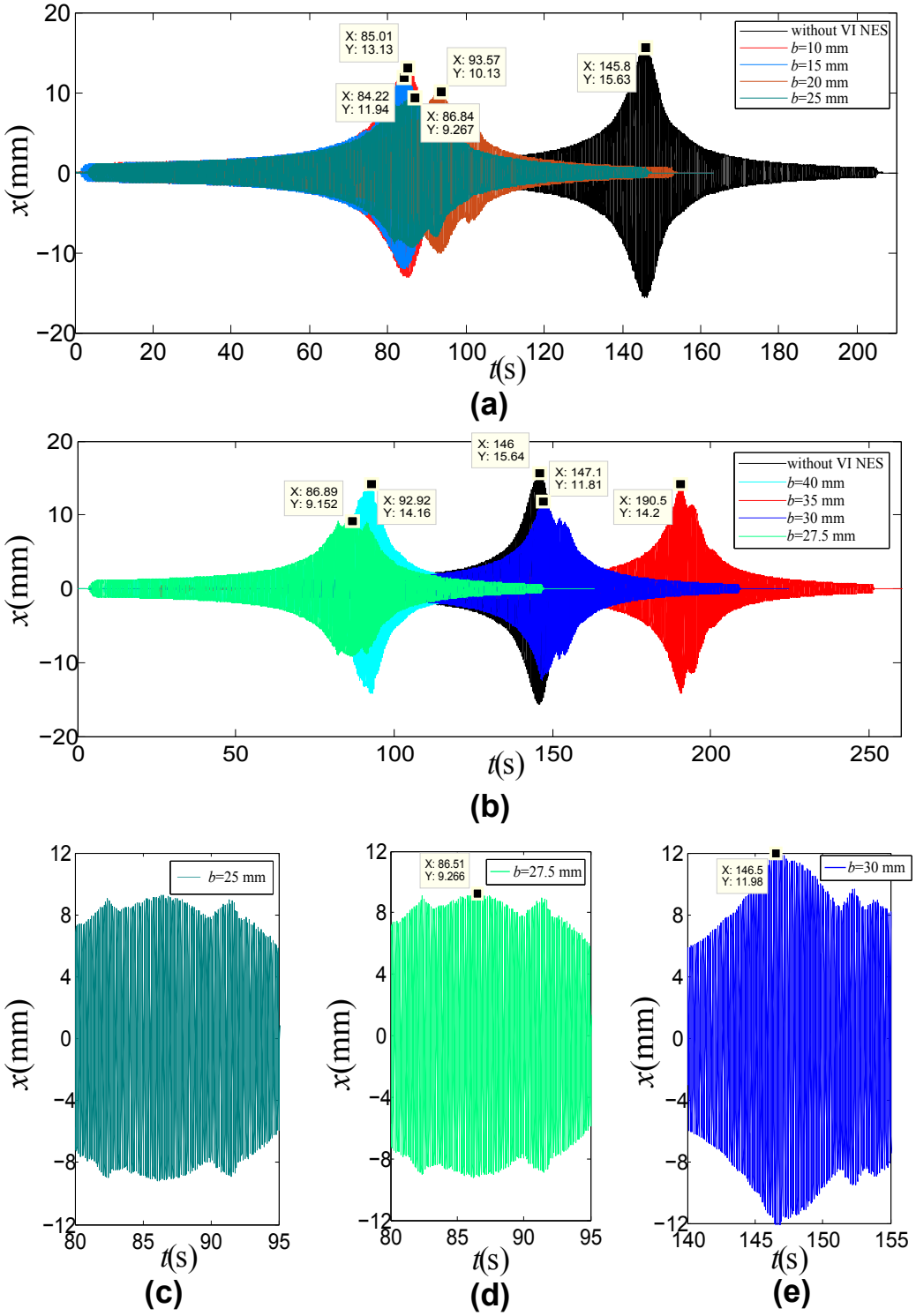

Fig. 3.9 The displacement history of the LO and the TET efficiency of VI NES under the periodic excitation with a range of frequency around f_0 for different b: (a) a small b with $z > 2$ or $z = 2$ at the point of resonance; (b) a large b with $z < 2$ at the point of resonance; (c) a detailed view for $b = 25\,mm$ around the point of resonance; (d) a detailed view for $b = 27.5\,mm$ around the point of resonance; (e) a detailed view for $b = 30\,mm$ around the point of resonance.

3.2.2 Transient excitation

Experimental setup

The same LO coupled with VI NES in Fig. 3.7 is used for the transient case as showed in Fig. 3.10 , so the parameters are almost the same as showed in Table 3.1 except a little addition of mass owing to the ring bolt. The LO is installed to a cast iron bench. One laser sensor and one accelerometer are used to measure the displacement and acceleration of LO respectively, meanwhile impact moments can be detected. For all tests, the initial displacement of LO is drawn to around $20\,mm$ which is realized by a stretching device displayed in Fig. 3.10(b). The location of the ball is random inside the cavity and it is supposed that it will not influence the stable response. The initial velocity of ball and LO is zero. Only the length of cavity is varied to see the transition of response regime for one specific length of cavity and further to compare the efficiency of different lengths of cavity.

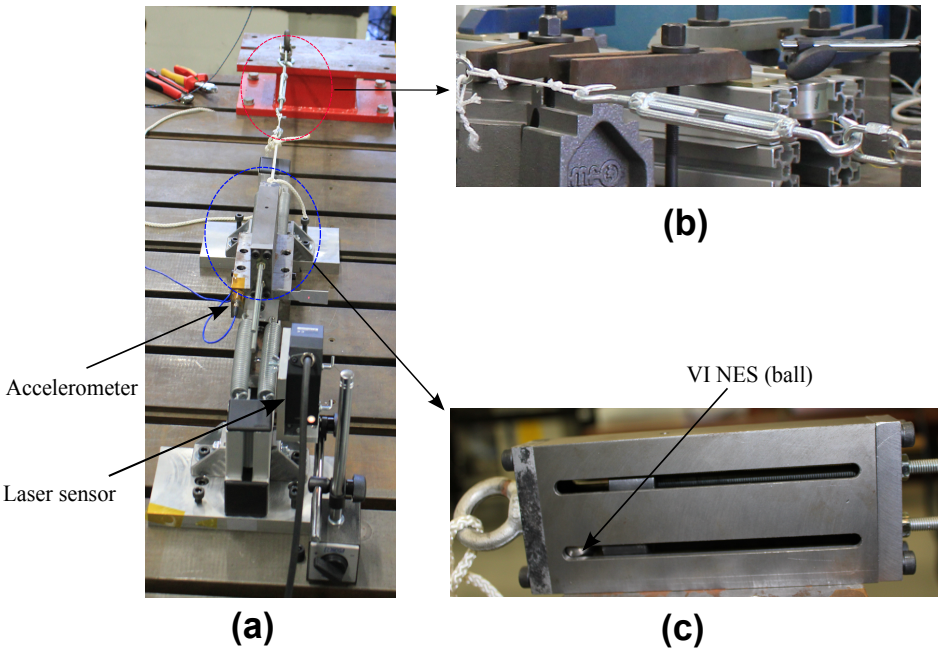

Fig. 3.10 Experimental setup: (a) the global configuration; (b) the displacement regulation device; (c) a detailed view of VI NES.

Efficiency of different transient response regimes

The response of LO with $b = 15\,mm$ is demonstrated in Fig. 3.11. The time history of displacement is displayed in Fig. 3.11(a) and it is observed that the displacement is not symmetric at the initial stage until the time around $t1 = 0.9254s$. However, the acceleration in this period is symmetric showed in Fig. 3.11(b).The pulse value of acceleration denotes an impact moment.

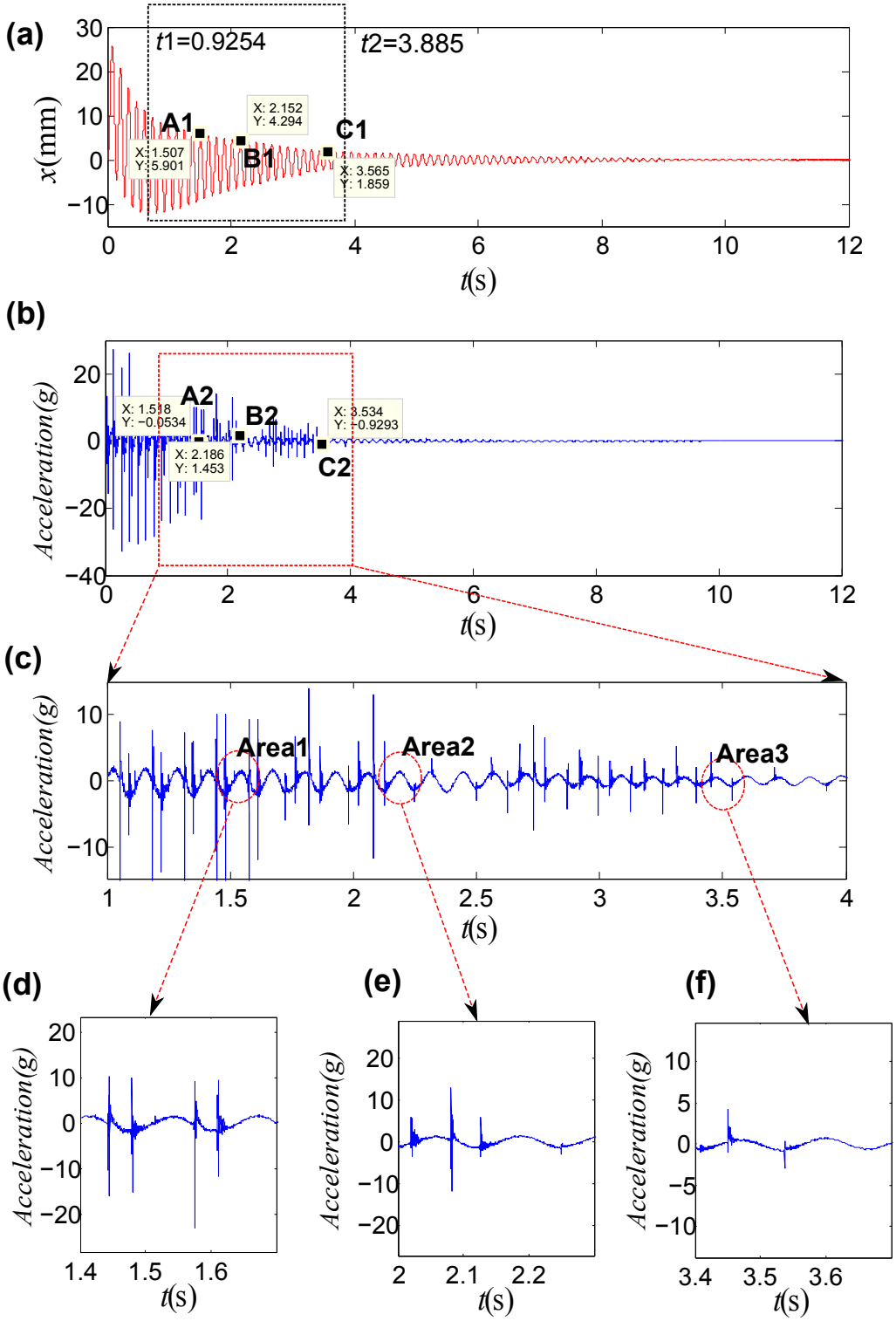

Fig. 3.11 Response of LO with $b = 15mm$: (a) time history of the displacement; (b) time history of the acceleration; (c) an enlarged view of acceleration; (d) an enlarged view of area1; (e) an enlarged view of area2; (f) an enlarged view of area3.

According to the number of impacts during one cycle of LO, different response regimes can be detected. An enlarged view of acceleration is showed in Fig. 3.11(c). The transition of impact number (i.e., z) can be clearly identified. The area 1,2 and 3 are enlarged in Fig. 3.11(d-f) respectively.

In area 1, the regime with three impacts per cycle disappears. In area 2, the regime with two impacts per cycle escapes into one impact during some cycles and will come back to the regime with two impacts per cycle. In area 3, the regime with two impacts per cycle escapes and cannot come back again. The different marked points correspond to different areas respectively. From regime with three impacts per cycle to regime with no impacts per cycle, different response regimes exist as represented in the SIM. To compare their efficiency, the decay rate of displacement amplitude during the period $[t1, t2]$ displayed in Fig. 3.11(a) is used.

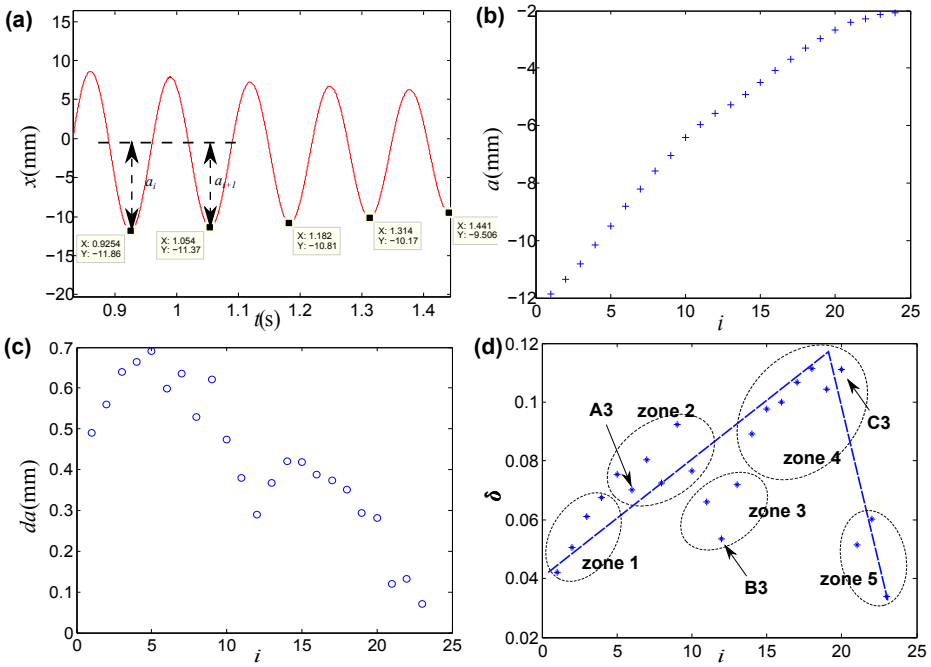

Fig. 3.12 Efficiency of different response regimes with $b = 15mm$: (a) enlarged view of time history of displacement; (b) time history of local minimal displacement; (c) decay rate; (d) relative decay rate.

An enlarged view of Fig. 3.11(a) is showed in Fig. 3.12(a). The local minimal displacements are marked out and represented by a_i and plotted in Fig. 3.12(b), which also represent its envelop. The variation of absolute value of difference (i.e., $da = a_{i+1} - a_i$) is demonstrated in Fig. 3.12(c). It is observed that the value of da varies during the whole process and cannot be approximated by a constant value. This means that the inclination rate is more complex than expected and cannot be described as linear, though it is truly different to the case without VI NES and is closer to a linear decay rate. Therefore, the index of linear decay rate in the former study of impact damper may cause

misunderstanding and it also should be noticed for other kinds of NES. Then the relative decay rate δ is used to compare different response regime. Specifically, δ is defined and calculated as follows:

$$\delta = \frac{da * 2}{a_{i+1} + a_i} \tag{3.1}$$

The results are showed in Fig. 3.12(d). In zone 1, the regime with three impacts per cycle exists. In zone 2 and 4, regime with two impacts per cycle exists. In zone 3, occasional short escape of two impacts per cycle appears. In zone 5, almost no impacts occur. The blue broken polyline can approximately describe the variation tendency of the efficiency of different response regimes. Except the phenomenon of occasional out of the excitation of VI NES, the obtained efficiency law agrees well with the former conclusion from the study of periodic excitation. The occasional out of excitation is probably related to the friction between ball and LO and it is not considered in our study.

Efficiency of different lengths of cavity

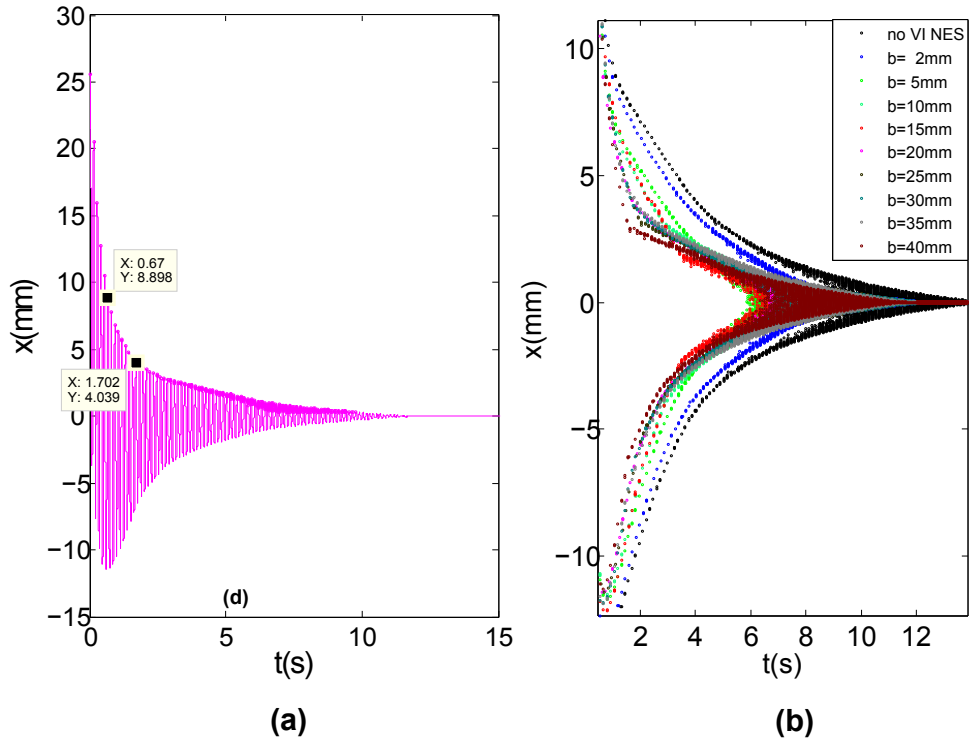

Fig. 3.13 Efficiency compare with different b: (a) envelop of $b = 20\,mm$; (b) imposed envelops of displacement of LO.

Except $b = 15\,mm$, other values of b have been to find the optimal value of b and the corresponding starting response regime. The time history of displacement for $b = 20\,mm$ is used to display the envelop extraction of each b and it is showed in Fig. 3.13(a). Its

local maximum and minimum is extracted and will constitute its own envelop. For for $b = 20\,mm$, only local maximum is showed. Because of the numerical precision, some local minimal and maximal values are presented by many values around the theoretical ones, especially for small displacement amplitude. However, it will not influence the analysis and can reflect the variation trend of amplitude any way. The envelop for different values of b is demonstrated in Fig. 3.13(b). With the increase of b, the decay rate becomes bigger until $b = 40\,mm$. For this value of b, the starting response regime is still that with two impacts per cycle. The b with larger value is not realized because of the limitation of experimental device (e.i. length of cavity). It means that the experimental results can just cover and validate the results with the increase of efficiency in the zone A and B marked out in Fig. 3.6 because of the limitation of b.

3.3 Conclusion

In this chapter, the efficiency comparison of different response regimes is carried out to explore a common optimization design criterion for different excitations. Firstly, it is numerically studied under periodic and transient excitations, respectively. The optimization design relation under different excitations is also analyzed. Then, the observed mechanism is experimentally validated.

It is observed that different response regimes possess different efficiency of vibration control, and correspondingly, an interaction force can describe a response regime from the analytical viewpoint. Evidently, response regimes and interacting force are the same for different excitations except that they are probably constant for periodic excitation and varying for transient excitation. This observation lays the common foundation for the optimization design of VI NES under different conditions, such as the type of excitation. Based on this idea, all optimization design criteria can be derived.

It is verified that the response regime between that with two impacts per cycle and SMR has the highest efficiency. Therefore, the ultimate objective of optimization design is to make this regime last as long as possible. For periodic excitation, the goal is to make this regime exist. In contrast, a compromise should be made to balance the duration time of different effective regimes and their existence. As for a range of frequency around resonance, it is observed that it can be simplified to the optimization design at resonance frequency.

From the observed results, a VI NES is only effective in a range of clearance. Therefore, there rests a problem about its activation, and it is studied in the next chapter.

CHAPTER 4

Activation mechanism of VI NES

Abstract

This chapter is dedicated to study the activation characteristics of VI NES and its application to the vibration control of nonlinear systems. Firstly, the activation characteristic is analytically analyzed and an optimization design criterion of VI NES for the vibration control of nonlinear systems is presented. Then, the same activation of VI NES with a same displacement amplitude but different frequencies is numerically verified. Thirdly, they are experimentally verified. Finally, an application of the optimization design method is performed to control the chatter during a turning process.

Contents

4.1 Analysis of SIM

For a fixed point of SIM as showed in Fig. 2.1, C and B is closely related to the displacement amplitude of LO and VI NES, respectively. During the analytical development, these two parameters are not changed despite the dimensionless process at the beginning. However, the frequency of LO is normalized and the velocity of VI NES is also scaled. It means that one point in the SIM actually represents different response regimes which have the same ratio between C and B but possess different frequencies of motion. In this way, different points of SIM possess different ratio and they together represent all possible response regimes.

Then two questions should be asked. Firstly, although the frequency can be different at the same point for different systems, the efficiency of energy reduction from the side of VI NES is the same ? Secondly, the optimal response, no matter in an interval of b with fixed excitations or in an range of displacement amplitude with a fixed b, will still be the same for linear systems with different natural frequencies or even nonlinear systems with varying frequency ?

From the viewpoint of VI NES, the above two questions can be answered together. The optimal response regime will still be optimal because it will still work at its best ability as long as it works at the corresponding response regime. For example, a ball realizes two impacts per cycle in p2 of SIM, and it is optimal as proved in the last chapter. However, that it will really influence the main systems remains a questions. Since it may impacts two impacts per cycle in a small object like a tea cup or a big object like a car. For the former, it can play an important role, but it is not the case for the latter. Anyway, it is activated at its best state. This point will be examined in detail in the following sections.

Actually, it is difficult to know the formation mechanism of a response regime by mathematical derivations for most nonlinear systems because of the underlying complex dynamics. Normally, just some information can be obtained by experimental observations or from a design objective. In this case, the VI NES shall be designed from the limited information of these nonlinear systems.

4.2 An optimization design criterion

The optimization design of VI NES coupled to a LO has been studied clear for different types of excitation. For the periodic excitation with single frequency, parameters should be designed to make the critical response regime between two impacts per cycle and SMR occur, which corresponds to the point p2 in Fig. 2.1. For transient excitation, the starting response regimes should also be that with two impacts per cycle, however it should be a little away from the former critical case to permit a long duration of this regime and it is recommended to be set at the boundary point p1 between symmetric and asymmetric two impacts per cycle or to the edging point p0 entering into the regime with more than two impacts per cycle in Fig. 2.1. For periodic excitation with a range

frequency, the optimization problem can be simplified to that of one frequency: the resonance frequency.

For a nonlinear system, its dynamic characteristics are difficult to be completely obtained by both analytical and numerical study. In this case, the idea is to apply a LO to represent the nonlinear system and then to design an optimal VI NES for this LO as an approximation to this nonlinear system. It is expected that this optimized VI NES will also be effective in two respects. In one respect, it still works at its maximal ability, i.e., its activation at optimal response regimes. In the other respect, linear approximation of nonlinear system will guarantee the similar role at energy reduction for nonlinear system.

Several conditions should be met to accomplish the above goal. Firstly, the mass ratio between VI NES and LO should be chosen the same as that in the nonlinear case and its feasibility depends on the acquirement of the mass of nonlinear system. Secondly, damping, stiffness and outside periodic force should be combined to create the same response as that of nonlinear system. Normally, its actual measured or designed amplitude is easier to know than the frequency. If its frequency could be known, the LO should be designed to possess the same frequency. If not, the condition of a same frequency should be insured by the design of an estimated frequency as close to the actual frequency of nonlinear system as possible.

From the above analysis, the characteristic of VI NES as broadband energy absorber is demonstrated from another direct perspective and expressed here more specifically, i.e., the same effectiveness for the same ratio between the displacement amplitude of main system and that of VI NES regardless of the underlying frequency. Moreover, the VI NES for a specific length of cavity can only be effective for a range of displacement amplitude of different main systems. This characteristic is essential for VI NES and for its optimization design for nonlinear systems. It will be validated from different points of view in the following parts.

4.3 Numerical observations

To guarantee the above mentioned design mechanism for nonlinear systems, several aspects of the activation characteristics of VI NES will be checked in this section. Firstly, will the three critical points (i.e., p0, p1 and p2) of the SIM still have the same value under different systems with different frequencies ? For this purpose, three linear systems with different natural frequencies and one duffing system with cubic nonlinearity are numerically studied. Moreover, whether the optimized parameters of one system are also optimal for the other systems with different frequencies are also checked. Secondly, since the ratio between the displacement amplitude of a main system and that of VI NES will be the same for a specific length of cavity, whether the displacement amplitude of the main system related to the above three points will be proportional to the length of cavity b will also be experimentally examined.

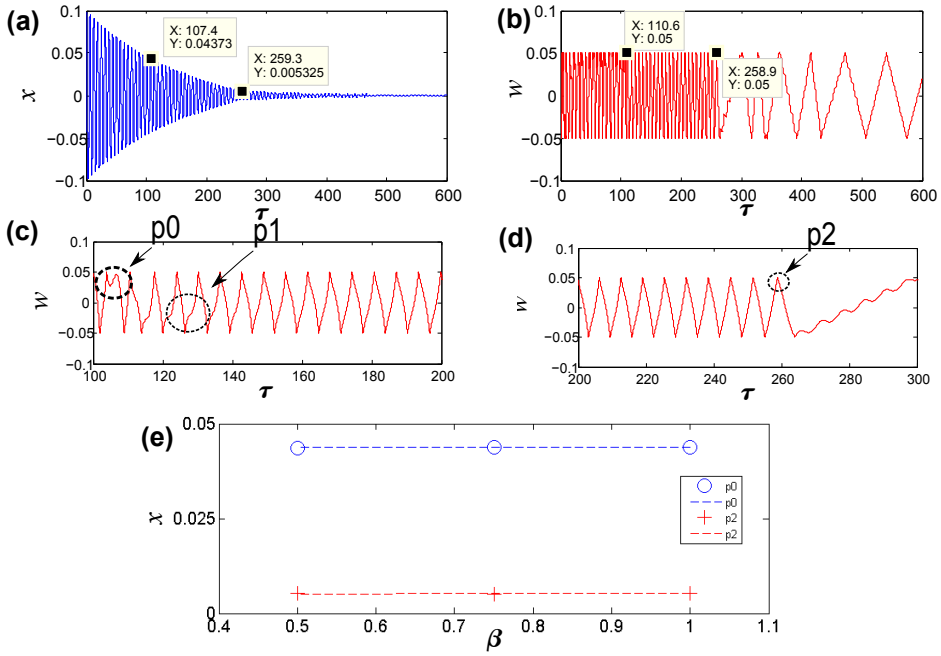

Fig. 4.1 Comparison of p0 and p2 for a LO with different natural frequencies by the displacement of LO and the relative displacement: (a) the time history of displacement x; (b) the time history of relative displacement w; (c) the judge of p0 and p1 from w; (d) the judge of p2 from w; (e) x related to p0 and p2.

4.3.1 LO and Duffing systems

Eq. (1.2) is modified as Eq. (4.1) to include a cubic term described by α and a proportional factor β is introduced to control the linear stiffness. The variation of β will be reflected in the parameter λ_1. For the moments of impact, Eq. (1.3) will still apply. The meaning of other parameters is the same as those in the last section. Eqs. (4.1) and (1.3) will be combined for numerical simulation and the following parameters are fixed except specially pointed out: $\epsilon = 0.84, r = 0.6$.

$$\begin{aligned} &\ddot{x} + \epsilon\lambda_1\dot{x} + x + \alpha x^3 = \epsilon G \sin\Omega\tau + \epsilon^2\lambda_1 G\Omega\cos\Omega\tau \\ &\epsilon\ddot{y} = 0 \\ &\forall\,|x-y| < b \end{aligned} \tag{4.1}$$

where

$$\epsilon = \frac{m_2}{m_1}, \quad {\omega_0}^2 = \frac{\beta k_1}{m_1}, \quad f_0 = \frac{\omega_0}{2\pi}, \quad \tau = \omega_0 t,$$
$$\lambda_1 = \frac{c_1}{m_2\omega_0}, \quad \Omega = \frac{\omega}{\omega_0}, \quad G = \frac{F}{\epsilon}$$

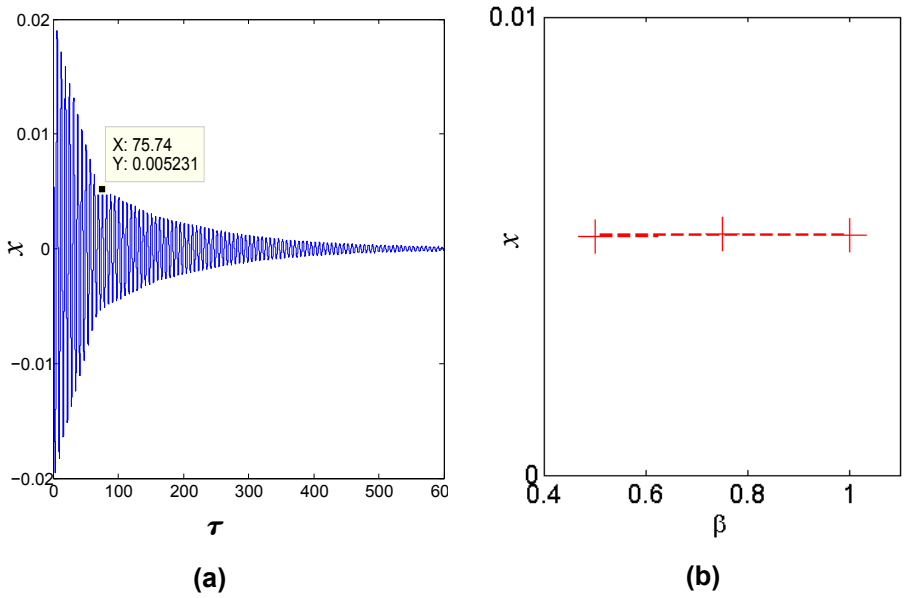

Fig. 4.2 Application of the optimal b from one specific LO to other two linear systems with different frequencies: (a) the time history of displacement of LO with $\beta = 1$; (b) x related to $p2$ for different β.

4.3.2 Free vibration of LO with different natural frequencies

The following parameters and initial conditions are used: $G = 0, \alpha = 0, b = 0.05, x_0 = 0.1, \dot{x_0} = 0, y_0 = b, \dot{y_0} = 0$. The following three values are consecutively chosen for β: 1, 0.75 and 0.5 to create three different linear systems. The results are showed in Fig. 4.1. For $\beta = 1$, the displacement of LO and relative displacement are displayed in Figs. 4.1 (a) and (b) respectively, among which the marked values for two points are judged from the special points p0 and p2 as showed in Figs. 4.1 (c-d). Because that the transition from regime with two asymmetric impacts per cycle to the symmetric case is difficult to distinguish, only p0 and p2 are used in the following results. In Fig. 4.1(e) , the corresponding value of x of p0 and p2 for these three different values of β is compared. The two broken lines are the line fitting of the circle and cross points and line fitting will also be used in the following parts to show the linear characteristic. It is observed that the value x related to the above two points is almost the same for the three cases of β.

When the parameters and initial conditions are fixed as: $G = 0, \beta = 1, \alpha = 0, x_0 = 0.02, \dot{x_0} = 0, y_0 = b, \dot{y_0} = 0$, different value of b is chosen to compare its efficiency for the same main system and $b = 0.05$ is found to be optimal. Then this optimal value of b is applied to the other systems with different β. The results are demonstrated in Fig. 4.2. The time history of displacement for $\beta = 1$ is displayed in Fig. 4.2(a) and x related to $p2$ is marked out. The comparison for three different β is showed in Fig. 4.2(b) . The three values are around 0.0052 which results in almost the same decay inclination for

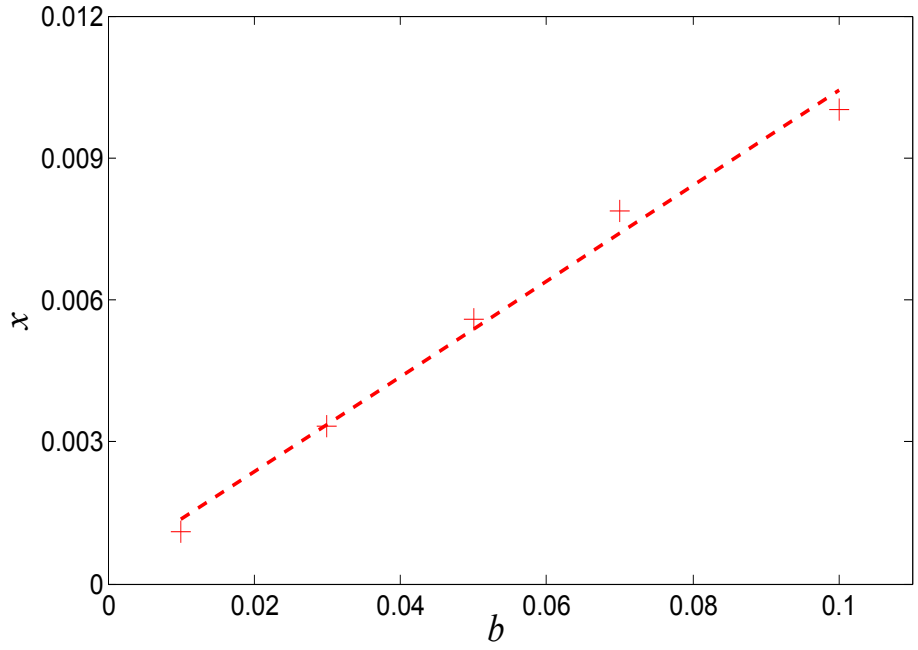

Fig. 4.3 x related to p2 obtained from the response of Duffing system with different b for VI NES.

these three systems.

4.3.3 Free vibration of different Duffing systems

For systems with cubic nonlinearity, the following parameters and initial conditions are used: $G = 0, \alpha = 250000, \beta = 1, x_0 = 0.02, \dot{x_0} = 0, y_0 = b, \dot{y_0} = 0$. Different values of b are chosen to compare their efficiency. As the way used in the above analysis, x related to p2 are compared and showed in Fig. 4.3. It is observed that the value of x for p2 is proportional to that of b and this characteristic will also be observed in the following experimental results. When the 95% of the energy of the main system is reduced, the percent of the accumulated energy dissipated by VI NES is recorded to compare the efficiency of different b. The result is displayed in Fig. 4.4(a). It is observed that the value around $b = 0.05$ is optimal not only because of the most reduced energy by VI NES but also the least time needed. Then this optimal value of b is fixed and α is varied to other two values: 0 and 2500000. The comparisons of x related to p2 are demonstrated in Fig. 4.4(b). The same mechanism is obtained as that for different linear systems with different frequencies as showed in Fig. 4.2(b).

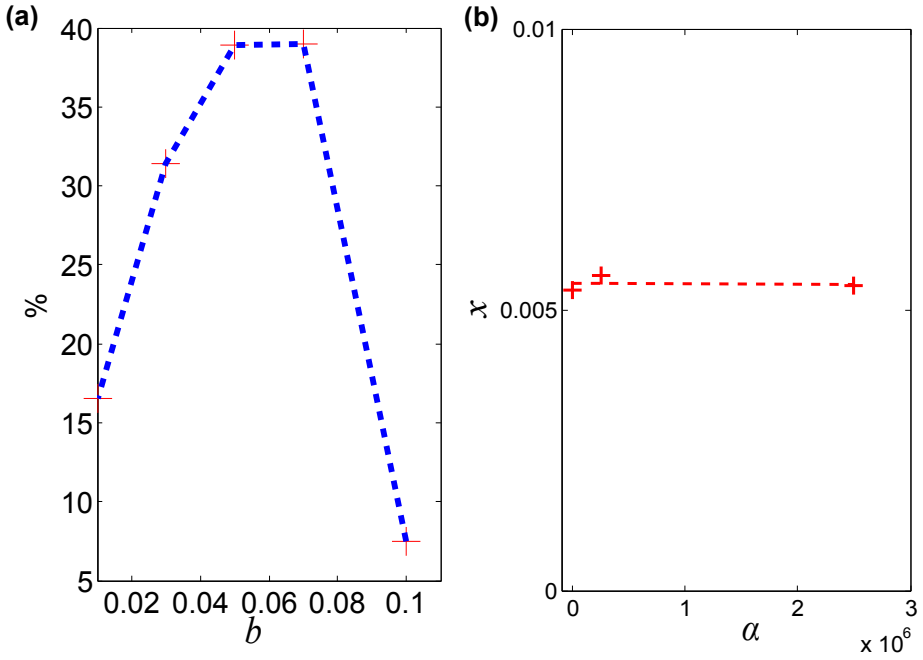

Fig. 4.4 The same optimized b for different duffing systems: (a) energy of the duffing system dissipated by VI NES with different value of b; (b) x related to p2 from the response of Duffing system with optimized b for different α.

4.4 Experimental observations

The objective in this part is to verify the proportional activation principle between the displacement amplitude of main system and the length of cavity b from the study of LO coupled with VI NES under different excitations. At first, the experimental device and parameters are introduced. Then the experimental results under a single frequency are showed. Finally, experimental results by sweep are presented.

4.4.1 Periodic excitation

The experimental device and parameters are the same as these in the last chapter, i.e., Fig. 3.7 and Table 3.1.

Single frequency excitation

The frequency of the shaker during sweep slowly varies from $7.82\,Hz$ to $7.84\,Hz$, which can be considered almost fixed to the value $7.83\,Hz$. This value is closed to the natural frequency of LO, i.e., $f_0 = 7.86\,Hz$. The acceleration of shaker is fixed to $0.06\,g$. The response coupled with VI NES is recorded for different values of b. It should be pointed out here that the unit of b expressed in the experimental results is mm which is different from that for numerical results (i.e., m).

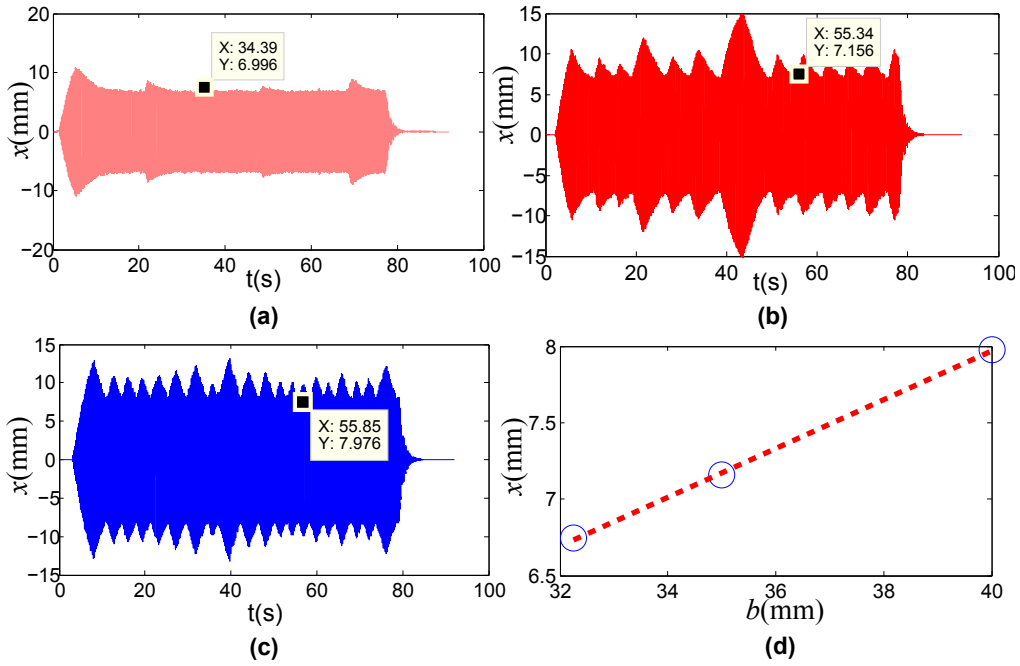

Fig. 4.5 Proportional activation characteristic of VI NES reflected by p2 of SIM: (a) $b = 32.5\,mm$; (b) $b = 35\,mm$; (c) $b = 40\,mm$.

The results are showed in Fig. 4.5. The whole time history of the displacement of LO is showed in Fig. 4.5 (a-c) for three different b respectively. Judging from the time range $20 - 70\,s$, SMR occurs at this stable area, the point of the minimal amplitude related to p2 is marked out around the same time moment and this minimal amplitude is equal to value of Y as marked out. The relation between different b and its corresponding minimal amplitude is represented by blue circles in Fig. 4.5(d) and is linearly interpolated. The consistency between the red broken line and circles proves the analytical obtained proportional characteristic to some extent, though the number of points is limited. Anyway, it could be observed from other results in addition to the experimental results here.

Excitation with a band of frequency

To observe the proportional activation characteristic of VI NES, the amplitude of LO related to the limit point p2 in SIM, i.e., the corresponding response regime limit between SMR and two impacts per cycle, is recorded for different values of b during the sweep process. The starting frequency f_s and the ending frequency f_e is showed in Table 3.1 and the acceleration of the shaker is also fixed to $0.06\,g$.

The displacement amplitudes of LO are marked out for different b and showed in Fig. 4.6(a) and (b). The shift of resonance peak between different experimental results comes from difference of the starting record time. The points of starting or ending the regime with two impacts per cycle are marked for different b and their specific judge

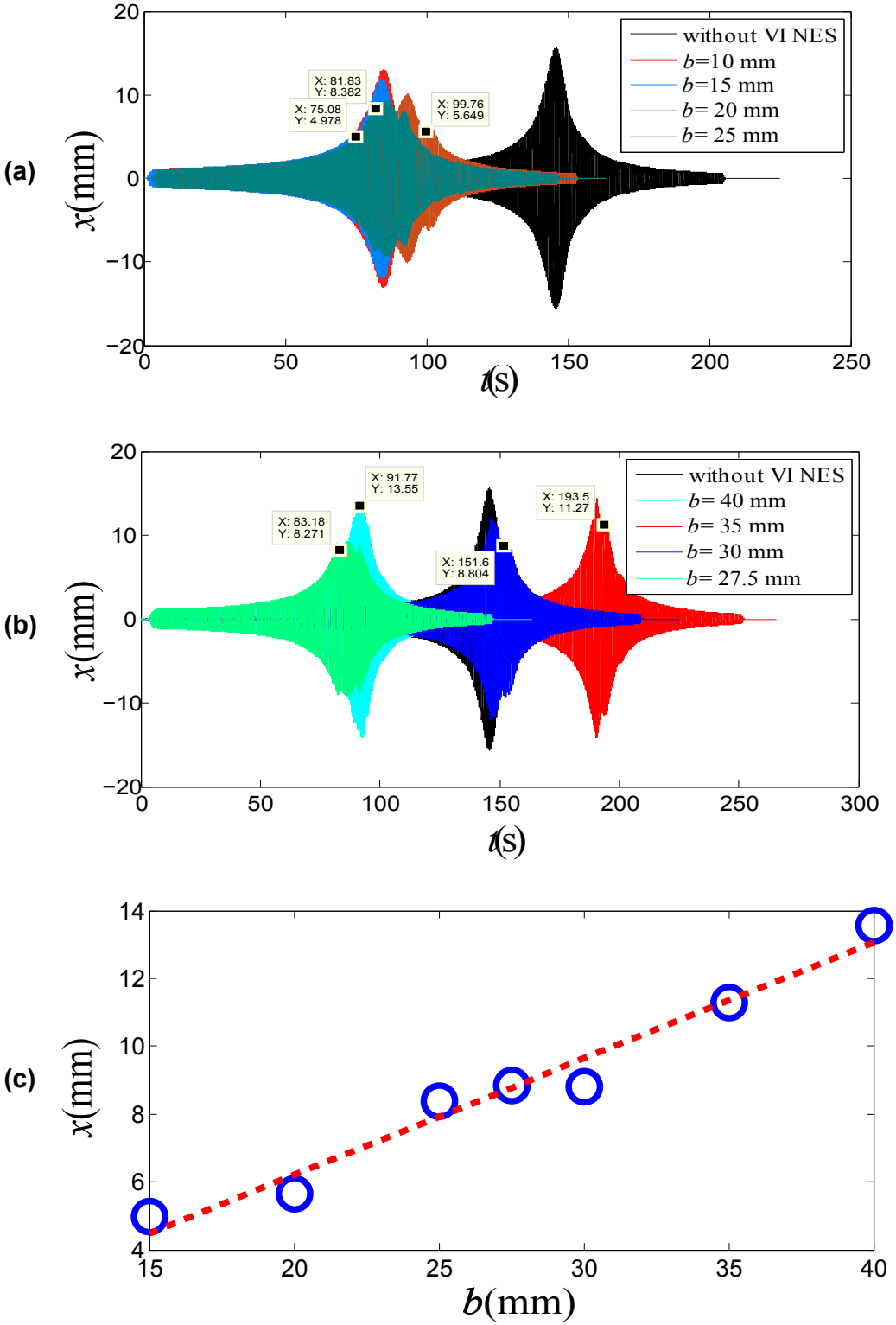

Fig. 4.6 Proportional activation characteristic of VI NES reflected by p2 of SIM under sweep experiment: (a) $b = 10\,mm, 15\,mm, 20\,mm\,and\,25\,mm$; (b) $b = 27.5\,mm, 30\,mm, 35\,mm\,and\,40\,mm$; (c) linear relation between b and x.

require the data of acceleration which could be seen during the analysis of the following experimental results. It should be pointed out here that these marked points are enough to coarsely describe the difference caused by b (i.e., the proportional characteristic), though it is difficult to accurately locate these points. Moreover, this point entering into or leaving from the regime of two impacts per cycle is evidently visible and distinguishable during the experimental process. As in the former part, these points are fitted by a red broken line showed in Fig. 4.6(c). These points almost locate in a line and prove again this proportional activation characteristic.

4.4.2 Transient excitation

Experimental configuration

In addition to the above experimental results under periodic excitation, three linear systems with different stiffness and one duffing system are experimentally studied under transient excitation. The objective here is to observe the dependence of the behavior of VI NES on the frequency. More specifically, it is to test that a VI NES with the same length of cavity will be excited at the same displacement level of main system with different frequency.

The same mass and damping of oscillator, same VI NES as showed in Fig. 4.7 will be used during the whole experimental process. Only the number of springs is changed from 4 springs to 3 springs or 2 springs, or even the direction of the springs is changed to another direction to create a duffing system. The oscillator is installed to a cast iron bench. Its displacement and acceleration are measured by an accelerometer and a laser sensor respectively. The LO is showed in detail in Fig. 4.7(a) and its stiffness can be changed by modifying the number of springs in its two sides. A detailed view of the fixation of springs is displayed in Fig. 4.7(b), in which two springs are used. If only one spring is used, this spring will be attached to the middle holes. During the experimental process, 4, 3 and 2 springs are consecutively applied. Their stiffness can be calculated according to the value of 4 springs as showed in Table 3.1. The displacement regulation device is showed in Fig. 4.7(c) and the initial displacement of LO is set to around $20\,mm$ for all tests. An enlarged view of VI NES is demonstrated in Fig. 4.7(d). Its initial location is random for all tests. The specific location is not so important, since only the stable process will be considered. In addition, the initial velocity of LO and VI NES is zero. The duffing system with the change of direction of springs from that of LO is showed in Fig. 4.7(e). It should be pointed out that only the stiffness is different for the above applied four systems.

Experimental results

The response for the case of LO with 4 springs and $b = 5\,mm$ is demonstrated in Fig. 4.8 to illustrate the process of identify the typical values related to two limit points p0 and p2 as previously introduced. The first limit point is that between the regime with

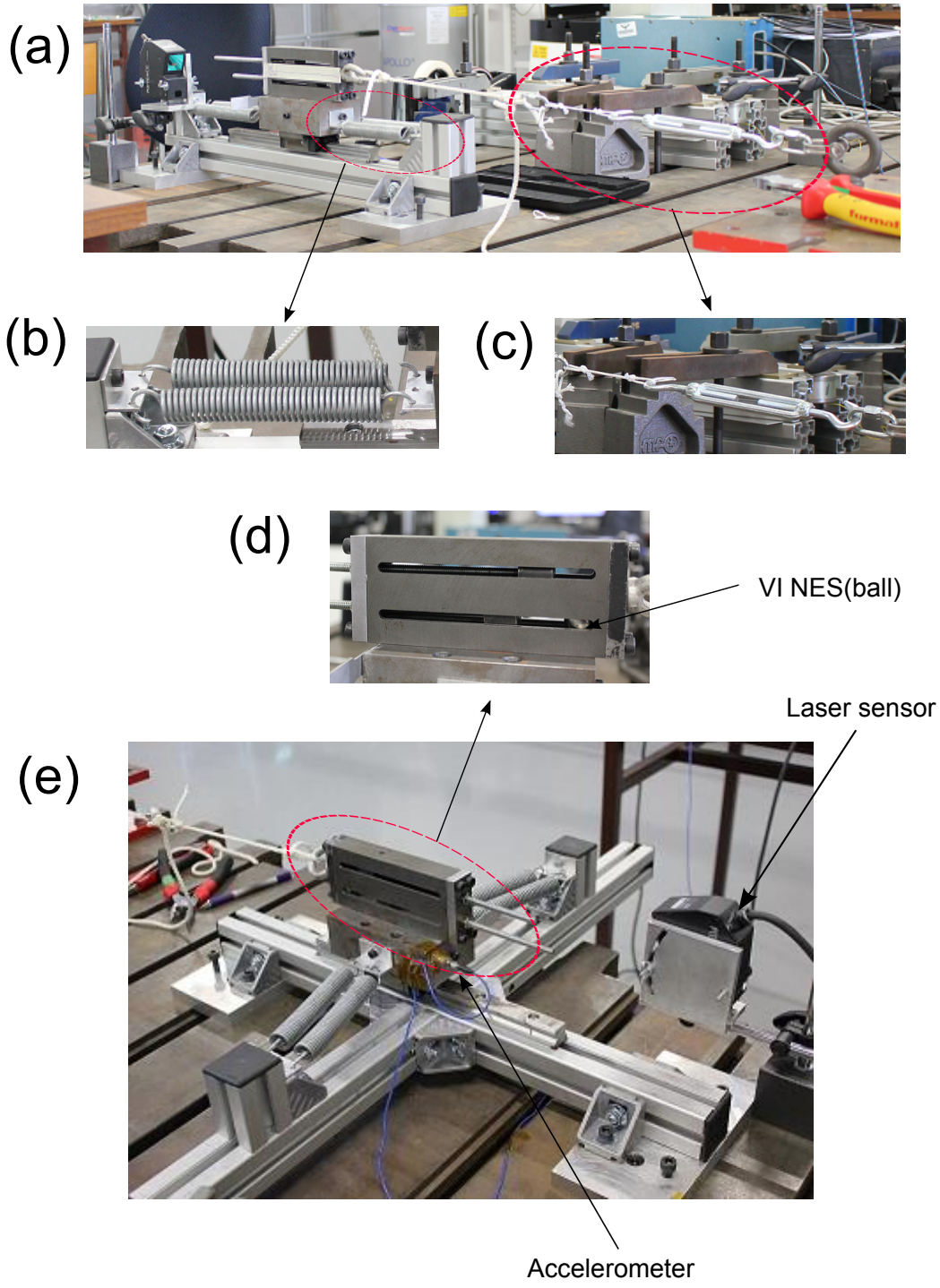

Fig. 4.7 Experimental setup: (a) the linear system with 4, 3 or 2 springs ; (b) the fixation of springs; (c) the initial displacement regulation device; (d) an enlarged view of VI NES; (e) the duffing system with 4 springs.

three impacts per cycle and that with two impacts per cycle, and the second is the one between the regime with two impacts per cycle and that with less than two impacts per cycle. The displacement is showed in Fig. 4.8(a), the first limit is between two points: the local maximum point A2 and point minimum A3. Similarly, the second limit point is between two other points: the local maximum point B2 and minimum point B3. The identification of these four points can be decided by the special points of the time history of acceleration as showed in Fig. 4.8(b) and this identification is also used for the above experimental results. Two periods are enlarged and displayed in Fig. 4.8(c) and (d). The point A1 is the last impact, which is denoted by the pulses, of the regime with three impacts per cycle. The point B1 is the last impact of the duration of the regime with two impacts per cycle and without stop. According to the times of A1 and B1, the special points A2, A3, B2 and B3 can be identified, and then their corresponding displacement amplitudes of main oscillator can be recorded, as showed in the side of each point.

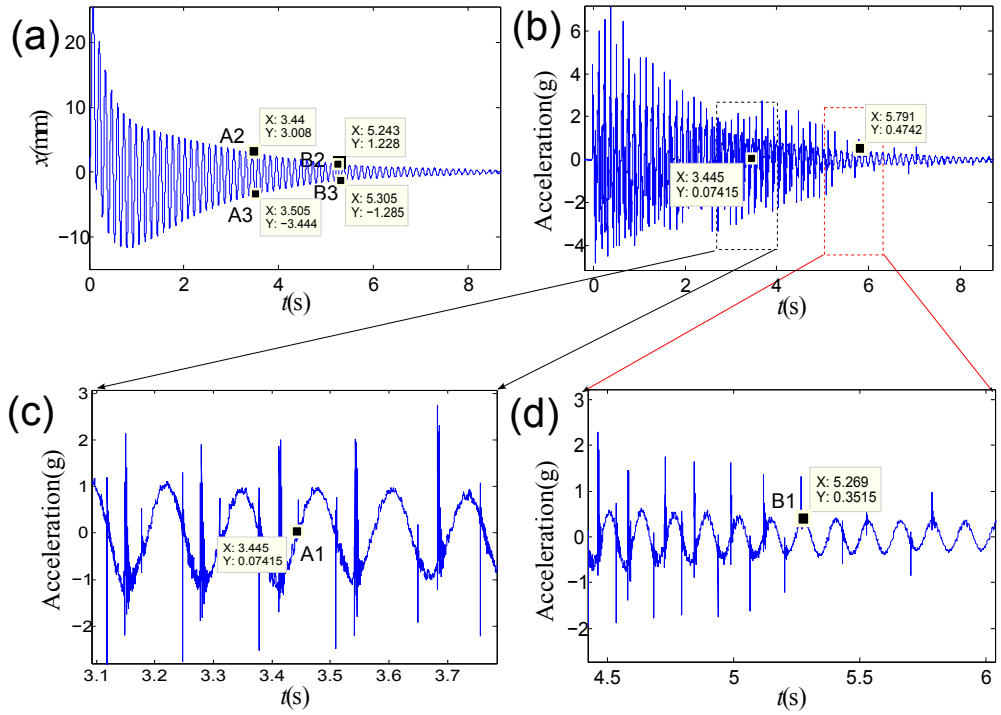

Fig. 4.8 LO with 4 springs and $b = 5\,mm$: (a) the time history of displacement; (b) the time history of acceleration; (c) an enlarged view of the time history of acceleration around point A1; (d) an enlarged view of the time history of acceleration around point B1.

For a main system with the same displacement amplitude, its energy will be bigger with a larger stiffness. For free vibration, there exist more oscillations during the decay process for larger stiffness. Therefore, it will be clearer to see the transition process of different response regimes with a larger stiffness for the same VI NES, since one response

regime will last longer. To illustrate the above transition phenomenon, the response history of a duffing system with 4 springs and $b = 5\,mm$ is displayed in Fig. 4.9. Its frequency is smaller than that of the corresponding LO with 4 springs. The application of points A1, A2, B2, and B3 to represent the two limit points of SIM will possess low accuracy than the former case, since the duration of each response regime is so short in the duffing case.

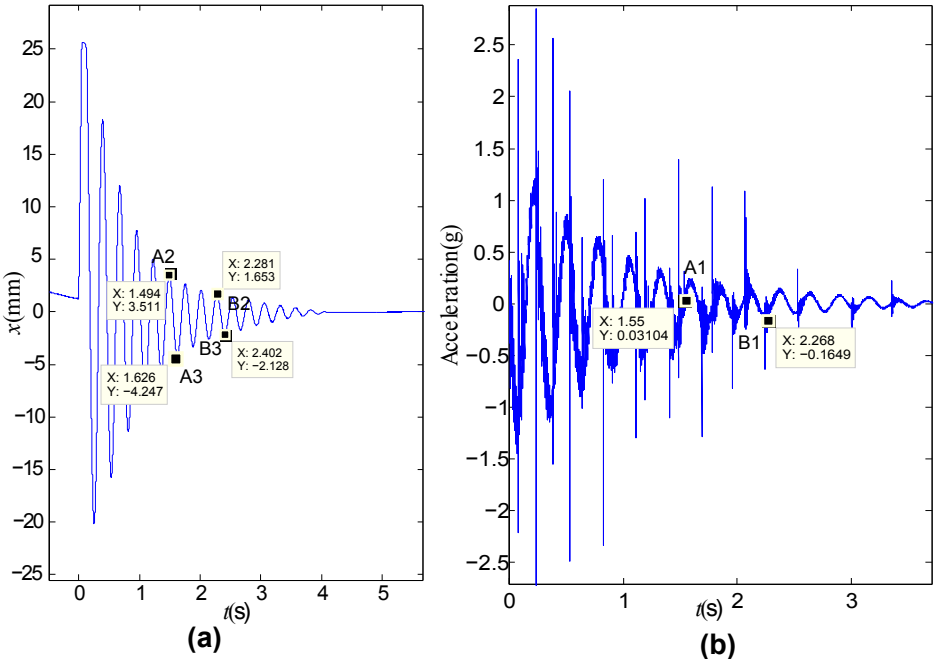

Fig. 4.9 Duffing system with 4 springs and $b = 5\,mm$: (a) the time history of displacement; (b) the time history of acceleration.

The amplitudes of main structure related to the two limit points p0 and p2 for different systems are compared and plotted in Fig. 4.10. As showed in Fig. 4.10(a), the first three values in the horizontal axis represent LO with 4, 3 and 2 springs respectively. And the last value represents the duffing system with 4 springs. The meaning of the value for the horizontal axis is the same for other three subfigures. Two lengths of cavity $b = 5\,mm$ and $10\,mm$ are applied and their results are showed in Fig. 4.10(a-b) and Fig. 4.10(c-d) respectively. The broken line is the curve fitting of the obtained data to show the variation trend. In Fig. 4.10(a), the results are showed by the amplitude of the positive side of displacement, A2 and A3 illustrate the first and second limit points respectively. The values of x are almost the same compared to its absolute value, which provides a direct proof for the activation characteristic of VI NES for systems with different frequencies mentioned in the former sections. The little increase of value with the decrease of number of springs is reasonable because that the description by measured data becomes coarse with the decrease of the stiffness. As for the comparison of LO with 2 springs with the duffing system with 4 springs, the difference is not significant because

that their stiffness are close and other unclear factors like friction may play the main role in deciding this value. The same conclusion can be obtained from the analysis of points A3 and B3 in the negative side of displacement as showed in Fig. 4.10(b). Moreover, the results showed in Fig. 4.10(c-d) for $b = 10\,mm$ also support the above analysis.

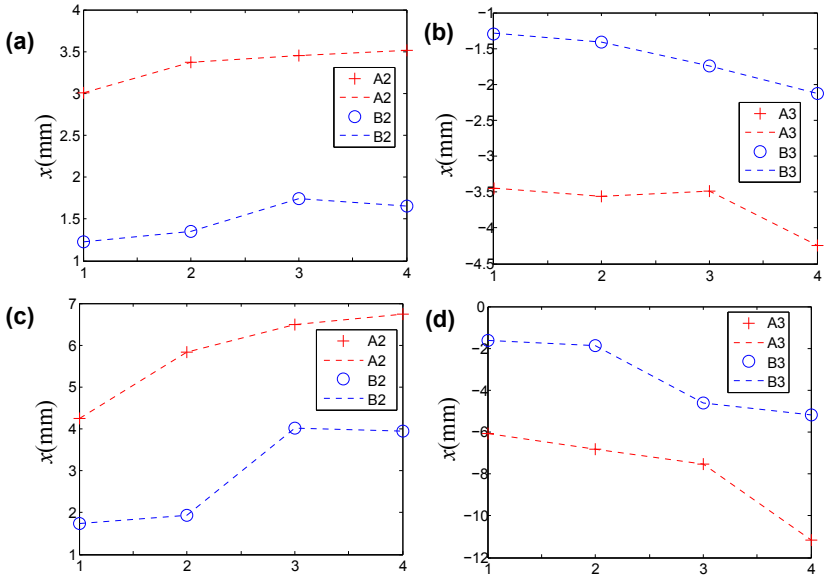

Fig. 4.10 Amplitude of the main structure around points A2, A3, B2 and B3 for three linear systems with 4, 3 and 2 springs and a duffing system with four springs and these four systems are presented by 1,2,3 and 4 in the horizontal axis respectively: (a) A2 and B2 with $b = 5\,mm$; (b) A3 and B3 with $b = 5\,mm$; (c) A2 and B2 with $b = 10\,mm$; (d) A3 and B3 with $b = 10\,mm$.

At the end, the complex of analysis should be pointed out to explain the possible errors. The time history of acceleration for the LO with 3 springs and $b = 10\,mm$ is showed in Fig. 4.11. Except A1 and B1, another special point C1 appears and denotes the occasional out of excitation of the regime with two impacts per cycle, but it will come back sometimes later. It probably results from the relative low amplitude and the corresponding low energy, and also the relative significant role of friction, since the friction is neglected during the whole study. In this situation, the above results in Fig. 4.10 seem at least acceptable.

4.5 An application to control chatter

In this section, an optimization design process of VI NES based on the above study will be applied to control the chatter of a cutting tool during the turning process. The simplified model and experimental parameters in [Gourc *et al.*, 2015b] will be used as showed in Table 4.1. The application of VI NES has been experimentally observed to be

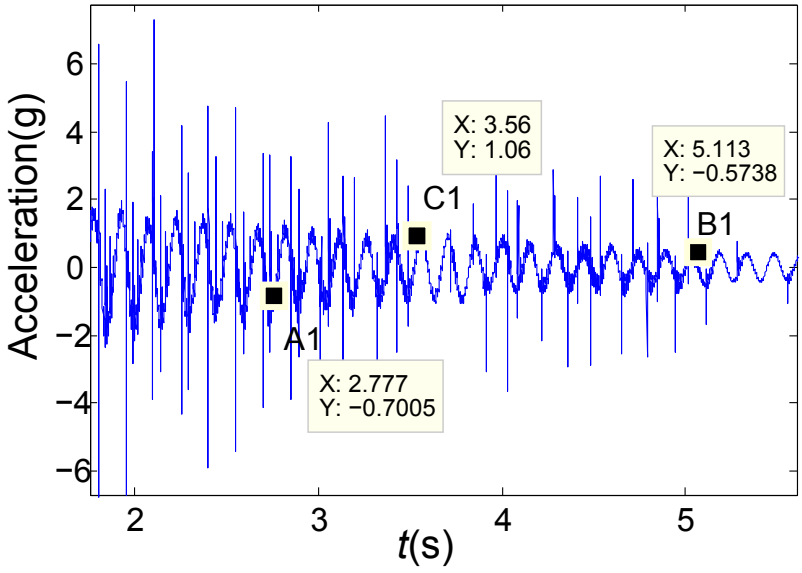

Fig. 4.11 One period of the time history of acceleration of the LO with 3 springs and $b = 10\,mm$.

efficient in quenching an unstable cutting in this paper. The objective here is to apply the above mentioned optimization design mechanism and to numerically validate its effectiveness. It is demonstrated that the bifurcation diagram with the increase of cutting parameters is complex [Nayfeh and Nayfeh, 2011] and the corresponding response regime is also complicated. Two typical cases will be chosen to demonstrate the optimization process. One case corresponds to the unstable cutting possessing an unstable cutting with a steady state response as well as a stable cutting with zero amplitude. The other case corresponds to the unstable cutting characterized by beating response.

4.5.1 Model of cutting tool coupled with VI NES

A simplified model of cutting tool coupled with a VI NES is represented in Fig. 4.12. The cutting tool is supposed to only vibrate in the feed direction and the workpiece is considered rigid. The corresponding equation of motion between impacts is written as follows:

$$\begin{aligned} &m_1\ddot{x} + c_1\dot{x} + k_1 x + k_2 x^3 = F_x \\ &F_x = p(\rho_1 \Delta h^1 + \rho_2 \Delta h^2 + \rho_3 \Delta h^3) \\ &\epsilon\ddot{y} = 0 \\ &\forall\, |x - y| < b \end{aligned} \tag{4.2}$$

The related parameters are expressed as follows:

$$\omega_0{}^2 = \frac{k_1}{m_1}, \quad f_1 = \frac{\omega_0}{2\pi}, \quad \mu_1 = \frac{c_1}{2m_2\omega_0} \tag{4.3}$$

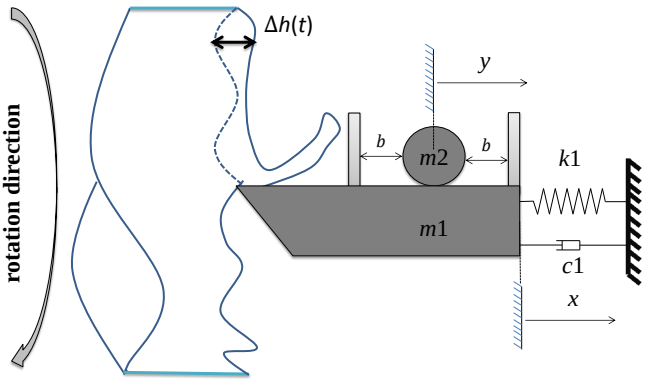

Fig. 4.12 Schema of a cutting tool system coupled with a VI NES.

where x, m_1, c_1, k_1 and k_3 are the displacement, mass, damping, coefficient of linear stiffness and coefficient of cubic stiffness of the cutting tool respectively. y and m_2 are displacement and mass of VI NES. The dots denote the differentiation with respect to time t. Δh is decided by the current displacement and the displacement trajectory left by the last pass. b represents the clearance. When $|x - y| = b$, impacts occur. The relation between after and before impact is obtained under the hypothesis of the simplified shock theory and the condition of total momentum conservation:

$$\begin{aligned} &x^+ = x^-, \quad y^+ = y^- \\ &m_1\dot{x}^+ + m_2\dot{y}^+ = m_1\dot{x}^- + m_2\dot{y}^-, \\ &\dot{x}^+ - \dot{y}^+ = -r\left(\dot{x}^- - \dot{y}^-\right), \\ &\text{for } |x - y| = b \end{aligned} \tag{4.4}$$

4.5.2 Optimization design of different cases

The fixed physical and cutting parameters are showed in Table 4.1. Only the cutting width h_0 and length of cavity b will be varied. At first, the system is not coupled with VI NES and the cutting width is varied to see the bifurcation. When $h_0 = 0.11\,mm$, the case with two fixed points is observed denoted as case 1 and the fixed point with beating response is located with $h_0 = 0.16\,mm$ and is denoted as case 2. The response regimes and the results for the above two cases without and with VI NES will be demonstrated.

Case 1

For $h_0 = 0.11\,mm$, the following initial conditions are fixed : $\dot{x_0} = 0, y_0 = b, \dot{y_0} = 0$. Only the initial displacement x_0 is changed. When x_0 is chosen to a large enough value

TABLE 4.1 Simulation parameters for cutting tool coupled with VI NES

Physical Parameters			
m_1	$3.1\,kg$	μ_1	$3\,\%$
f_1	$99.4\,Hz$	m_2	$32\,g$
Cutting Parameters			
p	$0.1\,mm$	ρ_1	$6109.6 * 10^6\,Nm^{-2}$
ρ_2	$-54141.6 * 10^9\,Nm^{-2}$	ρ_3	$203.769 * 10^{12}\,Nm^{-2}$
s	$1800\,rpm$		

such as $0.20\,mm$ and $0.01\,mm$, the response x will be attracted to the same steady state value, which corresponds to the unstable cutting as showed in Fig. 4.13(a) and (b) respectively. If the initial condition is small enough, the response will decay to zero as displayed in Fig. 4.13(c).

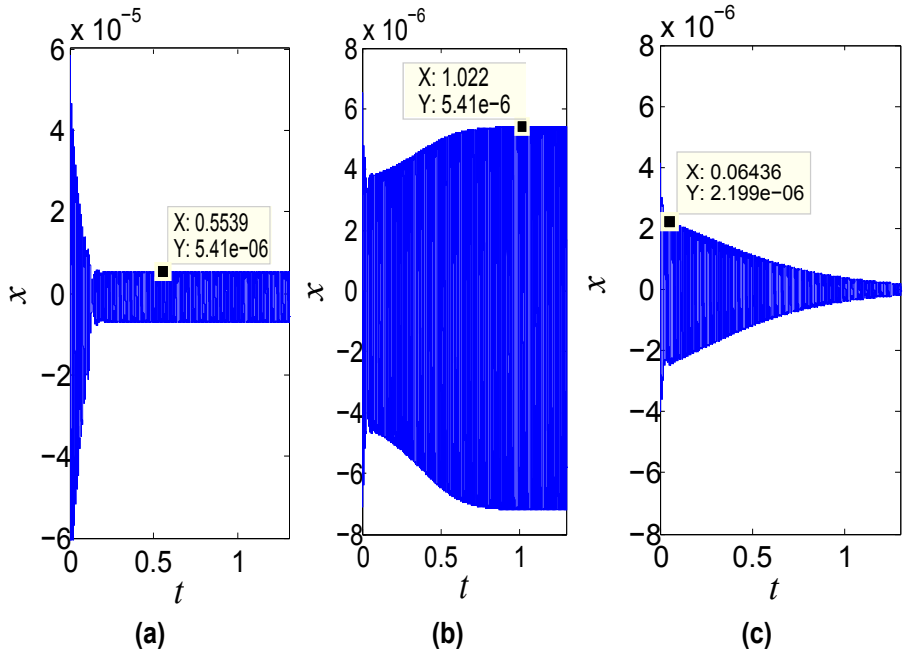

Fig. 4.13 Displacement of the cutting tool with different initial conditions for $h_0 = 0.11\,mm$ without VI NES: (a) $x_0 = 0.20\,mm$; (b) $x_0 = 0.01\,mm$; (c) $x_0 = 0.006\,mm$.

To design the length of cavity for VI NES, the analytical results in section 2 will be used. At first, a LO close to the turning system, i.e., with the same displacement amplitude is created. In addition, the corresponding LO will possess other same characteristics as cutting tool as many as possible. The frequency of outside force for the

imagined linear oscillator is fixed to the experimentally obtained frequency f_0 and its amplitude will be chosen in order that the displacement amplitude of LO will be the same as that of cutting tool. Then b is designed to make the objective displacement amplitude of cutting tool locate in p2 of the corresponding SIM under periodic force and in p1 for transient excitation. For cutting tool, its final steady state, i.e., a steady non-zero or zero amplitude, is applied to decide which points will be chosen.

For the first two initial conditions, it is periodic and its stable amplitude is $5.41 * 10^{-3}\,mm$ and b is chosen to p2. For the third initial condition, it is transient and its displacement at the starting point $2.199 * 10^{-3}\,mm$ is chosen to make it locate at p1. The effect with VI NES is demonstrated in Fig. 4.14. For the first two initial conditions, the unstable state is improved to stable state and the vibration is completely controlled as showed in Fig. 4.14(a-b). Meanwhile, the transient process of energy dissipation is accelerated. This is the same case for the third initial conditions as showed in Fig. 4.14(c).

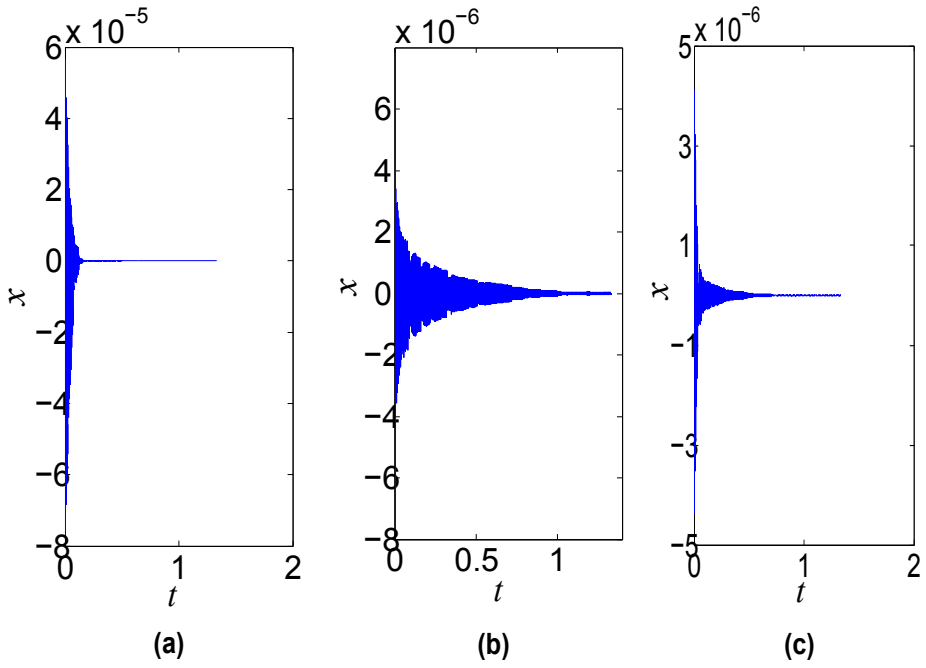

Fig. 4.14 Displacement of the cutting tool coupled with optimized VI NES for different initial conditions at $h_0 = 0.11\,mm$: (a) $x_0 = 0.20\,mm$ and $b = 2.2880 * 10^{-2}\,mm$; (b) $x_0 = 0.01\,mm$ and and $b = 2.2880 * 10^{-2}\,mm$; (c) $x_0 = 0.006\,mm$ and $b = 2.4604 * 10^{-3}\,mm$.

Case 2

Compared to case 1, the beating response occurs for $h_0 = 0.16\,mm$ as represented by the blue curve in Fig. 4.15(a). The amplitude of displacement is not steady. If the relative maximal value of point T1 is chosen as the target to choose the LO, the estimated amplitude will be high, the response should be designed according to p1 with a relative

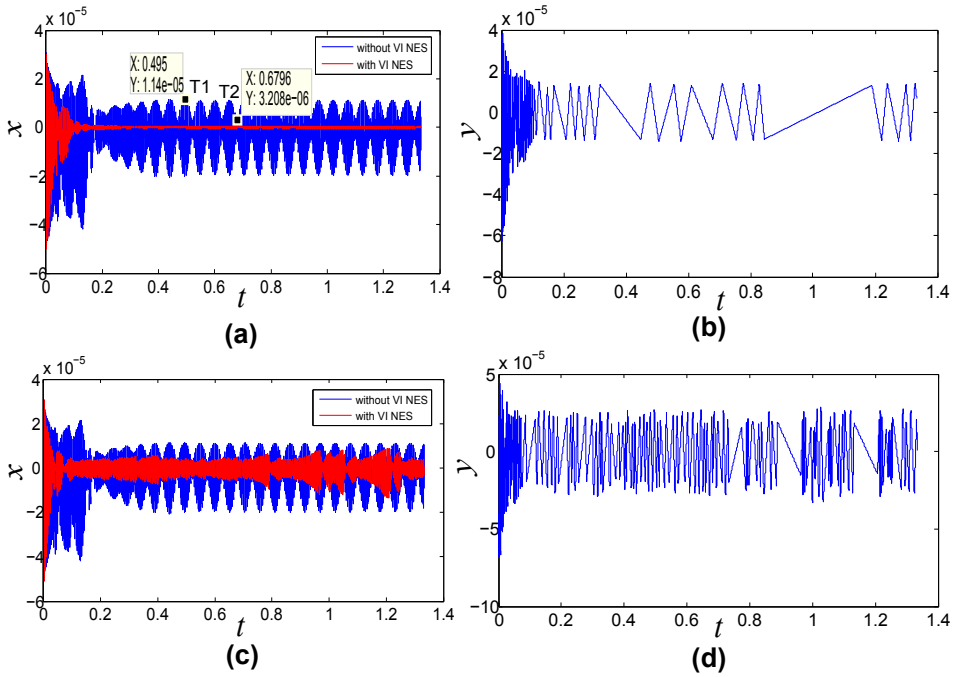

Fig. 4.15 Response comparison of the cutting tool without and with VI NES for $x_0 = 0.08\,mm$ and $h_0 = 0.16\,mm$: (a) x and $b = 1.3517 * 10^{-2}\,mm$; (b) y and $b = 1.3517 * 10^{-2}\,mm$; (c) x and $b = 1.2632 * 10^{-2}\,mm$; (d) y and $b = 1.2632 * 10^{-2}\,mm$.

high length of cavity of VI NES. In return, it will be a little small for the relative minimal value of point T2, the response should be designed according to p2.

When the relative minimal value $Y = 3.208 * 10^{-3}\,mm$ of T2 is chosen, the p1 is used as the targeted point. The result is showed in Fig. 4.15(a) and the displacement of the cutting tool in red curve is almost zero in this case. When the relative maximal value $Y = 1.14 * 10^{-2}\,mm$ of point T1 is chosen with t p2 as the target. The result in red curve is showed in Fig. 4.15(c) and the displacement of cutting tool is greater with this b. The displacements of VI NES y for these two designed value are showed in Figs. 4.15(b) and (d) respectively. For the first value of b, VI NES is more activated at the beginning. Once vibration is decreased to a little value, VI NES is no longer activated. For the second value in Fig. 4.15 (d), VI NES is also activated, but the vibration is not reduced as the first value and VI NES is occasionally activated.

In summary, the optimization design process proposed for VI NES is effective for the unstable cutting during the turning process. It demonstrates the possibility of optimal design of VI NES for nonlinear systems.

4.6 Conclusion

In this chapter, the activation mechanism is further investigated and is applied to the optimization design of VI NES for the vibration control of nonlinear systems. Firstly, the

activation characteristic is analyzed with the help of SIM. Then, an optimization design procedure is proposed for the vibration control of nonlinear systems. Before its application, some aspects of the activation mechanism are numerically and experimentally validated. Finally, an application to control chatter during a turning process is carried out.

Considering the difficulty encountered during the study of nonlinear systems coupled with VI NES, the optimization design objective is simplified to the activation of VI NES. When VI NES is activated at its best state, its role at vibration control will depend on its relative importance compared to other factors. However, it may be the best choice to design VI NES considering the complication of nonlinearity.

To support the above optimization design objective, different aspects are validated. From experimental results, the almost same activation of VI NES for different systems with different frequencies is important to design VI NES coupled to nonlinear systems. The preliminary application to chatter control during a turning process is numerically proved effective by two cases studies, and this aspect should be further studied.

The proportional activation of VI NES at p2 of SIM demonstrates the principle of separate activation to some extent. This point will be further explored in the next chapter with the addition of another VI NES.

CHAPTER 5

Dynamics of two VI NES in parallel

Abstract

The objective of this chapter is to experimentally study the dynamics of two VI NES in parallel and the possibility of efficiency and robustness improvement. Specifically, a LO coupled with two VI NES in parallel is studied. Firstly, experiments under periodic excitation are carried out for different combinations of clearances. Different response regimes are verified and improvement of robustness is observed. Then, experiments under transient excitation are performed and the principle of separate activation is observed.

Contents

5.1 Background

From the former study about one VI NES, it is observed that a VI NES with a fixed clearance will only be activated at a range of displacement amplitude of main system. Therefore, it is natural to conceive multiple VI NES with their own changeable clearances to improve the efficiency of vibration control. Around this idea, considerable studies around the concept of particle dampers have been performed [Olson, 2003]. However, the analytical study in the context of TET is few.

Recently, a LO coupled with two VI NES in parallel is analytically studied with multiple scales method by E. GOURC [Gourc, 2013]. The principle of separate activation, which is firstly obtained from NES with cubic nonlinearity [Vaurigaud *et al.*, 2011 ; Savadkoohi *et al.*, 2012], is analytically obtained for VI NES for the first time. In addition, fixed points are obtained and applied to predict the response regimes, and numerical results have verified the good consistency of analytical results.

Therefore, the objective here is to experimentally validate the already obtained analytical and numerical results. Specifically, it is to observe the possible response regimes and compare their efficiency under periodic excitation in one side. Then, the principle of separate activation is studied under transient excitation in the other side.

5.2 Mechanical model

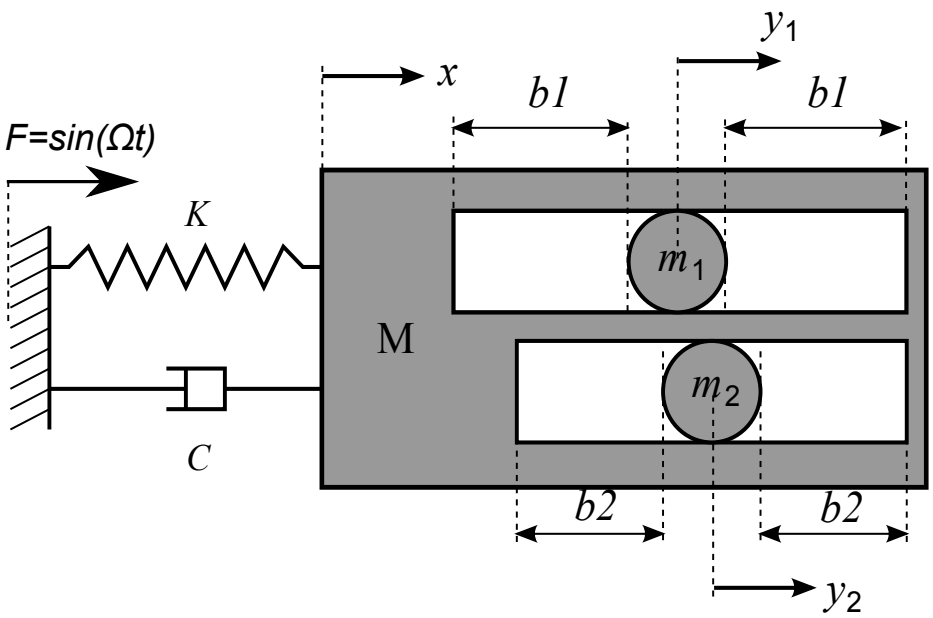

Fig. 5.1 Schema of LO with two VI NES coupled in parallel [Gourc, 2013].

Two VI NES in parallel are attached to a periodically forced LO as presented in Fig.

5.1. Each of them has its own clearance ($b1$ and $b2$) and can move freely inside LO. Its equation of motion between impacts is expressed as follows:

$$\begin{aligned} &M\frac{d^2x}{dt^2} + C\frac{dx}{dt} + Kx = F\sin\Omega t \\ &m_1\frac{d^2y_1}{dt^2} = 0, \quad \forall|x-y_1| < b1 \\ &m_2\frac{d^2y_2}{dt^2} = 0, \quad \forall|x-y_2| < b2 \end{aligned} \tag{5.1}$$

where x, M, C and K are the displacement, mass, damping and stiffness of the LO, respectively. y_i and m_i are displacement and mass of the i^{th} VI NES (i=1,2). $F\sin(\Omega t)$ is the displacement imposed on the base.

Its motion relation once impacts can be obtained with the condition of simplified impact theory and the momentum conservation, and it can be written as follows:

$$\begin{aligned} &\forall|x-y_1| = b1 \quad x_+ = x_-, \quad y_{1+} = y_{1-}, \quad y_{2+} = y_{2-} \\ &\text{or } |x-y_2| = b2 \quad M\frac{dx_+}{dt} + m_1\frac{dy_{1+}}{dt} + m_2\frac{dy_{2+}}{dt} = M\frac{dx_-}{dt} + m_1\frac{dy_{1-}}{dt} + m_2\frac{dy_{2-}}{dt} \\ &\text{if } |x-y_1| = b1 \quad \frac{dx_+}{dt} - \frac{dy_{1+}}{dt} = -r\left(\frac{dx_-}{dt} - \frac{dy_{1-}}{dt}\right), \quad \frac{dy_{2+}}{dt} = \frac{dy_{2+}}{dt} \\ &\text{if } |x-y_2| = b2 \quad \frac{dx_+}{dt} - \frac{dy_{2+}}{dt} = -r\left(\frac{dx_-}{dt} - \frac{dy_{2-}}{dt}\right), \quad \frac{dy_{1+}}{dt} = \frac{dy_{1+}}{dt} \end{aligned} \tag{5.2}$$

The subscripts $+$ and $-$ indicate time immediately after and before impacts. r represents the restitution coefficient of impact.

5.3 Experimental observations

In this section, experiments are done for periodic and transient excitation respectively to compare the case with one VI NES and that with two VI NES. For periodic excitation, the experimentally obtained and used parameters are displayed at the first place. Then, the results under excitation with a single frequency and a range of frequency around resonance frequency are demonstrated to show the possible response regimes, and to compare the efficiency under different combinations of length of cavity. Regarding transient excitation, the same experimental device is applied and the objective is to verify the principle of separate activation.

5.3.1 Periodic excitation

Experimental setup

The global experimental configuration is showed in Fig. 5.2(a). Two VI NES are put inside two clearances of LO in parallel as demonstrated in Fig. 5.2 (b), and they can move freely inside. The whole system is embedded on an electrodynamic shaker with a

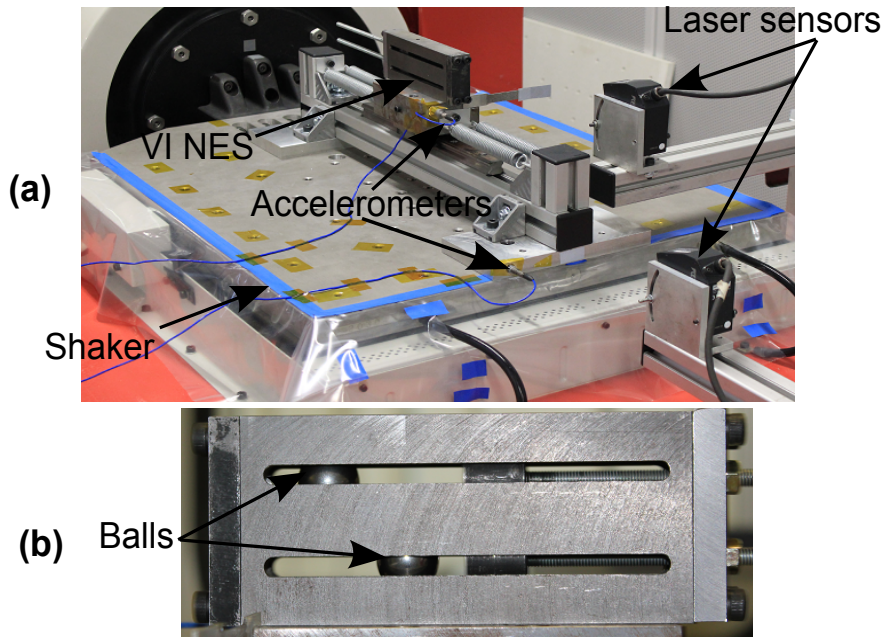

Fig. 5.2 Experimental setup: (a) global configuration; (b) detailed view of VI NES.

TABLE 5.1 Experimental parameters

Physical Parameters			
M	4.7 kg	C	3.02 Ns/m
K	$11.47 \cdot 10^3$ N/m		
m_1	32 g	m_2	32 g
b_1	$0 - 50$ mm	b_2	$0 - 50$ mm
Reduced Parameters			
ϵ	0.76 %	λ_1	1.91
f_0	7.86 Hz		
Single frequency test			
	f_r		$7.82 - 7.84$ Hz
Shaker acceleration			0.06 g
Frequency band test			
	$f_s - f_e$		$6.5 - 9$ Hz
Shaker acceleration			0.06 g

maximal force 10 kN. The displacement of LO as well as the imposed displacement of the shaker are measured by contact-less laser displacement sensors. Their accelerations are measured by accelerometers and the impacts between VI NES and LO can be judged from the sudden changes of the acceleration of LO. A detailed view of the configuration for two VI NES is presented in Fig. 5.2 (b). It simply consists of two closed clearances of lengths $d + 2 \cdot b1$ and $d + 2 \cdot b2$, respectively, where d is the diameter of both balls (VI NES). $b1$ and $b2$ are lengths of the above clearance and the below clearance, respectively, and each can be adjusted by a cylinder. The cylinder and the cover at the opposite side are made of hardened steel. The parameters of this system have been identified by performing modal analysis and are summarized in Table 5.1.

Single frequency excitation

The frequency of the sinusoidal excitation is slowly varied from 7.82 Hz to 7.84 Hz during 80 s, which can be considered almost fixed to the value 7.83 Hz. This value is closed to the natural frequency of LO ($f_0 = 7.86$ Hz). The acceleration of the shaker is fixed to 0.06 g. During the whole experimental process, the time histories of displacement and acceleration of LO are recorded.

With the change of the number of VI NES and different combinations of clearances b1 and b2, different periodic and transient response regimes are observed and demonstrated here. They are identified by the difference of impact numbers per cycle of LO, which can be judged from the time history of the acceleration of LO.

At first, the time history of the acceleration of LO without VI NES is showed in Fig. 5.3(a) as a reference. Although there exist small shakes at some of its maximal place, no impacts exist. In addition, its amplitude is highest compared to other cases coupled with VI NES. Then, the time history of the acceleration of LO with a VI NES for a clearance of 30 mm is showed in Fig. 5.3(b) as another reference. This value of clearance is proved to be almost optimal in the sense of vibration control and the response regime is two impacts per cycle (see chapter 3). It is not so easy to distinguish impacts because the order of impact strength is close to that of the acceleration of LO, but the impact number is observable during the process of experiment. Moreover, the peaks of acceleration are evidently reduced compared to the results in Fig. 5.3(a).

With the addition of another ball and different combinations of clearances, the response regimes will be more complicated. However, the possible variations are always based on the above two cases. Then, the regime with four impacts per cycle is observed with the addition of a second ball with clearance $b1 = 5$ mm (another ball with clearance $b2 = 30$ mm), and both ball impact twice per cycle as showed in Fig. 5.3(c), and the four impact moments during one cycle are marked out in rectangles. The acceleration of LO is further decreased compared to the optimized one ball case with 30 mm clearance, and this efficiency improvement cannot be easily judged here and will be demonstrated from the viewpoint of displacement later.

When the clearance of the added ball is increased to 40 mm, the response is compli-

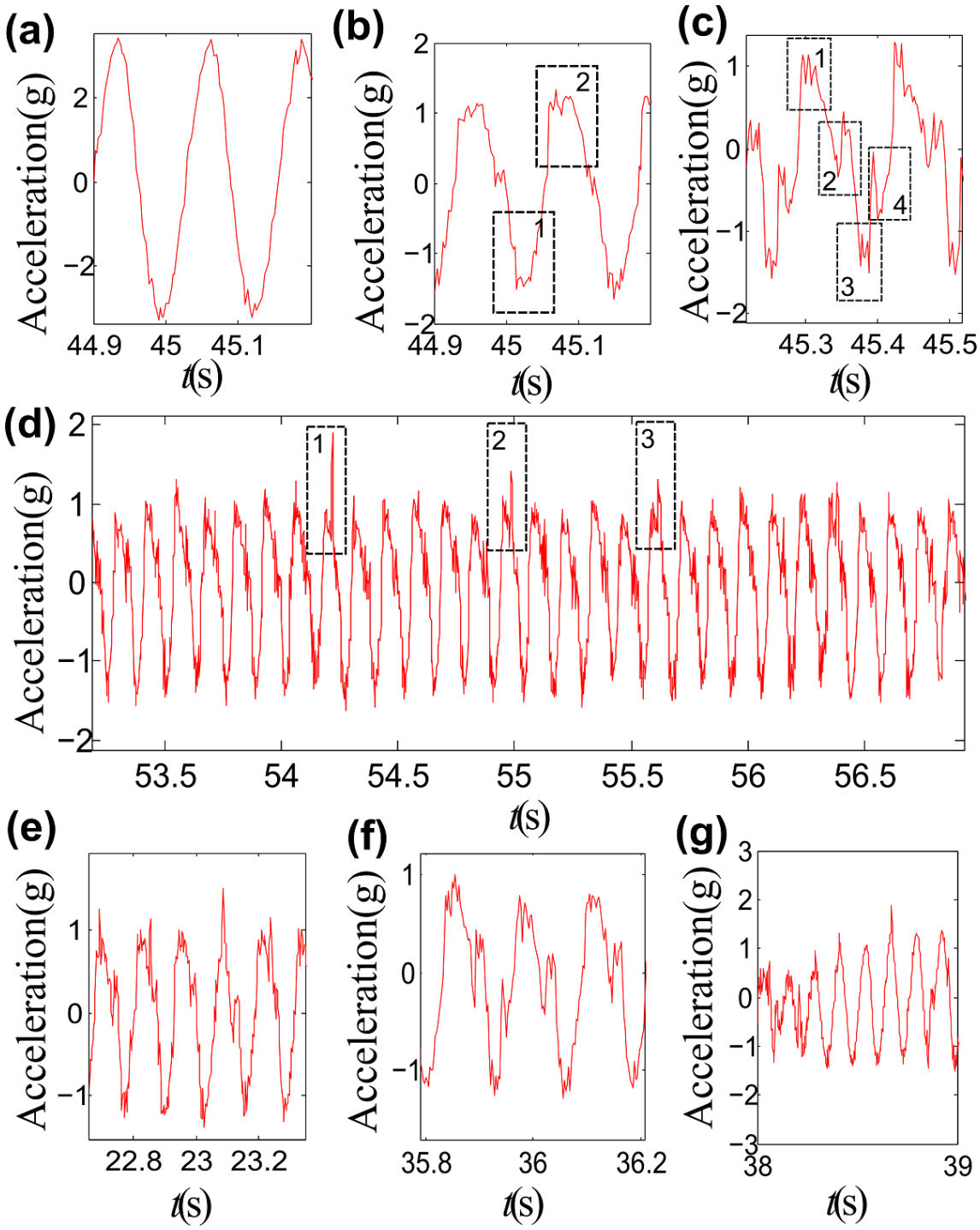

Fig. 5.3 Typical response regimes by comparison of impact numbers per cycle of the acceleration of LO and some impacts moments are marked out in rectangle: (a) no impact and no VI NES; (b) two impacts per cycle; (c) four impacts per cycle; (d) one VI NES impacts once during many cycles and another VI NES impacts twice per cycle; (e) one period of a response with at least one VI NES in the state of two impacts per cycle; (f) one period of a response with both VI NES in the state of two impacts per cycle; (g) one period of a response with both VI NES out of activation and no impact.

cated as displayed in Fig. 5.3(d). The ball below with $b2 = 30$ mm continuously impacts twice per cycle. In contrast, the added ball impacts only once during many cycles (> 1), and a few of them are marked out in rectangles.

In addition to the above relative stable response regimes, there exist some even more complicated transient response regimes during one time history for some combinations of clearances. For the case with $b1 = b2 = 30$ mm, there are some periods as showed in Fig. 5.3(e), in which just one ball is activated with two impacts per cycle, but this activated state can alternate between these two balls. This phenomenon is complicated, and it cannot be judged from the results showed here and can just be observed in the test site. There are also some periods, two balls impact twice per cycle as showed in Fig. 5.3(f) and there are even some periods there are almost no impacts as showed in Fig. 5.3(g).

Therefore, the strong nonlinear coupling between these two balls and LO is well observed by the complicated variations of response regimes during one time history. The above mentioned basic response regimes will be applied to explain the complication variation of efficiency, and this point is closely related to the targeted energy transfer by transient resonance captures.

In chapter 3, it is observed that the optimal response regime is the one with two impacts per cycle and around the entrance of SMR. The idea of optimization design is to make efficient response regimes occur for different excitations. This idea can still apply in the optimization design of two VI NES, namely to make each VI NES activated at its best state with two impacts per cycle.

Then, the efficiency comparison of different combinations of clearances is performed here to observe the possible relation between the types of response regimes and their efficiency. The two cases without VI NES and with one optimized VI NES (30 mm clearance) are chosen as two references as showed in Fig. 5.4(a-b).

The length of the down clearance $b2$ is fixed to 30 mm and only the upper clearance $b1$ is varied from 5 mm to 50 mm. Here, only the time histories of displacement are demonstrated for $b1 = 30$ mm and $b1 = 5$ mm, respectively. The former is displayed in Fig. 5.4(a), there are three typical areas A1, A2 and A3, which correspond to typical response regimes from Fig. 5.3(e) to Fig. 5.3(g), respectively. In area A1, there is a small decrease of amplitude compared to the one VI NES case in red curve. In area A2, both ball impact twice per cycle and the amplitude is lowest. In area A3, the occasional out of activation for both balls and the amplitude increases. In the whole process, there are many transitions between them, which results in the complicated variation of displacement amplitude of LO. It is a direct proof of nonlinear coupling between two VI NES and LO. In addition, the efficiency is highest when both balls impact twice per cycle, which is the most effective form of transient resonance captures.

This efficient targeted energy transfer is better demonstrated by the decrease of b1 to 5 mm as showed in Fig. 5.4(b). This time, both VI NES impact twice per cycle and it means the permanent resonance captures.

With the excitation of LO at the beginning, different activation amplitudes of LO with

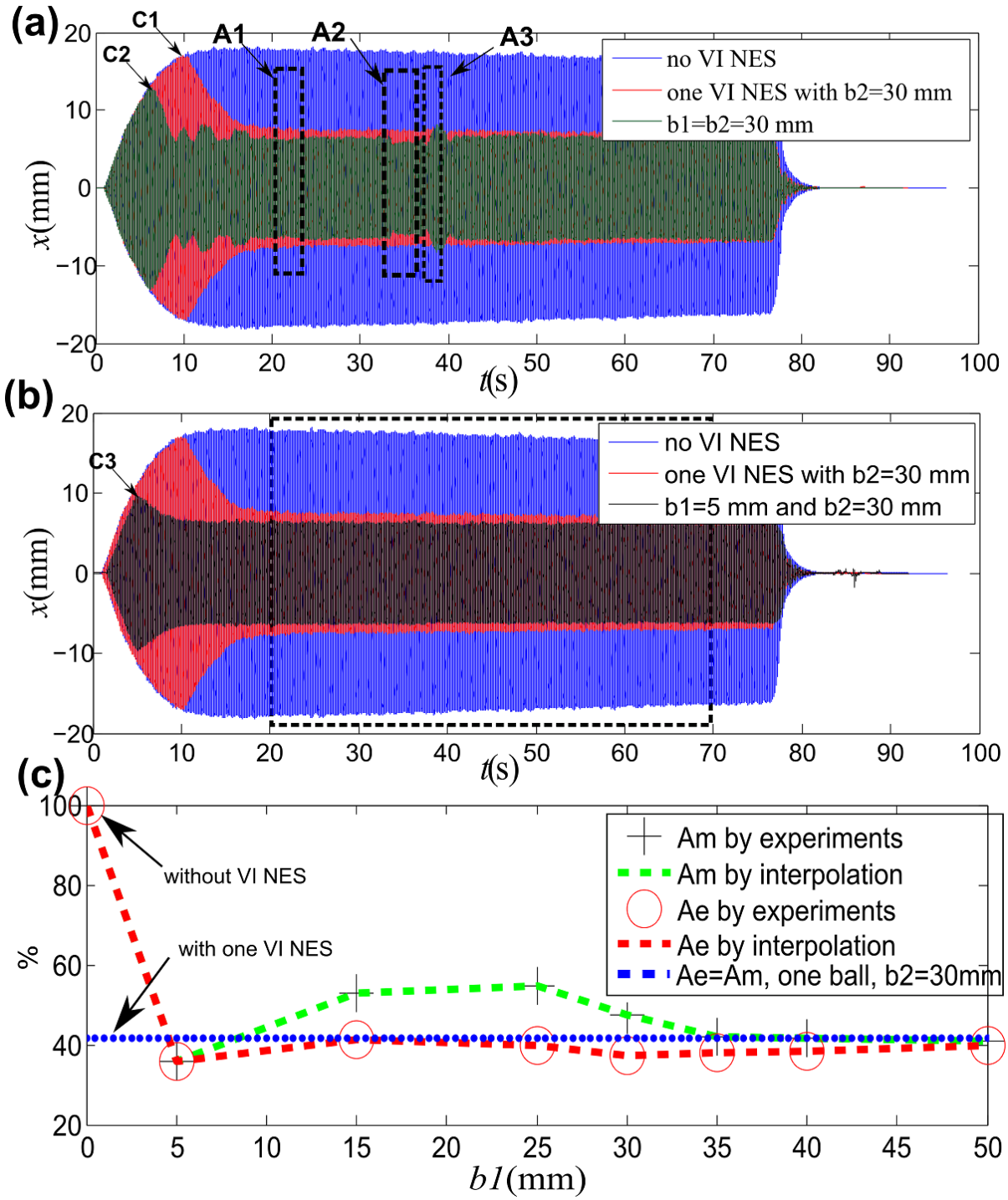

Fig. 5.4 Typical response regimes and their efficiency comparison with different combinations of clearances: (a-b) response regimes; (c) efficiency comparison by average and maximal amplitude ratios (Ae and Am).

different combinations of clearances are observed, namely C1, C2 and C3 in Fig. 5.4(a-b). With the increase of VI NES from 0 to 1, and then 2, the amplitude is evidently decreased at the activation point of VI NES. The same conclusion is obtained when the value of another clearance is decreased. In this sense, the robustness and efficiency can be improved.

Then, the average and maximal amplitude ratios between the case with VI NES and without NES are calculated for all cases during a stable time period (20-70 s), and the results are showed in Fig. 5.4(c). Compared to the case without VI NES and with one VI NES, the optimal case is the addition of another VI NES with a small clearance 5 mm. For other cases with large clearances, it cannot improve the efficiency and, in return, it will result in the occasional out of activation of VI NES, and meanwhile, the large displacement of LO.

According to the optimization design criterion proposed in chapter 3, the design of parameters is to make the efficient response regimes appear and it means the most efficient transfer and dissipation of energy. From the above experimental results with limited combinations of clearances, this optimization design criterion still applies since both balls impacts twice in the optimal case with $b1 = 5$ mm. However, the phase difference of two VI NES cannot be measured or calculated, it may be another factor related to efficiency.

Except the above combinations of clearances, experiments with the same clearance for both VI NES are also performed. The average and maximal amplitude ratios are also calculated and showed in Fig. 5.5. From the viewpoint of Ae, the case with $b1 = b2 = 30$ mm is optimal. On the contrary, the case with $b1 = b2 = 15$ mm is optimal in terms of Am. Generally speaking, they are less effective than the combination with $b1 = 5$ mm and b2=30 mm.

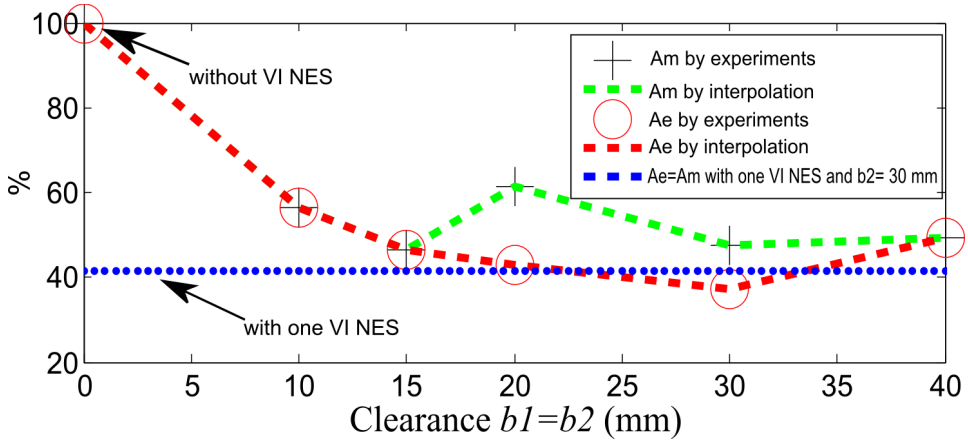

Fig. 5.5 Efficiency comparison of different response regimes with the same clearance for both VI NES.

As a summary, the objective to find the relation between response regimes and their efficiency is accomplished in two steps. The first step is to find basic response regimes.

Then, they are applied to explain the complicated variation of response. As a result, a general design criterion can also be proposed here: the design of two VI NES is to make them activated around most efficient response regimes.

Excitation with a band of frequency

Then, the band of excitation frequency is enlarged around the natural frequency of LO. The objective here is to study the influence of different combinations of clearances on the response regimes and their efficiency. The starting frequency f_s and ending frequency f_e during this sweep is showed in Table 5.1 and the acceleration is still fixed to 0.06 g.

For the above experimental configuration, the one VI NES case with a clearance 27.5 mm has been observed optimal. Here the clearance of an added VI NES is selected around this value. The displacement of LO is recorded for different combinations of $b1$ and $b2$ and is showed in Fig. 5.6. The results with fixed $b2 = 27.5$ mm and varying $b1$ are showed in Fig. 5.6(a). The combination of $b1 = 12.5$ mm and $b2 = 27.5$ mm is generally more optimal in this case. Then, the results with equal $b1$ and $b2$ are showed in Fig. 5.6(b). For frequencies a little below the resonance frequency, the combination of $b1 = 27.5$ mm and $b2 = 27.5$ mm is better, but the other two are better for frequencies a little higher than the resonance frequency. To have a close view, the results between two relative optimal cases are compared in Fig. 5.6(c). In area A, it is observed that VI NES can be activated at a lower value of displacement amplitude for a smaller $b1$. In area B, two VI NES are in regime with two impacts per cycle for $b1 = 27.5$ mm. On the contrary, one ball occasionally gets out of activation for $b1 = 12.5$ mm and results in the transient build-up of amplitude. In area C, low $b1 = 12.5$ mm still can be activated for lower amplitude and results in the reduction of amplitude. As has been demonstrated under the excitation with a fixed frequency, the variation of motion for LO and both VI NES can be more complicated than the above-mentioned characteristics. Except the observed relation between efficiency and the response regimes, it is desirable to obtain further information but this kind of try would be difficult.

Therefore, the following optimization design criterion is recommended. If just one ball is applied, it is recommended that VI NES should be optimized at the point of natural frequency. If two VI NES are applied to improve the robustness and increase efficiency, a smaller length of clearance should be chosen compared to the optimized clearance of the one ball case to avoid the occasional failure.

5.3.2 Transient excitation

Experimental setup

The same experimental device as the periodic case is used, but it is attached to a cast iron bench as showed in Fig. 5.7(a). The addition of a small ring bolt for pre-stretch will not influence the total mass of LO and its influence can be neglected. Therefore, its parameters are nearly the same as these in Table 5.1. One laser sensor and one

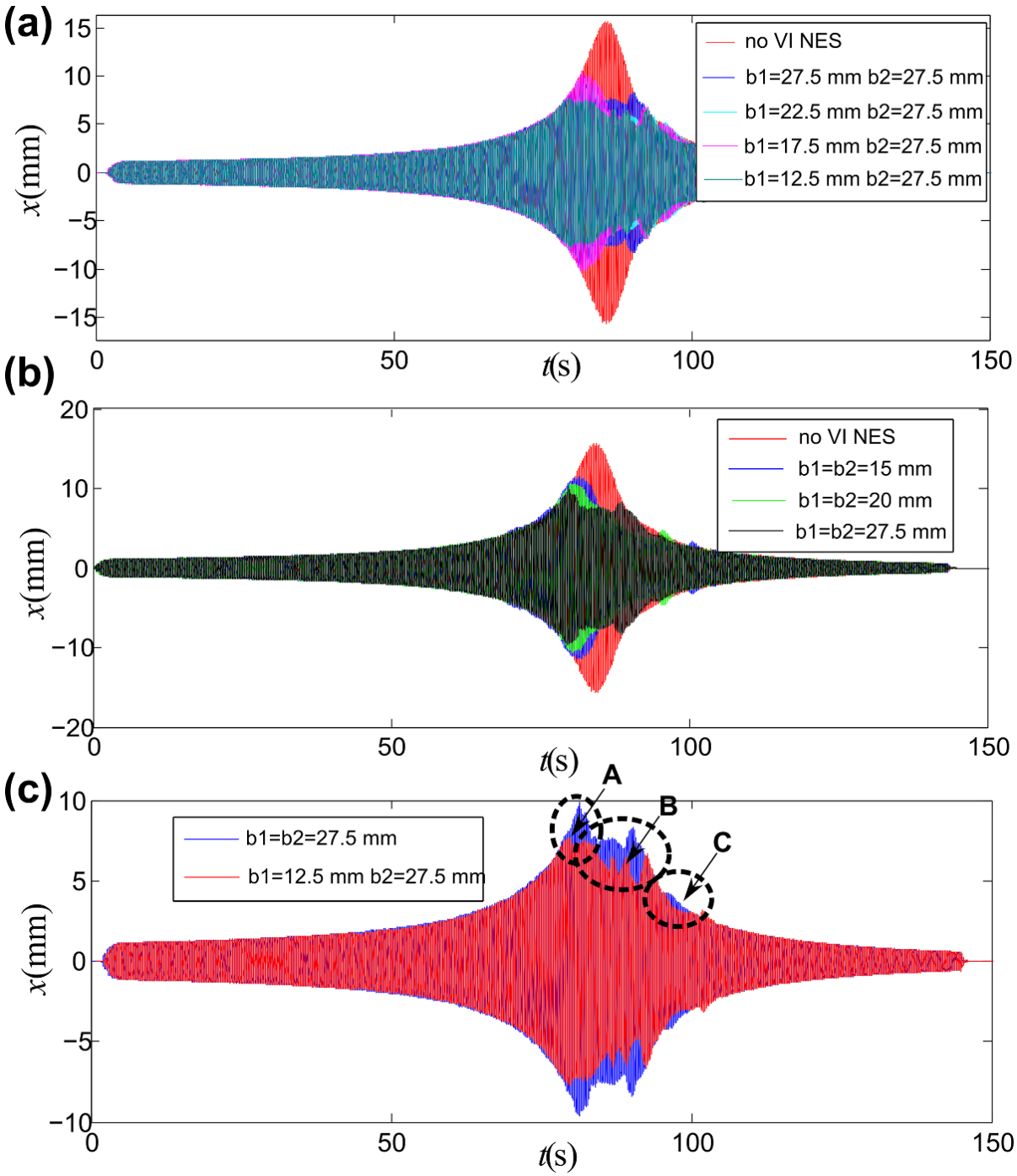

Fig. 5.6 Responses of LO during the sweep experiments and efficiency comparison: (a) with different $b1$ and $b2$; (b) with the same $b1$ and $b2$; (c) the efficiency comparison for two relative optimal cases.

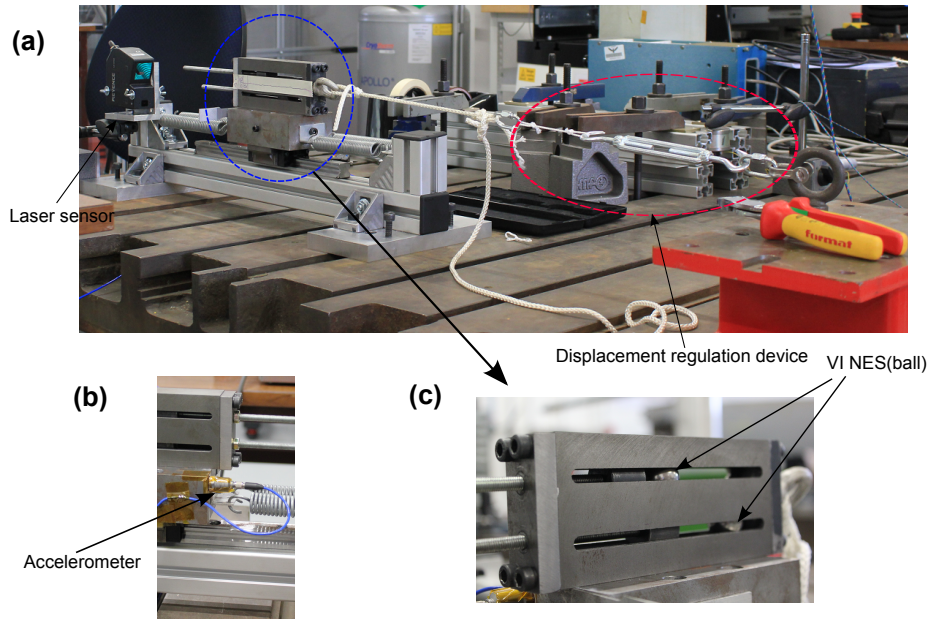

Fig. 5.7 Experimental setup: (a) global configuration; (b) installation of accelerometer; (c) detailed view of VI NES.

accelerometer are used to measure the displacement and acceleration of LO, respectively. The fixation of accelerometer is showed in Fig. 5.7(b) and a detailed view of VI NES is displayed in Fig. 5.7(c). The number of balls can be changed. The initial displacement of LO is regulated by a device and is fixed to 20 mm for all tests. The initial location of two balls are at random, and the velocities for LO and both balls are zero. Since only the stable transition process is studied and the transient process quickly disappears, the initial conditions will not influence the expected conclusion.

Principle of separate activation

With two sets of $b1$ and $b2$, the responses of two cases are compared here. For the case with one VI NES ($b2 = 20$ mm), the time history of displacement of LO is represented by the red curve in Fig. 5.8(a) and its corresponding acceleration is showed in Fig. 5.8(b). The points A1 and A2 are related to the transition from the regime with two impacts per cycle to that without any continuous period of two impacts per cycle.

For the case with two balls ($b1 = 2$ mm and $b2 = 20$ mm), the time history of displacement of LO is represented by the blue curve in Fig. 5.8(a) and its corresponding acceleration is showed in Fig. 5.8(c). The first VI NES with $b2 = 20$ mm gets out of two impacts per cycle around points B1 and B2. The second VI NES with a small clearance $b1 = 2$ mm gets out of two impacts per cycle around points C1 and C2. In zone 1, the first VI NES with a large clearance is activated with two impacts per cycle. In zone 2, the first VI NES gets out of activation and the second VI NES with a small clearance is

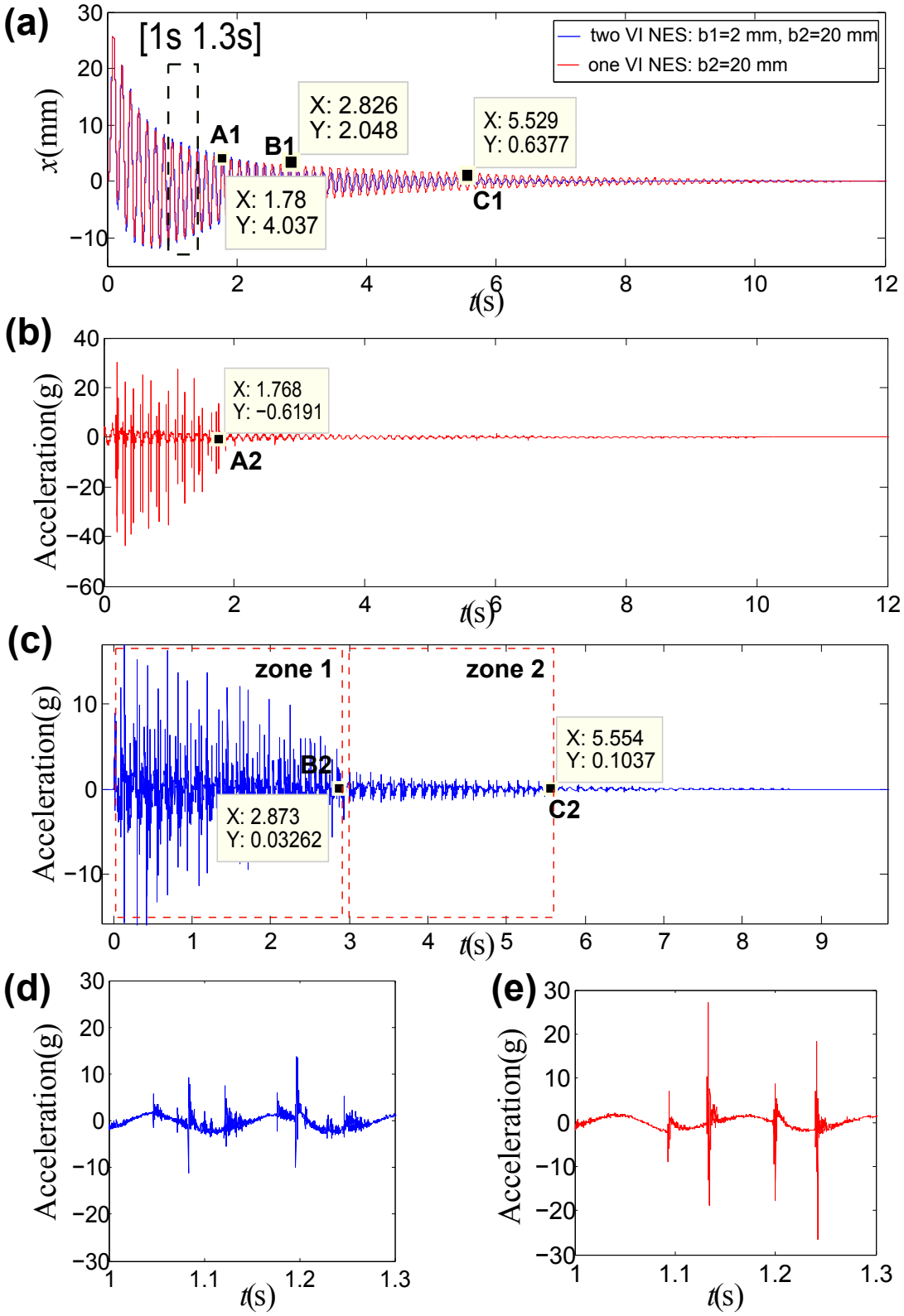

Fig. 5.8 Response comparison between LO coupled with one VI NES and two VI NES: (a) an imposed time history of displacement; (b) a time history of acceleration with one VI NES; (c) a time history of acceleration with two VI NES; (d) a detailed view of one period of acceleration with two VI NES; (e) a detailed view of one period of acceleration with one VI NES.

activated with two impacts per cycle. In the sense of the activation with two impacts per cycle, the principle of separate activation of VI NES with different clearances is observed here. This definition of activation is important, since the regime with two impacts per cycle is most efficient in vibration control.

Then, the decay rates of displacements for both cases are compared. Before point A1, there is almost no difference, since the first VI NES with large clearance is activated with two impacts per cycle and the second VI NES behaves in low efficient regime (more than two impacts per cycle). Between A1 and B1, the role of the second VI NES increases but still small. In contrast, it plays an important role between B1 and C1 since it is activated with two impacts per cycle and the first VI NES is totally out of excitation. The difference of decay rates in this period is relative large. Here, the role of separate activation in vibration control is evident, and the two VI NES with difference clearances can be effective at different ranges of displacement amplitude. More importantly, this effectiveness is related to the efficient response regime with two impacts per cycle.

During the above transition process, the first VI NES changes from two impacts per cycle to the state with no continuous periods of two impacts per cycle (i.e., permanent out of activation), the limit point is A1. It means that it plays the main role in vibration control before A1. In contrast, the second VI NES changes from more than two impacts per cycle to two impacts per cycle, and finally out of activation, it plays a main role in vibration control between B1 and C1. Between A1 and B1, it is the overlapping period. Evidently, the second VI NES undergoes more response regimes and could possess four impacts per cycle, three impacts per cycle and two impacts per cycle etc., which are closely related to different transient resonance captures.

In addition to displacement decay rates, impacts reflected by acceleration can also reveal some important characteristics. The time histories of acceleration of LO from 1 s to 1.3 s are taken out for both cases, as showed in Fig. 5.8(d) for two VI NES case and in Fig. 5.8(e) for one VI NES case. With the addition of another ball, the impact strengths are decreased and the impacts are scattered. As observed by other researchers, the regime with strong impact strengths but less impact numbers is replaced by that with weak and more impacts, but the whole energy reduction rate is not improved.

The principle of separate activation is also observed from results with other combinations of clearances as showed in Fig. 5.9. The separate points for the out of activation of the VI NES with a large clearance are marked out in each subfigure. The horizontal arrows demonstrate the two activation levels for two different clearances, and the vertical arrows denote the change between them.

In summary, the principle of separate activation of VI NES is observed, and the effectiveness of the vibration control can be increased to a large range of displacement amplitude of LO. Moreover, the addition of VI NES can reduce impact strengths and scatter impacts though it may not increase the efficiency of vibration control.

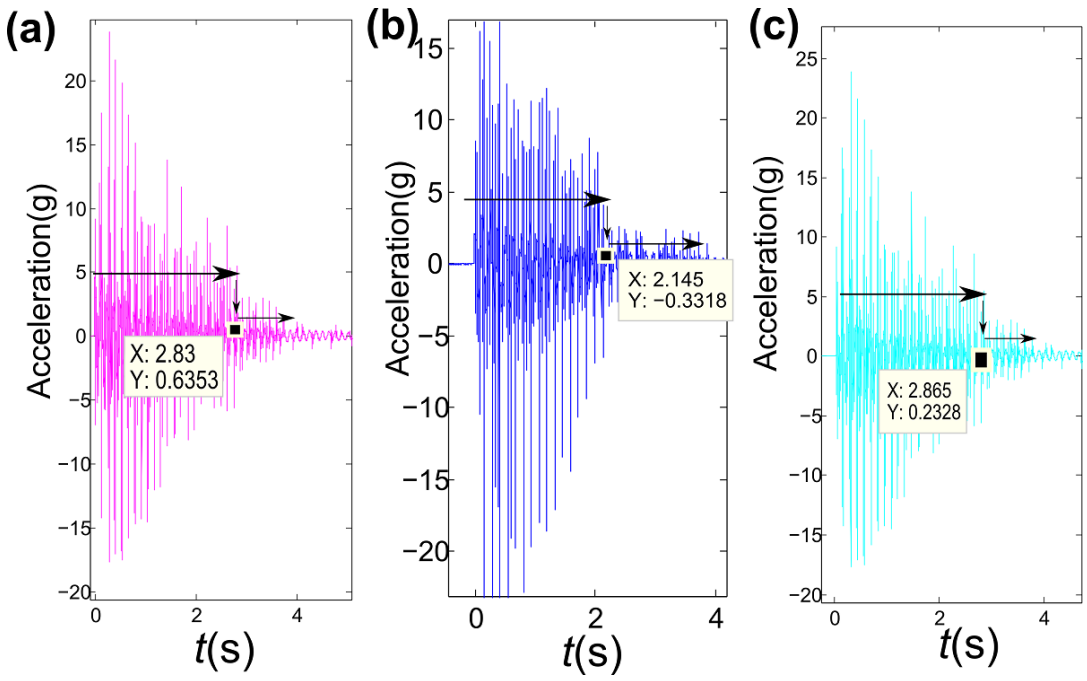

Fig. 5.9 Principle of separate activation: (a) $b1 = 5$ mm and $b2 = 20$ mm; (b) $b1 = 5$ mm and $b2 = 30$ mm; (c) $b1 = 5$ mm and $b2 = 40$ mm.

5.4 Conclusion

In this chapter, a LO coupled with two VI NES in parallel is experimentally studied under periodic and transient excitations. At first, its mechanical model and equation of motion are presented. Then, experiments under both periodic and transient excitations are performed, respectively.

Through experiments under different excitations, different response regimes are observed and their relation to their efficiency is analyzed. Whatever types of excitation, it is more effective as long as the two VI NES are activated with two impacts per cycle or around this regime. In addition to this common law, the results are complicated from the viewpoint of each excitation type. This observation proves the relevance and effectiveness of analytical study around SIM, more precisely, around the response regime with two impacts per cycle (i.e., resonance captures).

More specifically about experimental results, several points should be pointed out. Firstly , different basic periodic and transient response regimes are observed and analyzed from the experimental results under excitation with a fixed frequency. In addition, more complicated responses are observed but they can be explained by these basic response regimes. Then, they are applied to explain the complicated variation of response regimes, not only for excitation with a fixed frequency and a range frequency, but also for transient excitation. All observations here prove the important role of the regime with two impacts per cycle. Under transient excitation, this role is further demonstrated by the separate activation of VI NES of different clearances. This separate activation of VI NES with two

impacts per cycle can be applied to control vibration at different levels of displacement amplitude. Sometimes, although the addition of VI NES cannot improve the efficiency of vibration control, the impacts are scattered and their strengths are reduced.

Conclusion

The work of this thesis is dedicated to the passive vibration control through a nonlinear energy absorber termed as VI NES. All studies, no matter analytical, numerical or experimental, are tightly around the five questions raised in the introduction. The responses are almost positive as follows:

- The interacting force can play the intermediate and central role for the explanation of different response regimes.
- The influence of parameters on the occurrence of response regimes and on their efficiency can be studied respectively.
- The underlying optimization design mechanism for different types of excitation is based on the efficiency of response regimes and it is the same in this sense.
- The optimization design of VI NES to control vibration of nonlinear systems can be simplified to the optimal activation of VI NES for a corresponding linear system.
- The principle of separate activation can improve the efficiency and robustness of the vibration control.

Developed around them, the work of this thesis is organized in five chapters. In the first chapter, the general background and the state of the art is introduced. The latter is developed around two axes: NES with cubic nonlinearity and VI NES. The general study results are presented for cubic NES. More importantly, its unresolved problems are exposed, e.g., whether the optimization design mechanism under different excitations is the same and how to optimize NES for nonlinear systems. As for VI NES (impact damper), its former study demonstrates that its main limitation results from the used analytical method. Therefore, it is clear that the objective is to further study this energy absorber in the new context of TET.

In the second chapter, a general equation of motion including an interacting force is established to describe the variation of non-stationary responses. Except fixed points for steady state responses, this interacting force is not constant and cannot be analytically calculated, but it has proved convenient and easier in explaining and understanding the actual variation of responses. Based on the observation that the 1:1 resonance is the main responsible for efficient TET, it is interested in the study of influences of different parameters on the occurrence of response regimes around 1:1 resonance, which is identified as two impacts two cycle of LO. Based on this idea, the goal of optimal design of different parameters is the same, i.e., to make the regime with two impacts per cycle appear. In addition, the bifurcation and its variation routes, which have been observed so different by different study results, can be explained in the same mechanism this time.

The experimental results have showed the existence of different response regimes and proved a typical bifurcation route: from one type of highly irregular response to regular response like two impacts per cycle, and finally to another highly irregular response regimes. About SMR, its chaotic and strongly modulated characteristic are experimentally observed and explained this time, and its phenomenon of TET is explained in detail. The efficiency comparison of different response regimes is carried out in the next chapter with more details.

In chapter three, the optimization design mechanism for different types of excitation is studied. For periodic excitation with a single frequency, the response regime between that with two impacts per cycle and SMR is proved to be the most efficient by numerical and experimental results. For transient excitation, the initial starting response should be designed a little distant from the optimal response regime and make the efficient TET last for a while. For the actual optimal design of VI NES for a range of frequency around resonance frequency, the optimal objective can be simplified to the optimization design of VI NES under the excitation with the resonance frequency. In a word, the optimization design for different excitations is based on the same efficiency law of response regimes. Therefore, their optimization design mechanism is the same in this sense.

Since VI NES will be excited at its best state with the regime of two impacts per cycle, this characteristic is applied to the optimal design for the vibration control of nonlinear systems in chapter four. Through an analytical analysis of SIM, it is found that VI NES will be activated at some range of displacement amplitude of LO and will have the same state of activation for systems with different frequencies. Based on this, a deign procedure of VI NES is proposed for nonlinear systems, i.e., to optimally design VI NES for a corresponding LO that is chosen most similar to the original nonlinear system. Then, this characteristic of VI NES is observed by comparing the response of three LO with different stiffness and one duffing system by numerical and experimental results. Finally, this characteristic and design procedure is applied to control the chatter of a turning system. The preliminary numerical results are positive.

Finally, a LO coupled with two VI NES in parallel under periodic excitation is studied to improve the efficiency and robustness. The former analytical development is analyzed. The analytical results can be applied to calculate fixed points and judge different response regimes, especially SMR. Different response regimes are observed by experimental tests. From the limited experimental results, it is observed that the efficiency of vibration control depends on the number of VI NES activated with two impacts per cycle. For example, under periodic excitations, two VI NES activated with two impacts per cycle is more effective than the case with just one VI NES activated. Under transient excitation, two VI NES, which are designed with different clearances and activated with this response regime, can control the vibration at different levels of displacement amplitude. However, the addition of another ball may result in the occasional out of activation of the other VI NES and even both VI NES. Therefore, the length of cavity should be carefully selected.

Following this work, several points of research can be envisaged:

- One VI NES

- ➔ Response regimes should be studied further, especially the chaotic characteristic of SMR and some highly irregular responses. Lyapunov exponent should be calculated.
- ➔ The other impact model maybe adopted to improve the accuracy.
- ➔ The activation characteristics of VI NES should be studied further, especially with more precise experimental validations.
- ➔ The study is limited to periodic and transient excitation, and other excitation such as random excitation should be studied.

- Multi VI NES
  - ➔ Since the activation of VI NES depends on the range of displacement amplitude of LO and clearance, it is desirable to further study the combination of different VI NES with different clearances or even other parameters.
  - ➔ It is possible to increase the number of VI NES or change the configuration of multi VI NES.
- Other NES
  - ➔ Although the optimization design mechanism for different excitations is obtained just for VI NES, it is studied under the context of TET, and therefore it is reasonable to generalize the results to other NES or even other absorbers.
  - ➔ The characteristic of VI NES to be excited at a range of displacement amplitude of main systems with the same effectiveness for different frequencies is interesting. Actually every NES should possess its own characteristic (e.g., bi-stable) and it is desirable to study and apply the own characteristic.
  - ➔ The idea that the optimization design of VI NES coupled to nonlinear systems can be simplified to the optimization design of VI NES coupled to a LO close to the objective nonlinear system should be generalized to other types of NES, or more general, energy absorbers.
- Applications
  - ➔ Further study about the application of VI NES to the control of chatter, e.g., experimental validations.
  - ➔ Further study about the application of VI NES to control vibration of other nonlinear systems.

Glossary of principle abbreviations

FEP:	Frequency Energy Plot
HBM:	Harmonic Balance Method
LO:	Linear Oscillator
LPT:	Limiting Phase Trajectories
MSM:	Multiple Scales Method
NES:	Nonlinear Energy Sink
NNM:	Nonlinear Normal Mode
SIM:	Slow Invariant Manifold
SMR:	Strongly Modulated Response
TET:	Targeted Energy Transfer
TMD:	Tuned Mass Damper
VI NES:	Vibro-Impact Nonlinear Energy Sink

Bibliography

[Avramov and Gendelman, 2010] Avramov, K. and Gendelman, O. (2010). On interaction of vibrating beam with essentially nonlinear absorber. *Meccanica*, 45(3):355–365. *Cited page 17*

[Babitsky, 2013] Babitsky, V. I. (2013). *Theory of vibro-impact systems and applications*. Springer Science & Business Media. *Cited page 19*

[Bapat, 1995] Bapat, C. (1995). The general motion of an inclined impact damper with friction. *Journal of Sound and Vibration*, 184(3):417–427. *Cited page 46*

[Bapat and Bapat, 1988] Bapat, C. and Bapat, C. (1988). Impact-pair under periodic excitation. *Journal of Sound and Vibration*, 120(1):53–61. *Cited page 20*

[Bapat *et al.*, 1983] Bapat, C., Popplewell, N. and McLachlan, K. (1983). Stable periodic motions of an impact-pair. *Journal of Sound and Vibration*, 87(1):19–40. *4 citations pages 20, 26, 37, and 46*

[Bapat and Sankar, 1985] Bapat, C. and Sankar, S. (1985). Single unit impact damper in free and forced vibration. *Journal of Sound and Vibration*, 99(1):85–94. *3 citations pages 20, 55, and 56*

[Bellet *et al.*, 2012] Bellet, R., Cochelin, B., Côte, R. and Mattei, P.-O. (2012). Enhancing the dynamic range of targeted energy transfer in acoustics using several nonlinear membrane absorbers. *Journal of Sound and Vibration*, 331(26):5657–5668. *Cited page 17*

[Bellet *et al.*, 2010] Bellet, R., Cochelin, B., Herzog, P. and Mattei, P.-O. (2010). Experimental study of targeted energy transfer from an acoustic system to a nonlinear membrane absorber. *Journal of Sound and Vibration*, 329(14):2768–2791. *2 citations pages 17 and 18*

[Benacchio *et al.*, 2016] Benacchio, S., Malher, A., Boisson, J. and Touzé, C. (2016). Design of a magnetic vibration absorber with tunable stiffnesses. *Nonlinear Dynamics*, pages 1–19. *Cited page 11*

[Bergeot *et al.*, 2016] Bergeot, B., Bellizzi, S. and Cochelin, B. (2016). Analysis of steady-state response regimes of a helicopter ground resonance model including a non-linear energy sink attachment. *International Journal of Non-Linear Mechanics*, 78:72–89. *Cited page 18*

[Blazejczyk-Okolewska, 2001] Blazejczyk-Okolewska, B. (2001). Analysis of an impact damper of vibrations. *Chaos, Solitons & Fractals*, 12(11):1983–1988. *Cited page 21*

[Brown, 1988] Brown, G. V. (1988). Survey of impact damper performance. *Cited page 20*

[Cochelin and Vergez, 2009] Cochelin, B. and Vergez, C. (2009). Manlab, an interactive path following software. *Cited page 13*

[Dhooge *et al.*, 2003] Dhooge, A., Govaerts, W. and Kuznetsov, Y. A. (2003). Matcont: a matlab package for numerical bifurcation analysis of odes. *ACM Transactions on Mathematical Software (TOMS)*, 29(2):141–164. *Cited page 13*

[Doedel *et al.*, 2007] Doedel, E. J., Fairgrieve, T. F., Sandstede, B., Champneys, A. R., Kuznetsov, Y. A. and Wang, X. (2007). Auto-07p: Continuation and bifurcation software for ordinary differential equations. *Cited page 13*

[Ema and Marui, 1994] Ema, S. and Marui, E. (1994). A fundamental study on impact dampers. *International Journal of Machine Tools and Manufacture*, 34(3):407–421. *Cited page 20*

[Festjens *et al.*, 2014] Festjens, H., Chevallier, G. and Dion, J. (2014). Nonlinear model order reduction of jointed structures for dynamic analysis. *Journal of Sound and Vibration*, 333(7):2100–2113. *Cited page 12*

[Frahm, 1911] Frahm, H. (1911). Device for damping vibrations of bodies. US Patent 989,958. *Cited page 10*

[Gendelman, 2012] Gendelman, O. (2012). Analytic treatment of a system with a vibro-impact nonlinear energy sink. *Journal of Sound and Vibration*, 331(21):4599–4608. *3 citations pages 11, 21, and 39*

[Gendelman and Alloni, 2015] Gendelman, O. and Alloni, A. (2015). Dynamics of forced system with vibro-impact energy sink. *Journal of Sound and Vibration*, 358:301–314. *7 citations pages 11, 16, 21, 32, 35, 39, and 57*

[Gendelman and Alloni, 2016] Gendelman, O. and Alloni, A. (2016). Forced system with vibro-impact energy sink: Chaotic strongly modulated responses. *Procedia IUTAM*, 19:53–64. *6 citations pages 11, 21, 32, 35, 39, and 57*

[Gendelman and Bar, 2010] Gendelman, O. and Bar, T. (2010). Bifurcations of self-excitation regimes in a van der pol oscillator with a nonlinear energy sink. *Physica D: Nonlinear Phenomena*, 239(3):220–229. *Cited page 18*

[Gendelman *et al.*, 2001] Gendelman, O., Manevitch, L., Vakakis, A. and M'Closkey, R. (2001). Energy pumping in nonlinear mechanical oscillators: Part i: Dynamics of the underlying hamiltonian systems. *Journal of Applied Mechanics*, 68(1):34–41. *2 citations pages 11 and 14*

[Gendelman *et al.*, 2012] Gendelman, O., Sigalov, G., Manevitch, L., Mane, M., Vakakis, A. and Bergman, L. (2012). Dynamics of an eccentric rotational nonlinear energy sink. *Journal of applied mechanics*, 79(1):011–012. *Cited page 11*

[Gendelman *et al.*, 2008] Gendelman, O., Starosvetsky, Y. and Feldman, M. (2008). Attractors of harmonically forced linear oscillator with attached nonlinear

energy sink i: Description of response regimes. *Nonlinear Dynamics*, 51(1-2):31–46. *Cited page 17*

[Gendelman, 2004] Gendelman, O. V. (2004). Bifurcations of nonlinear normal modes of linear oscillator with strongly nonlinear damped attachment. *Nonlinear Dynamics*, 37(2):115–128. *Cited page 15*

[Georgiades and Vakakis, 2007a] Georgiades, F. and Vakakis, A. (2007a). Dynamics of a linear beam with an attached local nonlinear energy sink. *Communications in Nonlinear Science and Numerical Simulation*, 12(5):643–651. *Cited page 17*

[Georgiades and Vakakis, 2007b] Georgiades, F. and Vakakis, A. (2007b). Passive targeted energy transfers and strong modal interactions in a thin plate with strongly nonlinear end attachments of different configurations. *in ASME 2007 International Design Engineering Technical Conferences and Computers and Information in Engineering Conference*, pages 1355–1370. American Society of Mechanical Engineers. *Cited page 17*

[Georgiades *et al.*, 2007] Georgiades, F., Vakakis, A. F. and Kerschen, G. (2007). Broadband passive targeted energy pumping from a linear dispersive rod to a lightweight essentially non-linear end attachment. *International Journal of Non-Linear Mechanics*, 42(5):773–788. *Cited page 17*

[Gourc, 2013] Gourc, E. (2013). *Etude du contrôle passif par pompage énergétique sous sollicitation harmonique: Analyses théoriques et expérimentales.* Thèse de doctorat, Toulouse, INSA. *3 citations pages 22, 30, and 88*

[Gourc *et al.*, 2014] Gourc, E., Michon, G., Seguy, S. and Berlioz, A. (2014). Experimental investigation and design optimization of targeted energy transfer under periodic forcing. *Journal of Vibration and Acoustics*, 136(2):021021. *2 citations pages 16 and 17*

[Gourc *et al.*, 2015a] Gourc, E., Michon, G., Seguy, S. and Berlioz, A. (2015a). Targeted energy transfer under harmonic forcing with a vibro-impact nonlinear energy sink: Analytical and experimental developments. *Journal of Vibration and Acoustics*, 137(3):031008. *5 citations pages 11, 16, 20, 21, and 38*

[Gourc *et al.*, 2015b] Gourc, E., Seguy, S., Michon, G., Berlioz, A. and Mann, B. (2015b). Quenching chatter instability in turning process with a vibro-impact nonlinear energy sink. *Journal of Sound and Vibration*, 355:392–406. *3 citations pages 18, 21, and 80*

[Hahn, 1996] Hahn, S. L. (1996). *Hilbert transforms in signal processing.* Artech House. *Cited page 14*

[Huang, 2014] Huang, N. E. (2014). *Hilbert-Huang transform and its applications*, volume 16. World Scientific. *Cited page 14*

[Ibrahim, 2009] Ibrahim, R. A. (2009). *Vibro-impact dynamics: modeling, mapping and applications*, volume 43. Springer Science & Business Media. *4 citations pages 19, 20, 23, and 39*

[Karayannis *et al.*, 2008] Karayannis, I., Vakakis, A. and Georgiades, F. (2008). Vibro-impact attachments as shock absorbers. *Proceedings of the Institution of Mechanical Engineers, Part C: Journal of Mechanical Engineering Science*, 222(10):1899–1908. *Cited page 11*

[Kerschen *et al.*, 2008] Kerschen, G., Gendelman, O., Vakakis, A. F., Bergman, L. A. and McFarland, D. M. (2008). Impulsive periodic and quasi-periodic orbits of coupled oscillators with essential stiffness nonlinearity. *Communications in Nonlinear Science and Numerical Simulation*, 13(5):959–978. *Cited page 16*

[Kerschen *et al.*, 2009] Kerschen, G., Peeters, M., Golinval, J.-C. and Vakakis, A. F. (2009). Nonlinear normal modes, part i: A useful framework for the structural dynamicist. *Mechanical Systems and Signal Processing*, 23(1):170–194. *Cited page 12*

[Kerschen *et al.*, 2006] Kerschen, G., Worden, K., Vakakis, A. F. and Golinval, J.-C. (2006). Past, present and future of nonlinear system identification in structural dynamics. *Mechanical systems and signal processing*, 20(3):505–592. *Cited page 7*

[Korsch *et al.*, 2007] Korsch, H. J., Jodl, H.-J. and Hartmann, T. (2007). *Chaos: a program collection for the PC*. Springer Science & Business Media. *Cited page 41*

[Lamarque *et al.*, 2011] Lamarque, C.-H., Gendelman, O. V., Savadkoohi, A. T. and Etcheverria, E. (2011). Targeted energy transfer in mechanical systems by means of non-smooth nonlinear energy sink. *Acta mechanica*, 221(1-2):175–200. *2 citations pages 11 and 16*

[Lee *et al.*, 2009] Lee, Y., Nucera, F., Vakakis, A., McFarland, D. and Bergman, L. (2009). Periodic orbits, damped transitions and targeted energy transfers in oscillators with vibro-impact attachments. *Physica D: Nonlinear Phenomena*, 238(18):1868–1896. *3 citations pages 11, 20, and 21*

[Lee *et al.*, 2007] Lee, Y., Vakakis, A., Bergman, L., McFarland, D. M. and Kerschen, G. (2007). Suppression aeroelastic instability using broadband passive targeted energy transfers, part 1: Theory. *AIAA journal*, 45(3):693–711. *Cited page 18*

[Lee *et al.*, 2008] Lee, Y., Vakakis, A. F., Bergman, L., McFarland, D., Kerschen, G., Nucera, F., Tsakirtzis, S. and Panagopoulos, P. (2008). Passive non-linear targeted energy transfer and its applications to vibration absorption: a review. *Proceedings of the Institution of Mechanical Engineers, Part K: Journal of Multi-body Dynamics*, 222(2):77–134. *2 citations pages 11 and 14*

[Lee *et al.*, 2005] Lee, Y. S., Kerschen, G., Vakakis, A. F., Panagopoulos, P., Bergman, L. and McFarland, D. M. (2005). Complicated dynamics of a linear oscillator with a light, essentially nonlinear attachment. *Physica D: Nonlinear Phenomena*, 204(1):41–69. *Cited page 12*

[Lieber and Jensen, 1945] Lieber, P. and Jensen, D. (1945). An acceleration damper: development, design and some applications. *Trans. ASME*, 67(10):523–530. *Cited page 19*

[Manevitch, 2001] Manevitch, L. (2001). The description of localized normal modes in a chain of nonlinear coupled oscillators using complex variables. *Nonlinear Dynamics*, 25(1-3):95–109. *Cited page 13*

[Manevitch *et al.*, 2007a] Manevitch, L. I., Gourdon, E. and Lamarque, C.-H. (2007a). Parameters optimization for energy pumping in strongly nonhomogeneous 2 dof system. *Chaos, Solitons & Fractals*, 31(4):900–911. *Cited page 17*

[Manevitch *et al.*, 2007b] Manevitch, L. I., Gourdon, E. and Lamarque, C.-H. (2007b). Towards the design of an optimal energetic sink in a strongly inhomogeneous two-degree-of-freedom system. *Journal of Applied Mechanics*, 74(6):1078–1086. *Cited page 17*

[Mariani *et al.*, 2011] Mariani, R., Bellizzi, S., Cochelin, B., Herzog, P. and Mattei, P.-O. (2011). Toward an adjustable nonlinear low frequency acoustic absorber. *Journal of Sound and Vibration*, 330(22):5245–5258. *Cited page 17*

[Masri, 1969] Masri, S. (1969). Analytical and experimental studies of multiple-unit impact dampers. *The Journal of the Acoustical Society of America*, 45(5):1111–1117. *Cited page 20*

[Masri, 1970] Masri, S. (1970). General motion of impact dampers. *The Journal of the Acoustical Society of America*, 47(1B):229–237. *Cited page 20*

[Masri and Caughey, 1966] Masri, S. and Caughey, T. (1966). On the stability of the impact damper. *Journal of Applied Mechanics*, 33(3):586–592. *Cited page 20*

[Masri, 1965] Masri, S. F. (1965). Analytical and experimental studies of impact dampers. *2 citations pages 20 and 26*

[Mattei *et al.*, 2016] Mattei, P.-O., Ponçot, R., Pachebat, M. and Côte, R. (2016). Nonlinear targeted energy transfer of two coupled cantilever beams coupled to a bistable light attachment. *Journal of Sound and Vibration*, 373:29–51. *Cited page 11*

[Nayfeh, 1995] Nayfeh, A. H. (1995). On direct methods for constructing nonlinear normal modes of continuous systems. *Journal of Vibration and Control*, 1(4):389–430. *Cited page 13*

[Nayfeh, 2011] Nayfeh, A. H. (2011). *Introduction to perturbation techniques*. John Wiley & Sons. *Cited page 12*

[Nayfeh and Balachandran, 2008] Nayfeh, A. H. and Balachandran, B. (2008). *Applied nonlinear dynamics: analytical, computational and experimental methods*. John Wiley & Sons. *Cited page 13*

[Nayfeh and Nayfeh, 2011] Nayfeh, A. H. and Nayfeh, N. A. (2011). Analysis of the cutting tool on a lathe. *Nonlinear Dynamics*, 63(3):395–416. *Cited page 81*

[Nguyen and Pernot, 2012] Nguyen, T. A. and Pernot, S. (2012). Design criteria for optimally tuned nonlinear energy sinks—part 1: transient regime. *Nonlinear dynamics*, 69(1-2):1–19. *2 citations pages 17 and 55*

[Nucera *et al.*, 2008] Nucera, F., Lo Iacono, F., McFarland, D., Bergman, L. and Vakakis, A. (2008). Application of broadband nonlinear targeted energy transfers for seismic mitigation of a shear frame: Experimental results. *Journal of Sound and Vibration*, 313(1):57–76. *2 citations pages 11 and 21*

[Nucera *et al.*, 2007] Nucera, F., Vakakis, A., McFarland, D., Bergman, L. and Kerschen, G. (2007). Targeted energy transfers in vibro-impact oscillators for seismic mitigation. *Nonlinear Dynamics*, 50(3):651–677. *2 citations pages 11 and 21*

[Olson, 2003] Olson, S. E. (2003). An analytical particle damping model. *Journal of Sound and Vibration*, 264(5):1155–1166. *Cited page 88*

[Panagopoulos *et al.*, 2007] Panagopoulos, P., Georgiades, F., Tsakirtzis, S., Vakakis, A. F. and Bergman, L. A. (2007). Multi-scaled analysis of the damped dynamics of an elastic rod with an essentially nonlinear end attachment. *International Journal of Solids and Structures*, 44(18):6256–6278. *Cited page 17*

[Peeters *et al.*, 2009] Peeters, M., Viguié, R., Sérandour, G., Kerschen, G. and Golinval, J.-C. (2009). Nonlinear normal modes, part ii: Toward a practical computation using numerical continuation techniques. *Mechanical systems and signal processing*, 23(1):195–216. *2 citations pages 12 and 13*

[Peng *et al.*, 2005] Peng, Z., Peter, W. T. and Chu, F. (2005). An improved hilbert–huang transform and its application in vibration signal analysis. *Journal of sound and vibration*, 286(1):187–205. *Cited page 14*

[Pennisi *et al.*, 2016] Pennisi, G., Stéphan, C. and Michon, G. (2016). *Vibro-Impact NES: A Correlation Between Experimental Investigation and Analytical Description*, pages 137–142. Springer International Publishing, Cham. *Cited page 11*

[Peterka, 1996] Peterka, F. (1996). Bifurcations and transition phenomena in an impact oscillator. *Chaos, Solitons & Fractals*, 7(10):1635–1647. *Cited page 36*

[Peterka, 2003] Peterka, F. (2003). More detail view on the dynamics of the impact damper. *Mechanics, Automatic Control and Robotics*, 3(14):907–920. *2 citations pages 26 and 31*

[Peterka and Blazejczyk-Okolewska, 2005] Peterka, F. and Blazejczyk-Okolewska, B. (2005). Some aspects of the dynamical behavior of the impact damper. *Journal of Vibration and Control*, 11(4):459–479. *Cited page 21*

[Pilipchuk, 2002] Pilipchuk, V. (2002). Some remarks on non-smooth transformations of space and time for vibrating systems with rigid barriers. *Journal of applied mathematics and mechanics*, 66(1):31–37. *2 citations pages 13 and 24*

[Pilipchuk, 2015] Pilipchuk, V. (2015). Closed-form solutions for oscillators with inelastic impacts. *Journal of Sound and Vibration*, 359:154–167. *2 citations pages 13 and 24*

[Popplewell *et al.*, 1983] Popplewell, N., Bapat, C. and McLachlan, K. (1983). Stable periodic vibroimpacts of an oscillator. *Journal of Sound and Vibration*, 87(1): 41–59. *Cited page 20*

[Popplewell and Liao, 1991] Popplewell, N. and Liao, M. (1991). A simple design procedure for optimum impact dampers. *Journal of Sound and Vibration*, 146(3):519–526. *Cited page 20*

[Rosenberg, 1960] Rosenberg, R. M. (1960). Normal modes of nonlinear dual-mode systems. *Journal of Applied Mechanics*, 27(2):263–268. *Cited page 12*

[Savadkoohi *et al.*, 2012] Savadkoohi, A. T., Vaurigaud, B., Lamarque, C.-H. and Pernot, S. (2012). Targeted energy transfer with parallel nonlinear energy sinks, part ii: theory and experiments. *Nonlinear dynamics*, 67(1):37–46. *2 citations pages 18 and 88*

[Sigalov *et al.*, 2012] Sigalov, G., Gendelman, O., Al-Shudeifat, M., Manevitch, L., Vakakis, A. and Bergman, L. (2012). Resonance captures and targeted energy transfers in an inertially-coupled rotational nonlinear energy sink. *Nonlinear dynamics*, 69(4):1693–1704. *2 citations pages 11 and 16*

[Starosvetsky and Gendelman, 2008] Starosvetsky, Y. and Gendelman, O. (2008). Attractors of harmonically forced linear oscillator with attached nonlinear energy sink. ii: Optimization of a nonlinear vibration absorber. *Nonlinear Dynamics*, 51(1-2):47–57. *Cited page 17*

[Starosvetsky and Gendelman, 2011] Starosvetsky, Y. and Gendelman, O. (2011). Response regimes in forced system with non-linear energy sink: quasi-periodic and random forcing. *Nonlinear Dynamics*, 64(1-2):177–195. *Cited page 17*

[Sung and Yu, 1992] Sung, C. and Yu, W. (1992). Dynamics of a harmonically excited impact damper: bifurcations and chaotic motion. *Journal of Sound and Vibration*, 158(2):317–329. *Cited page 21*

[Tsakirtzis *et al.*, 2007] Tsakirtzis, S., Panagopoulos, P. N., Kerschen, G., Gendelman, O., Vakakis, A. F. and Bergman, L. A. (2007). Complex dynamics and targeted energy transfer in linear oscillators coupled to multi-degree-of-freedom essentially nonlinear attachments. *Nonlinear Dynamics*, 48(3):285–318. *Cited page 17*

[Vakakis and Gendelman, 2001] Vakakis, A. and Gendelman, O. (2001). Energy pumping in nonlinear mechanical oscillators: Part ii: Resonance capture. *Journal of Applied Mechanics*, 68(1):42–48. *2 citations pages 11 and 14*

[Vakakis *et al.*, 2003] Vakakis, A., Manevitch, L., Gendelman, O. and Bergman, L. (2003). Dynamics of linear discrete systems connected to local, essentially non-linear attachments. *Journal of Sound and Vibration*, 264(3):559–577. *Cited page 14*

[Vakakis *et al.*, 2008] Vakakis, A. F., Gendelman, O. V., Bergman, L. A., McFarland, D. M., Kerschen, G. and Lee, Y. S. (2008). *Nonlinear targeted energy transfer in mechanical and structural systems*, volume 156. Springer Science & Business Media. *Cited page 11*

[Vaurigaud *et al.*, 2011] Vaurigaud, B., Savadkoohi, A. T. and Lamarque, C.-H. (2011). Targeted energy transfer with parallel nonlinear energy sinks. part

i: design theory and numerical results. *Nonlinear dynamics*, 66(4):763–780. *2 citations pages 18 and 88*

[Yoshitake *et al.*, 2007] Yoshitake, Y., Harada, A., Kitayama, S. and Kouya, K. (2007). Periodic solutions, bifurcations, chaos and vibration quenching in impact damper. *Journal of System Design and Dynamics*, 1(1):39–50. *2 citations pages 21 and 38*

Publications

The work of thesis has produced the following publications:

Journal papers

- T. Li, S. Seguy and A. Berlioz. Dynamics of cubic and vibro-impact nonlinear energy sink: analytical, numerical and experimental analysis. Journal of Vibration and Acoustics, Transactions of the ASME. 138(3)031010-9. 2016
- T. Li, S. Seguy and A. Berlioz. On the dynamics around targeted energy transfer for vibro-impact nonlinear energy sink. Nonlinear Dynamics. (DOI 10.1007/s11071-016-3127-0)
- T. Li, S. Seguy and A. Berlioz. Optimization mechanism of targeted energy transfer with vibro-impact energy sink under periodic and transient excitation.Nonlinear Dynamics. (DOI: 10.1007/s11071-016-3200-8)
- T. Li, D. Qiu, S. Seguy and A. Berlioz. Optimization of vibro-impact energy sink for nonlinear systems. Journal of Sound and Vibration. (submitted 12/Sep/2016)
- T. Li, E. Gourc, S. Seguy and A. Berlioz. Dynamics of two vibro-impact nonlinear energy sinks in parallel under periodic and transient excitation. International Journal of Nonlinear Mechanics. (submitted 07/Oct/2016 and needed revision 22/Nov/2016)

Conference papers

- T. Li, S. Seguy, A. Berlioz and E. Gourc. Analysis of a vibro-impact nonlinear energy sink: theoritical and numerical developments. Proceedings of 22ème Congrès Français de Mécanique, 24-28 août 2015, Lyon, France 2015
- T. Li, E. Gourc, S. Seguy and A. Berlioz. Analysis of a turning process strongly coupled to a vibro-impact nonlinear energy sink. Proceedings of Joint Conference on Mechanical, Design Engineering & Advanced Manufacturing, 18-20 juin 2014, Toulouse, France 2014

Résumé

De nos jours, malgré l'utilisation croissante de nouveaux matériaux avec notamment les matériaux composites, les phénomènes vibratoires complexes sont toujours présents, et ce quel que soit le critère recherché : sécurité, performance ou encore confort. Il existe différentes techniques permettant de contrôler les vibrations, les approches basées sur le contrôle passif sont prometteuses. Un dispositif bien connu est l'absorbeur linéaire – Amortisseur à Masse Accordée (AMA) – bien que largement utilisé, il a des limites lié à l'ajout de masse important et à un réglage précis de l'accord en fréquence. Depuis, quelques années un nouveau type d'absorbeur non linéaire appelé – Nonlinear Energy Sink (NES) – est largement étudié. Il est construit par le couplage non linéaire entre le système principal et une petite masse auxiliaire, le NES. Sous certaines conditions, l'énergie vibratoire du système principal peut être transférée de manière irréversible au NES pour être ensuite dissipée. De plus, la masse ajoutée est bien plus faible que dans le cas d'un AMA. Le phénomène de transfert irréversible d'énergie est appelé pompage énergétique. L'étude du pompage énergétique est très fournie, et concerne de nombreuses approches : des systèmes principaux linéaires à un degré de liberté, des systèmes non linéaires avec de nombreux degrés de liberté ou encore des NES avec des non linéarités cubique, linéaire par morceaux, à impact, le tout en régime transitoire, périodique ou encore aléatoire. Ces nombreux travaux de recherche sont prometteurs et méritent que l'on s'y intéresse.

Tous les absorbeurs d'énergie doivent être couplés au système principal, par exemple avec un ressort linéaire pour l'AMA, ou encore par les impacts pour un NES à Vibro Imapct (NES VI). Étant donné que l'énergie du système principal est transférée à travers ce couplage, il joue un rôle essentiel. Ce rôle peut être décrit sous différents aspects. Par exemple, l'existence du pompage énergétique dans une large bande de fréquence dépend directement de la caractéristique non linéaire du couplage. D'autres aspects sont liés, les modes non linéaires ou les régimes de réponse lors de l'étude des systèmes Hamiltoniens, sont réglés uniquement par le type de non linéarité du couplage. De plus, la force d'interaction peut également être utile, notamment pour l'étude analytique. Ainsi deux approches analytiques sont utilisées : l'étude des systèmes Hamiltoniens avec la présentation des résultats sous forme d'un diagramme énergie-fréquence et la méthode asymptotique avec des résultats sous la forme d'une variété invariante. Pourquoi, bien souvent, des paramètres tels que le type d'excitation sont négligés ? L'analyse de la force d'interaction, qui peut jouer un rôle d'intermédiaire, afin d'expliquer la dynamique d'un système avec différentes excitations extérieures.

Il a été montré que le régime de résonnance 1:1 permet l'efficacité maximale du transfert d'énergie, ou pompage énergétique. L'efficacité du pompage énergétique est fortement liée au régime vibratoire observé, l'étude du pompage peut donc être séparée en deux parties: l'influence des paramètres du système sur l'apparition des régimes vibratoire et l'efficacité des différents régimes vibratoire observés. Avec ce découpage, le rôle des différents paramètres peut être ramené sous le même angle d'étude. Ainsi pour l'optimisation de la conception, la sélection des paramètres doit permettre d'obtenir un régime vibratoire optimal. Étant donné que le régime de réponse existe à la fois pour une excitation périodique et transitoire, le mécanisme d'optimisation doit être expliqué d'une seule et même manière. Ainsi, si le régime optimal pour une excitation périodique avec une seule fréquence a été défini, le mécanisme optimal pour une excitation périodique avec un balayage en fréquence sera expliqué de la même manière.

Si la condition d'activation du NES est précisément définie, l'application du NES pour contrôler les systèmes non linéaires peut alors être simplifiée de la sorte : comment activer le NES et faire que son efficacité soit maximale. Ainsi l'amplitude du système principal non linéaire ne peut être garantie, mais par contre le NES sera activé avec une efficacité maximale. Peut-être que cet optimal ne sera pas le meilleur en théorie, mais il sera le meilleur en pratique.

De l'analyse ci-dessus, les cinq points suivants trouvent une réponse positive, à savoir:

1. Une force d'interaction peut jouer un rôle central pour l'explication des différents régimes vibratoires observés.
2. Il est possible d'étudier l'influence des paramètres du NES VI sur la présence des régimes vibratoire et sur leur efficacité.
3. Le mécanisme d'optimisation sous-jacent pour les différents types d'excitation est similaire.
4. La conception optimale du NES VI pour les systèmes non linéaires peut être simplifiée à l'optimisation du NES VI pour un système linéaire correspondant.
5. Le principe de l'activation séparée peut améliorer l'efficacité et la robustesse pour la réduction des vibrations.

À partir de ces points, ces travaux de thèse sont organisés autour de cinq chapitres.

Dans le premier chapitre, le contexte général est présenté. La bibliographie est ensuite développée autour de deux axes: le NES à non linéarité cubique et le NES VI. Les résultats généraux sont présentés pour le NES. L'accent est mis sur les problématiques, à savoir, comment optimiser un NES face à un système non linéaire ou encore comment identifier un mécanisme d'optimisation sous différentes excitations. Pour le NES VI, les études anciennes montrent les limites des approches analytiques utilisées. Par conséquent, le principal objectif est d'étudier cet absorbeur avec les nouveaux outils développés pour le pompage énergétique.

Le chapitre 2 vise à étudier l'influence des différents paramètres du NES VI sur les régimes vibratoires et sur les bifurcations. Une force d'interaction est introduite dans les

équations analytiques afin d'apporter une explication. Ensuite, les régimes de réponse typiques sont obtenus par simulation numérique et sont comparés à la variété invariante du système. Les régimes sont analysés précisément et l'influence des paramètres du NES VI est clairement explicitée. Enfin, une campagne expérimentale est menée afin de retrouver les régimes vibratoires et les bifurcations associées.

Le chapitre 3 vise à comparer l'efficacité des régimes, précédemment observés, pour définir les mécanismes pour l'optimisation de la conception face à différents types d'excitation. Dans un premier temps l'efficacité des différents régimes est analysée par simulation numérique sous excitation périodique et transitoire. Ces résultats sont analysés plus finement par une approche analytique. Dans un second temps, des essais expérimentaux sont réalisés en régime périodique avec une seule fréquence d'excitation, avec un balayage en fréquence et en régime transitoire. Les résultats, ainsi observés, sont cohérents avec les simulations numériques. Ils valident ainsi l'existence d'un critère commun pour l'optimisation de la conception du NES VI.

Dans le chapitre 4, les caractéristiques de l'activation du NES VI sont explorées et l'optimisation de la conception est étendue pour la réduction des vibrations sur des systèmes non linéaires. Dans une première partie, les caractéristiques de l'activation sont analysées à travers la variété invariante du système. Il est ainsi observé que l'activation du NES VI est proportionnelle et valable pour différentes fréquences d'excitation. Ces résultats permettent de développer un critère pour l'optimisation de la conception du NES VI dans le cas de système non linéaire. Dans une deuxième partie, les caractéristiques ainsi obtenues sont observées par la simulation numérique. Enfin, des expériences sont réalisées afin de valider le mécanisme d'activation. Une application pratique est conduite afin de réduire le broutement en tournage. Les résultats de la simulation numérique prouvent la faisabilité de la réduction des vibrations d'usinage.

Dans le chapitre 5, un oscillateur linéaire est couplé avec deux NES VI en parallèle afin d'améliorer l'efficacité et la robustesse. Les résultats analytiques et numériques existants sont brièvement rappelés. Ensuite, les résultats expérimentaux, en régime périodique, sont présentés, les différents régimes vibratoires sont observés. Par contre, les gains ne sont pas si évidents et certains cas peuvent conduire à la désactivation des deux NES VI. Pour éviter cet inconvénient, il faut choisir précisément la longueur de la cavité. Des essais en transitoire sont aussi conduits et le principe d'activation séparé est observé. Dans un objectif de réduction du niveau acoustique, l'addition d'une deuxième bille dans le NES VI est plus efficace.

Suite à ces travaux de thèse, plusieurs perspectives peuvent être envisagées:

- Les régimes vibratoires peuvent être analysés plus finement, notamment en calculant l'exposant de Lyapunov afin de caractériser les comportements chaotiques des réponses fortement modulées.
- La modélisation de l'impact mériterait d'être affinée afin d'améliorer la précision du modèle.
- L'étude s'est limitée aux excitations périodiques et transitoires, d'autres excitations pourraient être analysées, par exemple l'excitation aléatoire.

- Puisque l'activation du NES VI dépend directement de l'amplitude du système principal et de la course de la bille, il est intéressant de pousser l'étude en combinant différents NES VI avec différentes longueurs de cavité.
- Il serait intéressant de généraliser l'étude à d'autres types de NES, par exemple le NES rotatif ...
- Il serait également intéressant d'étudier expérimentalement l'application du NES VI pour la réduction des vibrations du broutement en usinage et sur d'autres applications non linéaires ...